

PhD degree in Medical Nanotechnology  
European School of Molecular Medicine (SEMM),  
CIMaINa, University of Milan

**An Electrochemical Detection System for Thiocholine Using  
Cluster-assembled Zirconia Modified Gold Electrodes**

*Alexandra Raileanu*

**Matricola n. R10787**

**Supervisor: Prof. Paolo Milani**

**CIMaINa (Interdisciplinary Centre for Nanostructured  
Materials and Interfaces )**

**University of Milan**

**Anno accademico 2016-2017**

# Contents

<b>List of abbreviations</b>	<b>4</b>
<b>List of figures</b>	<b>6</b>
<b>List of tables</b>	<b>10</b>
<b>Abstract</b>	<b>12</b>
<b>1. Introduction</b>	<b>13</b>
<b>1.1. What is a biosensor?</b>	<b>13</b>
<b>1.2. Electrochemical biosensors</b>	<b>15</b>
<b>1.3. Nanotechnology in biosensing applications</b>	<b>16</b>
<b>1.4. Nanostructured zirconium oxide used in biosensing applications</b>	<b>17</b>
<b>1.5. Means of enzymatic immobilization onto nanostructured surfaces</b>	<b>18</b>
<b>1.6. Acetylcholinesterase as component of a transducer used in electrochemical biosensing- Case of study</b>	<b>20</b>
<b>1.6.1 The importance of Acetylcholinesterase in the neurotransmission process</b>	<b>20</b>
<b>1.6.2. Organophosphates and their influence on the nervous system</b>	<b>21</b>
<b>1.6.3. Current methods of detection for organophosphorus compounds</b>	<b>23</b>
<b>1. 7. Aim of the project</b>	<b>25</b>
<b>2. Materials and methods</b>	<b>26</b>
<b>2.1. Electron beam evaporation</b>	<b>26</b>

<b>2.2. Supersonic cluster beam deposition technique</b>	<b>27</b>
<b>2.3. Surface morphology characterization of nanostructured zirconia- Atomic force microscopy analysis</b>	<b>30</b>
<b>2.4. Electrochemical characterization of the modified transducers</b>	<b>32</b>
<b>2.5. Enzymatic production of thiocholine</b>	<b>37</b>
<b>2.6. Amperometric detection of thiocholine</b>	<b>39</b>
<b>3. Results</b>	<b>41</b>
<b>3.1. Nanostructured Zirconia</b>	<b>42</b>
<b>3.1.1. Morphological characterization of first generation of modified electrodes</b>	<b>42</b>
<b>3.1.2. Electrochemical assessments preparation- “Quasi” Reference electrode production</b>	<b>44</b>
<b>3.1.3. Electrochemical behavior of first generation of the modified electrodes – Cyclic Voltammetry study</b>	<b>45</b>
<b>3.1.4. Electrochemical behavior of first generation of the modified electrodes – Electrochemical impedance spectroscopy study</b>	<b>46</b>
<b>3.2.1 Morphological characterization of second generation of the modified electrodes</b>	<b>48</b>
<b>3.2.2. Electrochemical characterization of second generation of the modified electrodes- Cyclic voltammetry study</b>	<b>50</b>
<b>3.2.3. Electrochemical characterization of second generation of modified electrodes - Electrochemical impedance spectroscopy study</b>	<b>55</b>
<b>3.3.1. Enzymatic production of Thiocholine</b>	<b>62</b>
<b>3.3.2. Electrochemical detection of Thiocholine</b>	<b>62</b>

<b>3.3.3. Electrochemical detection of Thiocholine-Electrochemical Impedance Spectroscopy</b>	<b>66</b>
<b>3.3.4. Electrochemical detection of Thiocholine- Chronoamperometry</b>	<b>71</b>
<b>4. Discussions</b>	<b>76</b>
<b>5. References</b>	<b>81</b>
<b>6. Appendix 1</b>	<b>93</b>

## **Glossary**

**ns- ZrO<sub>2</sub>** – Nanostructured zirconia

**SCBD** - Supersonic Cluster Beam Deposition

**PMCS**- Pulsed Microplasma Cluster Source

**AFM** - Atomic force microscopy

**ATCh** – Acetylthiocholine

**TCh** - Thiocholine

**AChE** - Acetylcholinesterase

**ATCh Cl** - Acetylthiocholine Chloride

**ATCh I** – Acetylthiocholine Iodide

**OP** – Organophosphate

**WE** - Working electrode

**RE** - Reference electrode

**CE** - Counter electrode

**KCl** - Potassium Chloride

**PBS** - Phosphate buffer solution

**Fe<sup>3+</sup>/Fe<sup>2+</sup>** - Potassium Ferricyanide/ Potassium Ferrocyanide

**EIS** - Electrochemical Impedance Spectroscopy

**CV** - Cyclic Voltammetry

**CA** - Chronoamperometry

**LOD** - Limit of detection

**DTNB** - 5, 5- dithio-bis-(2-nitrobenzoic acid)

**TNB** - 5-thio-2-nitrobenzoate

**Rs** - Solution resistance

**Rct** - Charge transfer resistance

**Cdl** - Double layer capacitance

## List of figures

<b>Fig. 1-</b> Representation of the main components of a biosensor	<b>14</b>
<b>Fig. 2-</b> Schematic representation of the role of AChE in the neurotransmission process	<b>21</b>
<b>Fig. 3-</b> Schematic representation of the pesticide cycle in nature	<b>22</b>
<b>Fig. 4-</b> Schematic representation of a normal hydrolysis in the esteratic site of the AChE enzyme in comparison to an irreversible inhibition process and a blockage of the binding site of the enzyme in the case of OPs usage	<b>23</b>
<b>Fig. 5-</b> Concept of OPs enzymatic electrochemical detection using immobilized AChE as biocatalyst for synthetically produced TCh	<b>25</b>
<b>Fig. 6A-</b> Schematic representation of the SCBD apparatus	<b>28</b>
<b>Fig. 6B-</b> Schematic representation of the elements used for the development of the modified electrodes	<b>28</b>
<b>Fig. 7-</b> Schematic representation of the pulsed microplasma cluster source	<b>29</b>
<b>Fig. 8-</b> Roughness Vs Thickness calibration curve	<b>30</b>
<b>Fig. 9-</b> Schematic representation of the operating principle of the AFM	<b>31</b>
<b>Fig. 10-</b> Schematic representation of a three-electrode electrochemical cell setup	<b>33</b>
<b>Fig. 11-</b> Cyclic voltammogram of a single electron oxidation-reduction reaction	<b>34</b>
<b>Fig. 12-</b> AFM analysis of nanostructured ZrO <sub>2</sub> surfaces for first generation of modified electrodes	<b>43</b>

<b>Fig. 13-</b> Calibration curve of the “Quasi” RE in KCl solution of difference concentrations	<b>44</b>
<b>Fig. 14-</b> Cyclic voltammograms for all types of ns-ZrO <sub>2</sub> modified working electrodes compared to the bare Au (Control)	<b>45</b>
<b>Fig. 15-</b> Nyquist plot of the commercial electrolyte at the surface of the modified electrodes compared to bare Au	<b>46</b>
<b>Fig. 16-</b> Representation of the Randles circuit model	<b>47</b>
<b>Fig. 17-</b> AFM analysis of nanostructured ZrO <sub>2</sub> surfaces	<b>49</b>
<b>Fig. 18-</b> Cyclic voltammograms for all types of ns-ZrO <sub>2</sub> modified working electrodes compared to the bare Au (Control)	<b>50</b>
<b>Fig. 19 a-</b> Cyclic voltammograms for NS-1 working electrodes performed in Fe <sup>3+</sup> /Fe <sup>2+</sup> at different scan rates (20 mV/s, 50 mV/s and 100 mV/s)	<b>52</b>
<b>Fig. 19 b-</b> Variation of anodic and cathodic current peak with the square root of scan rate for the NS-1 working electrodes	<b>52</b>
<b>Fig. 20 a-</b> Cyclic voltammograms for NS-2 working electrodes performed in Fe <sup>3+</sup> /Fe <sup>2+</sup> at different scan rates (20 mV/s, 50 mV/s and 100 mV/s)	<b>53</b>
<b>Fig. 20 b-</b> Variation of anodic and cathodic current peak with the square root of scan rate for the NS-2 working electrodes	<b>53</b>
<b>Fig. 21 a-</b> Cyclic voltammograms for NS-3 working electrodes performed in Fe <sup>3+</sup> /Fe <sup>2+</sup> at different scan rates (20 mV/s, 50 mV/s and 100 mV/s)	<b>54</b>
<b>Fig. 21 b-</b> Variation of anodic and cathodic current peak with the square root of scan rate for the NS-3 working electrodes	<b>54</b>
<b>Fig. 22-</b> Nyquist plot of PBS (0.1 M, pH= 7.5) at the surface of the modified transducers compared to bare Au electrodes	<b>55</b>
<b>Fig. 23-</b> Nyquist plot of the commercial electrolyte at the surface of the modified electrodes compared to bare Au sample at open potential circuit	<b>56</b>
<b>Fig. 24-</b> Nyquist plot of different concentration of commercial electrolyte solution at the surface of bare Au electrode	<b>58</b>

<b>Fig. 25-</b> Nyquist plot of different concentration of commercial electrolyte solution at the surface of NS-1 modified electrodes	<b>59</b>
<b>Fig. 26-</b> Nyquist plot of different concentration of commercial electrolyte solution at the surface of NS-2 modified electrodes	<b>60</b>
<b>Fig. 27-</b> Nyquist plot of different concentration of commercial electrolyte solution at the surface of NS-3 modified electrodes	<b>61</b>
<b>Fig. 28-</b> Calibration curve for Thiocoline using the spectrophotometric method	<b>62</b>
<b>Fig. 29-</b> Cyclic voltammograms of ATChCl and ATChI substrates (0.5 M) in PBS solution	<b>63</b>
<b>Fig. 30-</b> Cyclic voltammogram of TCh oxidation at the surface of Bare gold electrode	<b>64</b>
<b>Fig. 31-</b> Cyclic voltammogram of TCh oxidation at the surface of NS-1 modified electrode	<b>64</b>
<b>Fig. 32-</b> Cyclic voltammogram of TCh oxidation at the surface of NS-2 modified electrode	<b>65</b>
<b>Fig. 33-</b> Cyclic voltammogram of TCh oxidation at the surface of NS-3 modified electrode	<b>65</b>
<b>Fig. 34-</b> Nyquist plot of different concentrations of TCh solution at the surface of Bare Au electrodes at fixed potential	<b>67</b>
<b>Fig. 35-</b> Nyquist plot of different concentrations of TCh solution at the surface of NS-1 modified electrodes at fixed potential	<b>68</b>
<b>Fig. 36-</b> Nyquist plot of different concentrations of TCh solution at the surface of NS-2 modified electrodes at fixed potential	<b>69</b>
<b>Fig. 37-</b> Nyquist plot of different concentrations of TCh solution at the surface of NS-3 modified electrodes at fixed potential	<b>70</b>
<b>Fig. 38a-</b> Amperometric detection of TCh at the surface of Bare Au electrode	<b>71</b>

**Fig. 38b-** Concentration vs. Current of TCh amperometric detection at the surface of Bare Au electrodes 71

**Fig. 39a-** Amperometric detection of TCh at the surface of NS-1 modified electrode 72

**Fig. 39 b-** Concentration vs. Current of TCh amperometric detection at the surface of NS-1 modified electrodes 72

**Fig. 40a-** Amperometric detection of TCh at the surface of NS-2 modified electrode 73

**Fig. 40b-** Concentration vs. Current of TCh amperometric detection at the surface of NS-2 modified electrodes 73

**Fig. 41a-** Amperometric detection of TCh at the surface of NS-3 modified electrode 74

**Fig. 41b-** Concentration vs. Current of TCh amperometric detection at the surface of NS-3 modified electrodes 74

## List of Tables

- Table 1.** Thickness and morphology assessment values performed by tapping-mode AFM on cluster-assembled ZrO<sub>2</sub> nanostructured thin films grown by means of SCBD 44
- Table 2.** CV data of anodic and cathodic current peaks as well as the peak-to-peak separation for all types of ns-ZrO<sub>2</sub> modified working electrodes compared to the bare Au 45
- Table 3.** Charge transfer resistance, solution resistance and double layer capacitance values for the modified electrodes and bare Au sample in commercial electrolyte solution on cluster-assembled ZrO<sub>2</sub> nanostructured thin films grown by means of SCBD 47
- Table 4.** Thickness and morphology assessment values performed by tapping-mode AFM 48
- Table 5.** CV data of anodic and cathodic current peaks as well as the peak-to-peak separation for all types of ns-ZrO<sub>2</sub> modified working electrodes compared to the bare Au 50
- Table 6** Solution resistance values for the modified electrodes and bare Au (Control) in PBS solution 56
- Table 7** Charge transfer resistance and double layer capacitance values for the modified electrodes and bare Au sample in commercial electrolyte solution 57
- Table 8.** Charge transfer resistance and double layer capacitance values for the bare Au sample in commercial electrolyte solution with different concentrations 58

<b>Table 9.</b> Charge transfer resistance and double layer capacitance values for the NS-1 modified electrodes in commercial electrolyte solution with different concentrations	59
<b>Table 10.</b> Charge transfer resistance and double layer capacitance values for the NS-2 modified electrodes in commercial electrolyte solution with different concentrations	60
<b>Table 11.</b> Charge transfer resistance and double layer capacitance values for the NS-3 modified electrodes in commercial electrolyte solution with different concentrations	61
<b>Table 12.</b> Oxidation potentials and current peaks of TCh at the surface of the modified electrodes and Bare Au sample	66
<b>Table 13.</b> Charge transfer resistance and double layer capacitance values for the Bare Au electrodes in TCh solution with different concentrations	67
<b>Table 14.</b> Charge transfer resistance and double layer capacitance values for the NS-1 modified electrodes in TCh solution with different concentrations	68
<b>Table 15.</b> Charge transfer resistance and double layer capacitance values for the NS-2 modified electrodes in TCh solution with different concentrations	69
<b>Table 16.</b> Charge transfer resistance and double layer capacitance values for the NS-3 modified electrodes in TCh solution with different concentrations	70
<b>Table 17.</b> Limit of detection of TCh at the surface of the modified electrodes and Bare Au control	75

## Abstract

Rapid, low cost, sensitive and user friendly detection methods for pesticides that contain organophosphate compounds are important for environmental pollution control. Even though the current detection methods are very precise, they are meant only for laboratory use, they require highly trained personnel, are expensive, cumbersome and the usage of a large number of reactants and chemicals is needed. Nanotechnology combined with specific enzymes that are influenced by the presence of organophosphates could offer the alternative of designing specific biosensors that are more suitable for on-site detection. With this PhD work I intend to approach one of the drawbacks that are commonly found in designing a platform for portable electrochemical detection systems: a good communication between the materials that make up a transducer and the biological component which will interact with the analyte. Cluster-assembled zirconia nanostructured thin films, as a transducer component, have been optimized for a suitable immobilization of Acetylcholinesterase enzyme that acts as a catalyst for the breakdown of Acetylcholine. Moreover, the implementation of zirconia has shown to improve the electron transfer when used as part of the transducer in electrochemical assessments, which makes it a suitable candidate for the development of detection platforms for environment monitoring based on electrochemical techniques.

# 1

## Introduction

Nanotechnology has become in the past years one of the key factors in the development of biosensors used in fields such as food safety control, healthcare or environmental analysis. Current analysis methods are cumbersome, they require highly trained personnel, they are expensive and are not suitable for on-site usage. Therefore, a rapid, sensitive and user friendly device that can be used outside the laboratories by non-trained personal is required.

### 1.1 What is a biosensor?

According to IUPAC (International Union of Pure and Applied Chemistry), a biosensor is an analytical device that contains a biological element used for the detection of a specific bio-analyte and a transducer that converts a biological signal into an electrical signal [1].

A biosensing device consists of three elements: a bioreceptor, a transducer and a system that processes the signal (**Fig. 1**).

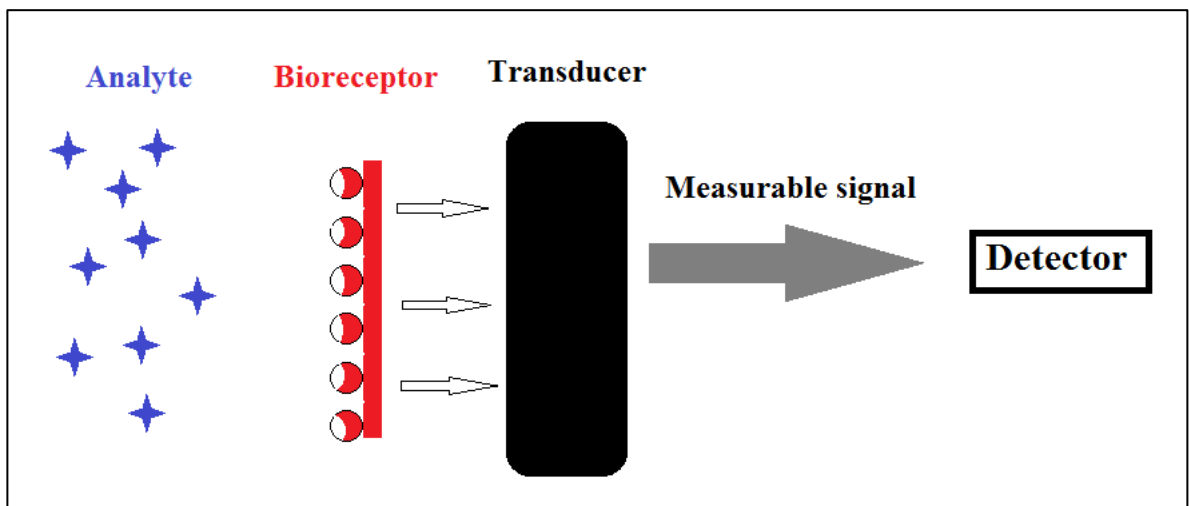


**Fig. 1-** Representation of the main components of a biosensor [2]

The classification of a biosensor can be made according to the type of bioreceptor or the transduction mechanism that is used.

Based on the transduction mechanism, there are:

- ✓ Electrochemical
- ✓ Piezoelectric
- ✓ Calorimetric
- ✓ Optical

Depending on the type of bioreceptor implemented, biosensors can be classified as:

- ✓ Enzymatic
- ✓ Antibody based
- ✓ DNA based
- ✓ Cell based
- ✓ Biomimetic

## **1.2. Electrochemical biosensors**

Among all types of biosensors, electrochemical detection devices are the most preferred due to their fast response time, the low-cost and also to the low complexity of handling by the users. The concept behind an electrochemical biosensor is the detection of an electrical signal correlated to an analyte concentration in a solution [3]. Many of the electrochemical detection systems do not require a complex instrumentation, microfabrication methods can easily be integrated in the production of the devices and they have a relative low-cost.

Even though L. C. Clark first developed a biosensor for blood glucose detection in 1962 [4], the path from research laboratories to the market of the portable electrochemical detection systems has been a cumbersome one. Issues as sensitivity, selectivity, rapid detection, ease of handling and simple production process of transducers have been the main challenges in order to develop biosensors for general use. Among the main tackled issues, the most important one is to realize a good interaction between the transducer and the biological component in order to obtain a good sensitivity and also to be able to maintain the integrity and activity of the bioreceptor. A solution for this issue is represented by the implementation of nanostructures that are biocompatible and also have good surface morphology characteristics to be appropriate for immobilization of biological compounds.

## **1.3 Nanotechnology in biosensing applications**

A nanomaterial can be defined according to the European regulations as a material with at least one dimension in the range of 1-100 nm [5]. The main advantages of the implementation of the nanomaterials in the structure of biosensors are: an increased active surface area, enhanced electron transfer and a better implementation of the bioreceptor.

The type of nanostructures that are implemented in detection systems are nanoparticles, nanowires, nanotubes, nanorods or quantum dots [6], [7]. Materials like gold, carbon, zinc, titanium or zirconium are often used and characteristics like biocompatibility and the ease of biomolecule immobilization are taken into consideration when producing a biosensor [8], [9]. Among these materials, carbon- and gold-based nanostructures are the most commonly used.

Gold nanoparticles are mainly used as components of biosensors due to their ability to increase the electronic signal when the biological material is in contact with the nanostructured surface [10]. For the development of amperometric biosensors several research groups have integrated noble nanostructures which were covered by a biorecognition element in order to enhance the amperometric signal [11], [12], [13].

In the past decades carbon-based nanostructures like graphene, carbon nanotubes, carbon nanofibers or carbon dots have been gaining more attention in the production of biosensors [14], [15]. Among all the carbon-based nanostructures, carbon nanotubes are the most intensively used in biosensing applications. Since their discovery in 1991 by Iijima, who first produced them by arc-discharge evaporation method [16] and their first integration in a biosensor by Britto et al. [17] they have been used in biosensing applications due to their higher sensitivity and faster response times compared to other carbon based electrodes [18], [19].

The process of nanostructures production is an important factor for the development of research in nanoscience. There are two main production techniques: the “bottom-up” and “top-down” technique.

When the “bottom-up” technique is used the nanostructured film is built starting from the bottom, by layering atom by atom/molecule by molecule/cluster by cluster, until

the desired structure is obtained and it is considered as a self-assembly process. Examples of “bottom-up” techniques are used for methods as electrochemical deposition [20], [21], screen printing [22], [23], chemical vapor deposition [24] or chemical deposition [25].

For the “top-down” technique, the bulk material is already available and processes like abrasion or etching are used to remove top layers of substrates until the design of the necessary film is acquired. One of the most common methods that use this technique is lithography [26].

When designing a transducer for biosensing applications, with components that involve nanostructures, the choice of technique plays an important role. The “top-down” techniques allow patterns that are on a large scale to be reduced to nanoscale but are not cheap or quick to manufacture, and the produced films may come with many defects due to the abrasions. They are also slow and not very suitable for large scale production. With the “bottom-up” techniques, the number of defects is lower, the fabrication process is less expensive and it also involves less chemicals and solvents.

#### **1.4 Nanostructured zirconium oxide used in biosensing applications**

Among different types of material used for the development of detection devices for biological applications, nanostructured metal oxides (NMO) have shown great potential as matrices for immobilizing biological components onto the transducer component of biosensors [27], [28], [29].

Zirconia ( $ZrO_2$ ) represents an attractive material to be implemented in the design of transducers since it has a high thermal, mechanical and chemical resistance, it is biocompatible, it has a high affinity towards the groups containing oxygen and it also expresses a high ion exchange capacity and redox activity [30], [31], [32]. During the past years,  $ZrO_2$  nanostructures have been successfully implemented in the design of detection

platforms by many research groups. In biomedical applications, ZrO<sub>2</sub> nanostructures have been used as part of biosensors for DNA detection [33], [34], detection of bilirubin [35], oral cancer or urea [36]. Besides biomedical applications, nanostructured ZrO<sub>2</sub>, both functionalized and unfunctionalized, have also been used as part of detection system for environmental pollution control [37], [38], [39], [40].

## **1.5 Means of enzymatic immobilization onto nanostructured surfaces**

The immobilization process of enzymes onto different type of supports is the most important step when taking into consideration the design of a transducer for a biosensor. Even though many research groups have been working on the development of biosensing devices, the number of detection system that get from the laboratories into the market is very low, mainly because of the challenge represented by obtaining a good interaction between the biologic compound and the support material. In order to overcome this issue several aspects must be taken into consideration when an enzymatic immobilization is performed. First of all, the process should be simple and it should involve a small number of chemicals and therefore the functionalized transducers would be affordable by common users [41]. The catalytic activity of the enzyme should be maintained after the immobilization, there should be no leakage of the immobilized biological material and the amount of enzyme would have to be kept as low as possible.

There are several methods of enzymatic immobilization onto nanostructured matrices for biosensing devices described in literature.

The *entrapment* method of enzymatic immobilization is described as an irreversible method in which the enzyme of interest is caged by covalent or non-covalent bonds within gels or fibers [42]. With this method the substrate and the product are allowed to pass through, but the enzyme is kept inside the matrix. The materials used for enzymatic

entrapment include polymers, sol-gels, polymer/sol-gel composites or other inorganic materials [43], [44]. Although it has been shown that by using this immobilization method the denaturation of the enzyme is avoided and that the mechanical stability is improved [45], there are some drawbacks when it comes to mass transfer between the analyte and the active site of the enzyme [46] or the possibility of enzyme leakage [47].

Another method of enzymatic immobilization is the *cross-linking* or carrier-free method where the enzyme acts as its own carrier [47]. The principle of this method is creating cross-linkages between the enzyme and the nanostructured surface. The most common and economical cross-linking agent is glutaraldehyde [48]. Although this method does not involve a support to prevent the enzyme leakage, it has been shown that it can lead to the dilution of the enzyme [47] and it can be also very costly [49].

One of the most commonly used method for irreversible enzyme immobilization is the *covalent binding* and the principle of this method involves using the functional groups of the enzyme that don't have a role in the catalytic activity. This immobilization method has been shown to be very effective in the case of enzymes of which activity can be restored and compared to other methods, it is possible to reuse the immobilized enzymes more often than other methods allow [50].

For enzymes of which the activity cannot be restored the most appropriate immobilization method is represented by the *physical adsorption* onto the nanostructured surfaces. It is one of the most simple immobilization methods since it does not require additional chemicals. For this reason as well as its low cost and the capability of retaining a higher enzyme activity, this method has a higher commercial potential [51].

## **1.6 Acetylcholinesterase as component of a transducer used in electrochemical biosensing- Case of study**

Given the knowledge and vast experience of our group in the production of nanostructured materials through a “bottom-up” technique [52] and also the studies performed on the interaction of biological components with nanostructured thin films [53], I took the advantage to develop a cluster- assembled nanostructured zirconia thin film (ns-ZrO<sub>2</sub>) for the realization of a detection platform suitable for biosensing applications.

The case studied in this work presents the use of Acetylcholinesterase enzyme as a catalyst for the electrochemical detection of Thiocholine (TCh).

### **1.6.1 The importance of Acetylcholinesterase in the neurotransmission process**

Acetylcholinesterase (AChE) is an enzyme located in the post-synaptic membrane and its main role is to catalyze the breakdown of acetylcholine (ACh) which functions as a neurotransmitter [54]. In a normal functioning environment, ACh is released from the pre-synaptic neuron and it is captured by the ACh receptors located in the post-synaptic neuron or muscle cell. When this happens, a signal is generated from the post-synaptic neuron and the release of AChE takes place. The AChE has the role of breaking down the unbound ACh into choline and acetic acid that will be reabsorbed by the pre-synaptic neuron and they will be transformed once again into ACh [55]. AChE is the primary enzyme that is inhibited by organophosphorus compounds found in nerve agents or pesticides. Once the enzymatic activity is inhibited, the released ACh can no longer be broken and the consequences of this process lead to neurological damages, paralysis, seizures and death

[56]. A schematic representation of the AChE in the neurotransmission is represented in Fig. 2.

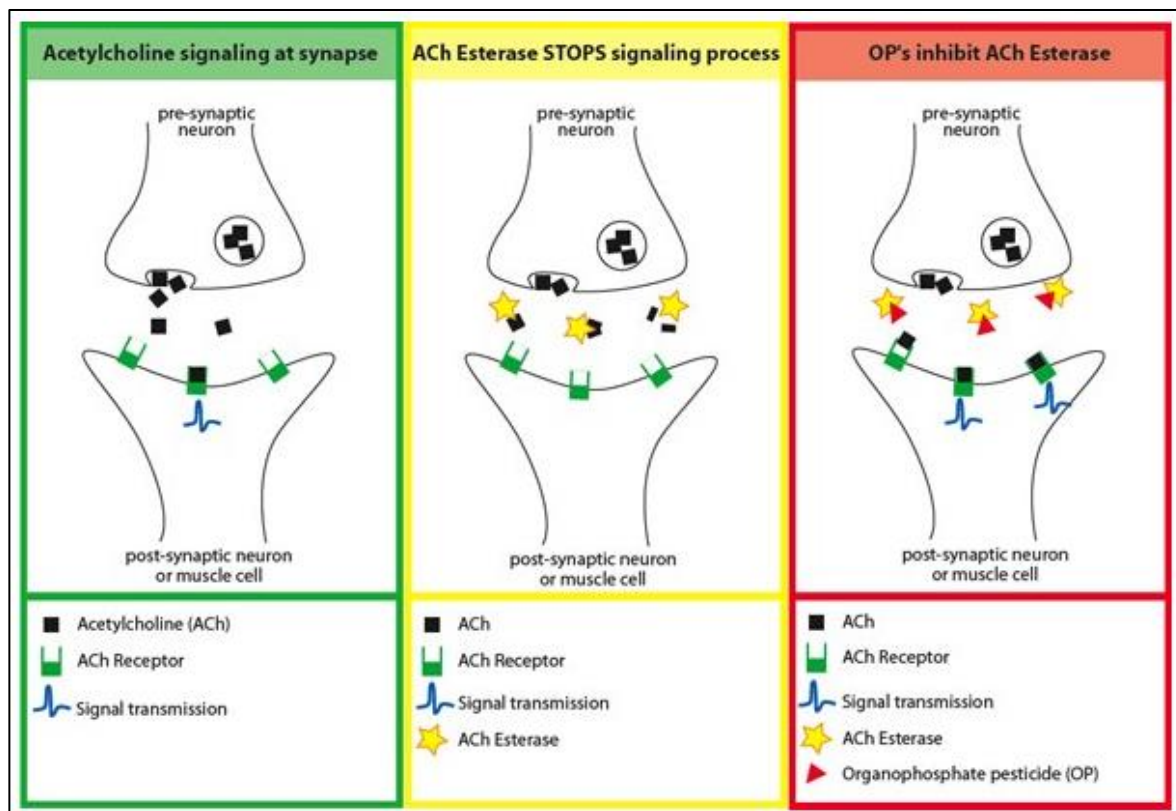
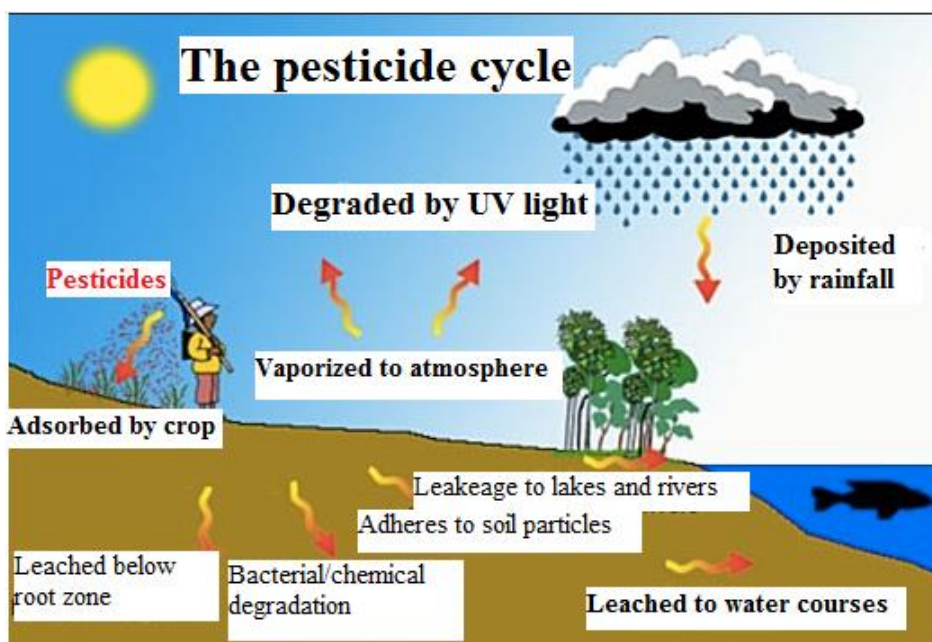


Fig. 2 – Schematic representation of the role of AChE in the neurotransmission process

[57]

### 1.6.2 Organophosphates and their influence on the nervous system

Organophosphate (OP) is a general term for esters of phosphoric acid. They are basic components found in pesticide, insecticide and nerve agents [58]. During the World War II, OPs have been at the base of known nerve agents like Sarin, Soman and VX nerve agent [59]. Since 1930, when this compound was developed by Gerhard Schrader for the IG Farben Company, it has been used as an insecticide and nowadays it still represents 50 % of used pesticides worldwide.



**Fig.3.** – Schematic representation of the pesticide cycle in nature [60]

Even though a big part of the pesticides activity is degraded by elements found in air and soil, intensive usage of these chemicals leave a higher level of residues that are deposited in water and soil and become dangerous for the environment as well as for the inhabitants of the area where the substances are used. A schematic representation of the cycle of pesticides in nature can be observed in **Fig. 3**.

Two of the most common commercialized pesticides based on OP compounds are Parathion and Malathion, which are frequently used in parks and public areas for mosquito control [61].

In section 1.6.1. the normal mechanism of AChE activity has been described. The inhibition process of the AChE enzyme can be reversible or irreversible. In the case of a reversible inhibition, the enzyme activity is stopped between a few seconds to a few minutes and afterwards the biological processes return to a normal function. In the case of

the irreversible inhibitors the biological function is stopped without any possibility of recovery and therefore leading to neurological damage [62] (**Fig. 4**).

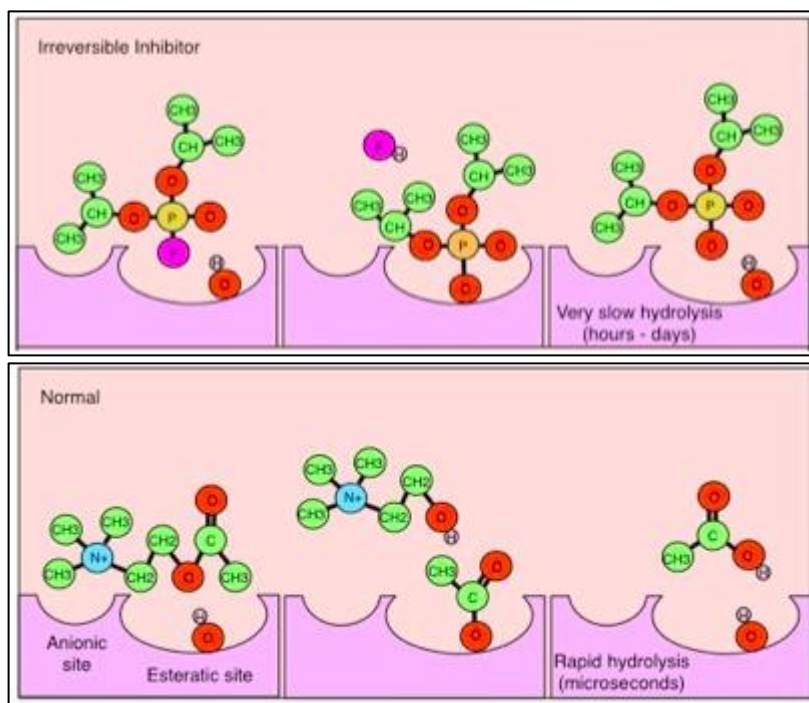


**Fig. 4-** Schematic representation of a normal hydrolysis in the esteratic site of the AChE enzyme (top image) in comparison to an irreversible inhibition process and a blockage of the binding site of the enzyme in the case of OPs usage (bottom image) [63]

### 1.6.3 Current methods of detection for organophosphorus compounds

Besides public areas, OP based pesticides are still intensively used for crop protection in developing countries and residue traces infiltrate in the soil, contaminating water sources and still represent a danger for the environment as well as for the population that inhabits the treated area [64].

In terms of OP contamination analysis, laboratory methods like gas chromatography [65], [66], high purity liquid chromatography (HPLC) [67] or fluorescence spectroscopy [68] are the main detection methods used. Although they are very precise and sensitive,

these methods are not suitable for on-site detection and they require highly trained personnel, are very expensive and require a high number of chemicals. Therefore, a higher demand for portable, sensitive, cheap and easy to use detection devices for OPs has been expressed.

In recent years, many research groups have been focusing on developing portable biosensors for OPs that are robust, precise and easy to use by consumers on-site.

Many research groups that have been working in the past years on the development of biosensors for OPs analysis use enzymatic detection with AChE as primary enzyme or bi-enzymatic systems [69], [70], [71], [72].

There are several techniques used in the enzymatic detection of OPs, such as optical methods [73] or fluorescence analysis [74], [75] but the most commonly used detection technique is the electrochemical method. Electrochemical detection systems for OPs that involve using AChE enzyme as biocatalyst are based on the anodic oxidation of the enzymatic product TCh, process that is described in more detail in Section 2.6. Voltammetric [76], [77] or impedance spectroscopy methods [76] have been used by several research groups but the most common electrochemical mean of TCh detection is the amperometric method [78], [79], [80], [81].

## 1.7. Aim of the project

The aim of this PhD project was to design and characterize a detection platform, based on cluster-assembled zirconia nanostructured thin film functionalized with Acetylcholinesterase, suitable for biosensing application in the field of environmental monitoring. The proof of concept to demonstrate the feasibility of the platform was to electrochemically detect TCh generated from the enzymatic reaction using AChE immobilized onto the nanostructured material, with a low limit of detection.

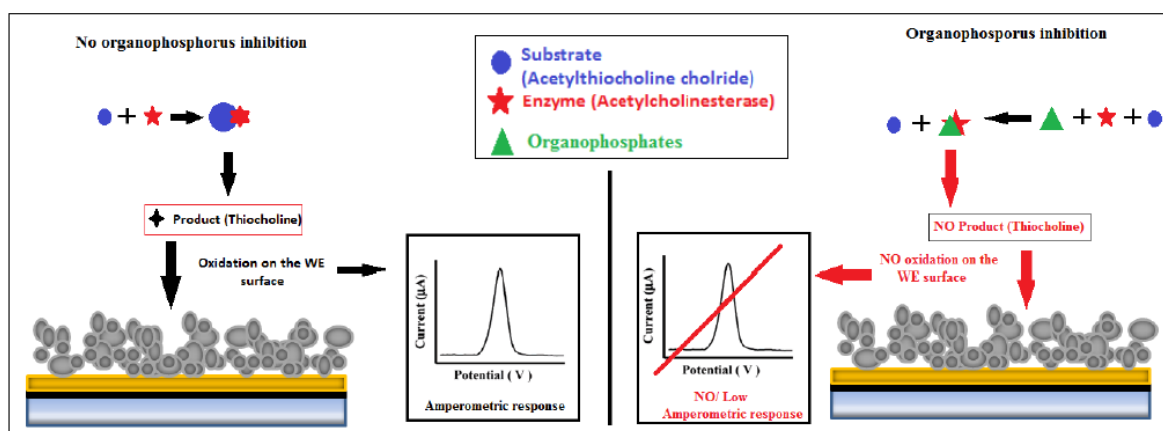


**Fig.5.** - Concept of OPs enzymatic electrochemical detection using immobilized AChE as biocatalyst for synthetically produced TCh

# 2

## Materials and methods

In this chapter, the materials and methods used for the development of the PhD study will be presented, along with a short theoretical overview for the background of the used techniques.

### 2.1 Electron beam evaporation

Electron beam (or E-beam) evaporation is a form of physical vapor deposition (PVD), technique which can be used to evaporate materials that cannot be processed through normal thermal evaporation. The working principle of an E-beam evaporator is based on generating an electron beam when an electrical current is applied to a tungsten filament. The electrons produced from the filament are then focused by magnets so they can reach the crucible which contains the material that needs to be evaporated. This process takes place in high vacuum chambers and it represents an ideal method for evaporating materials with high melting points like gold or titanium. Unlike other evaporation techniques, the E-beam evaporation heats only the material of interest and not the entire crucible, reducing therefore the risks of sample contamination and also reducing the possible damages of the substrate due to overheating [82], [83].

## **Experimental**

For the production of the modified electrodes, borosilicate glass coverslips with a diameter of 24 mm have been previously cleaned with ethanol under ultrasonication for 15 minutes, rinsed with deionized water and then dried with nitrogen flow. After cleaning they were placed in a sample holder and put in the e-beam evaporator. Once the pressure inside the deposition chamber was brought to  $6.0 \times 10^{-6}$  mbar and the beam was set at a voltage of 6kV, a flat thin film (15 nm thickness) of titanium was deposited while keeping a current value of 100 mA and a material deposition rate of  $0.2 \text{ \AA}/\text{sec}$ . After reaching the desired film thickness, the beam was turned off and the titanium crucible was replaced with the one containing gold. For the evaporation of the gold thin film (160nm thickness), the beam was turned back on and the voltage was set to 8 kV. The current used for the evaporation process was set at 320 mA and the deposition rate was kept at  $0.2 \text{ \AA}/\text{sec}$ .

### **2.2 Supersonic cluster beam deposition technique**

The cluster-assembled  $\text{ZrO}_2$  nanostructured thin films were produced with the Supersonic Cluster Beam Deposition (SCBD) technique. The process takes place under high vacuum conditions and it implies the production of a supersonic seeded beam of  $\text{ZrO}_2$  by a pulsed microplasma cluster source (PMCS). A schematic representation of the apparatus can be seen in **Fig. 6 A and B**.

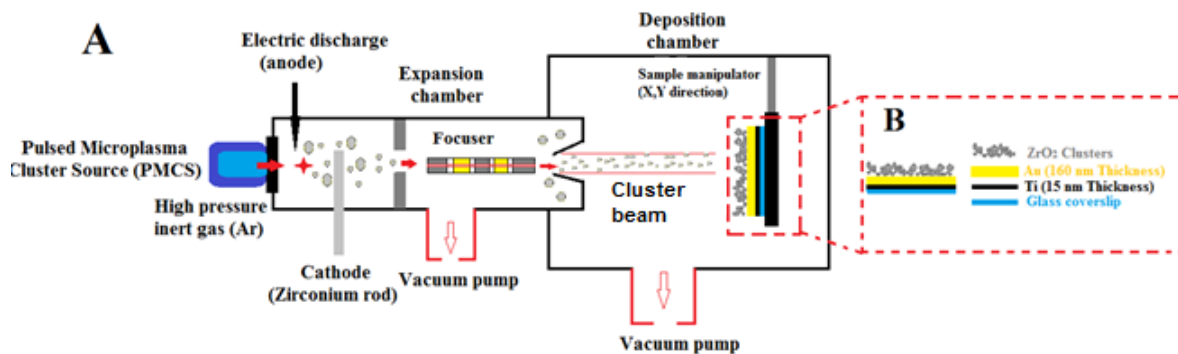


**Fig. 6 A-** Schematic representation of the SCBD apparatus (adapted with permission [84])

**B -** Schematic representation of the elements used for the development of the modified electrodes

The SCBD apparatus consists of two differentially pumped vacuum chambers, the first chamber called the ‘expansion chamber’ and the second one, the ‘deposition chamber’, which are separated by a gate. The cluster source (PMCS) is located in the expansion chamber and it consists of a ceramic hollow body in which an inert gas is introduced (Ar or He) through a pulsed valve (the pulse duration of the valve is of the order of hundreds of microseconds, at a pressure of 40 bar, and a repetition rate from 2 to 4 Hz). In the ceramic body there is also a rotating target that represents the cathode (for this study we are using a zirconium rod). When there is a high voltage applied between the cathode and the anode (850 V), the zirconium rod is sputtered and the vapor condenses into clusters which will be then extracted from the source through an expansion nozzle. A schematic representation of the PMCS can be observed in **Fig. 7**.

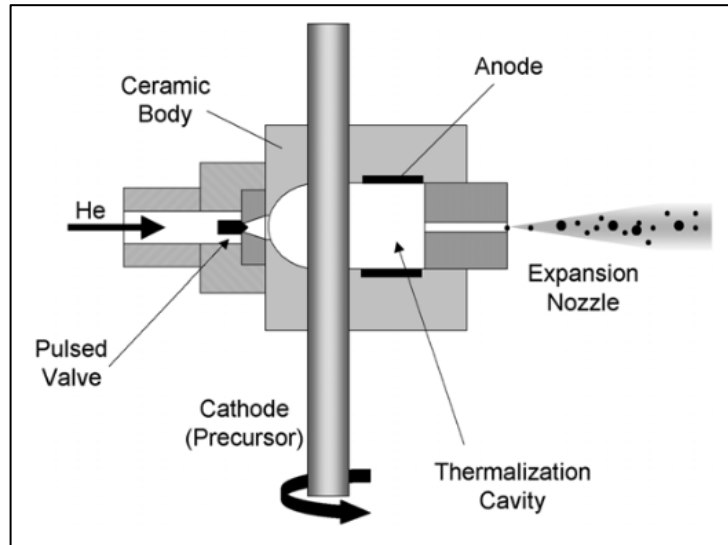


**Fig.7.** – Schematic representation of the pulsed microplasma cluster source (PMCS) [85]

The use of SCBD technique for the production of cluster assembled nanostructures allows a very good control of the cluster mass distribution and of the kinetic energy and it is possible to obtain high deposition rates [86] and well collimated beams [87]. The surface morphology characteristics such as roughness of the deposited thin films can be well controlled by adjusting the thickness of the deposited material since these two parameters are correlated by the calibration curve as shown in **Fig. 8**.

Surface morphology characteristics of the deposited thin films can be tuned depending on the application requirements, by adjusting the deposition rate, the distance between the exit point of the seeded beam and the substrate onto which we are making the deposition or the type of gas that is used [84].

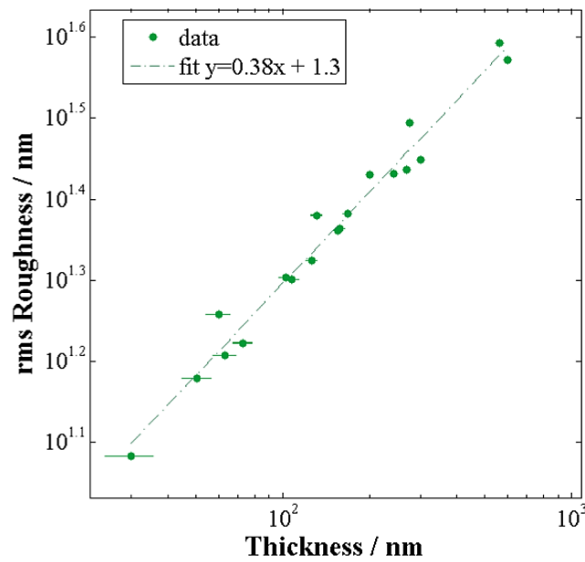


**Fig. 8** – Roughness Vs Thickness calibration curve- Log-log plot of the evolution of roughness of cluster-assembled ZrO<sub>2</sub> nanostructured thin film with thickness at room temperature and the corresponding linear fit [88]

## 2.3 Surface morphology characterization of nanostructured zirconia- Atomic Force Microscopy analysis

Atomic force microscopy (AFM) is a type of Scanning Probe Microscopy, derived from the Scanning Tunneling Microscopy (STM), when researches tried to develop a technique that was able to investigate electrically non-conductive materials like proteins [89], [90]. AFM is a high resolution scanning probe tool that helps obtaining direct images of material surfaces but can also give details regarding film roughness. In **Fig. 9** a schematic representation of the operation principle of the AFM can be observed.

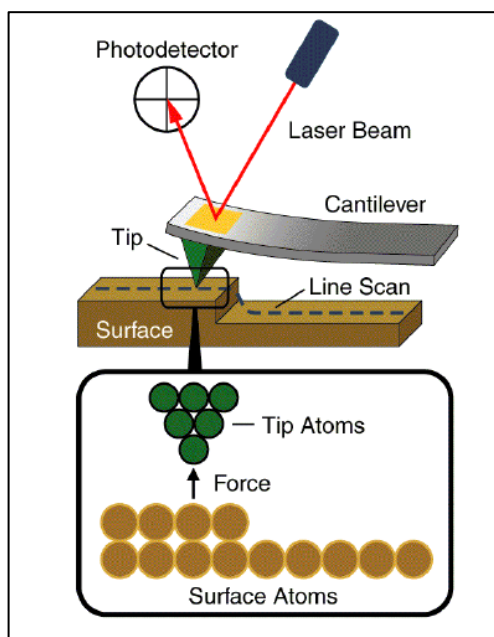


**Fig. 9**– Schematic representation of the operating principle of the AFM [91]

A very small sharp probe (nm size) is situated at one end of an elastic cantilever and scans an area of the surface of the sample. During the scanning process, the tip moves a few hundred Angstroms and a deflection of the laser aligned onto the cantilever is recorded at every interaction between the tip and the surface. There are two main operating modes of the AFM, contact or tapping mode. In the contact mode the tip has a physical contact with the surface of the sample, contact that causes the bending of the cantilever and the deflection can be measured. In the tapping mode, an oscillation of the cantilever is measured when the tip comes near the sample's surface. Unlike the contact mode, the tapping mode provides a higher resolution and the sample damaging can be kept to a minimum.

## **Experimental**

To characterize the surface morphology of the modified electrodes, a Multimode AFM equipped with a Nanoscope III Controller (Veeco Instruments) was used. The mode of

operating was tapping mode by using single crystal silicon tips (5-10 nm size) and the cantilever resonance was kept in the range of 200-300 kHz. The surface was characterized for areas of 2  $\mu\text{m}$  x 1  $\mu\text{m}$ , the scan rates were kept in the range of 1.5-2 Hz for each sample and the sampling resolution was 2048 x 512. For each sample three images were acquired and then processed using MATLAB<sup>®</sup> program [92]. During processing, the images have been flattened by line-by-line subtraction of the first and second order polynomials for artifacts removal due to sample tilt and scanner bow. From the AFM images, root-mean-square surface roughness (Rq) was calculated according to **Eq. 1**:

$$\boxed{Rq = \sqrt{\frac{1}{N} \sum_{i,j} (h_{ij} - \bar{h})^2}} \quad \text{Eq.1}$$

Where  $h_{ij}$  are the height values in the topographic map, N is the number of pixels and  $\bar{h}$  is the average height.

For all types of the modified electrodes as well as the bare Au samples, specific area, thickness and roughness characteristics were determined.

## 2.4 Electrochemical characterization of the modified transducers

Electrochemical assessments are usually performed in electrochemical cells with three electrodes setup, working electrode (WE), reference electrode (RE) and counter or auxiliary electrode (CE). The CE has the role of closing the current circuit in the electrochemical cell and it is usually made out of inert materials like platinum, gold or glassy carbon and it is not involved in the electrochemical reaction. Normally, the size of the CE must be 10 times larger than the size of the WE so the kinetics of the reaction will not be limited. The RE is the electrode with a stable and well-known potential and it is used as a point of reference in the electrochemical cell. With the help of the CE, the current flow

through the RE is kept close to zero. For the aqueous standard RE, hydrogen, saturated calomel or silver chloride is used. The WE is the electrode at which the reaction of interest takes place [93]. The common materials from which the WE are made of are inert materials such as gold, silver, platinum or glassy carbon. In **Fig.10** a schematic representation of a general three-electrode electrochemical cell can be observed.

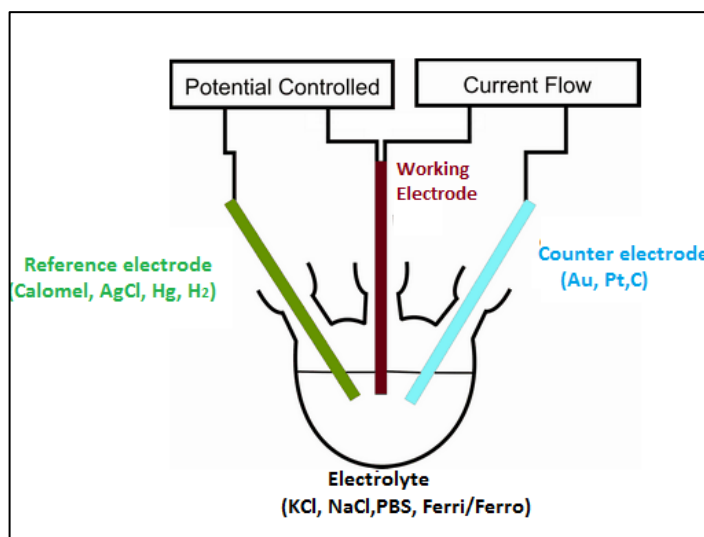


**Fig.10-** Schematic representation of a three-electrode electrochemical cell setup [94]

There are two main methods to determine the electrochemical behavior of electrodes, Cyclic Voltammetry and Electrochemical Impedance Spectroscopy.

*Cyclic Voltammetry (CV)* is a potentiometric electrochemical technique and it is the most commonly used method to study electroactive species. It is usually the first form of electroanalysis performed by researchers when it comes to studies regarding compounds, biological materials or electrodes surface [95]. When performing a CV measurement, the current at the working electrode is measured while the potential is controlled versus a RE. The potential applied to the WE is scanned linearly from a chosen starting point to a predetermined limit (interval known as ‘scan range’) and the current response is plotted as a function of potential. **Fig. 11** shows a typical cyclic voltammogram for a redox reaction.

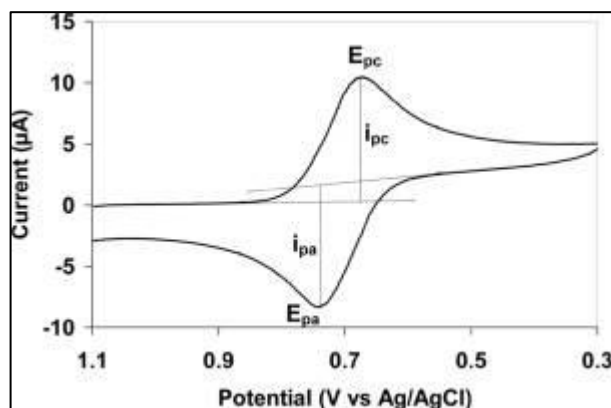


**Fig. 11** – Cyclic voltammogram of a single electron oxidation-reduction reaction [95]

When interpreting a cyclic voltammogram, the parameters of interest are:

**E<sub>pc</sub>** - the cathodic peak potential at which the oxidation of the electroactive species takes place

**I<sub>pc</sub>** - the cathodic peak current of the oxidation process

**E<sub>pa</sub>** - the anodic peak potential at which the reduction of the electroactive species takes place

**I<sub>pa</sub>** - the anodic peak current for the reduction process

Once these parameters are determined, the reversibility of the process can be evaluated. For this, the peak potential separation at all scan rates is calculated according to the **Eq. 2**.

$$\Delta E_p = (E_{pc} - E_{pa}) = 59.2/n \text{ mV} \quad \text{Eq. 2}$$

where n represents the number of electrons transferred

Another parameter to be determined is the current peak ratios according to the **Eq. 3**

$$I_{pa}/I_{pc} = 1 \quad \text{Eq. 3}$$

The last parameter to be determined is the dependence of the current peaks to different scan rates. For this, CVs in the presence of the same concentration of the electroactive species are submitted to different scan rates and the current peaks are measured. In a normal reversible reaction the current peaks should decrease linearly with the decrease of the scan rate.

The second electrochemical method used for characterizing the electrochemical behavior of working electrodes in the presence of the chosen electroactive species is *Electrochemical Impedance Spectroscopy (EIS)*. This electrochemical method represents a very complex, accurate and non-destructive mean of analyzing complex electrochemical resistances of a system and when it is used for biosensing it provides important information regarding the binding events on the transducer surface [96].

The principle behind this method is based on Ohm's law and it consists of measuring the response of a WE to a sinusoidal potential modulation at different frequencies (**Eq. 4**). These modulations can be superimposed either to an applied cathodic or anodic potential, where the reaction of interest takes place, or to an open circuit potential.

$$E= I Z \quad \text{Eq. 4}$$

**Where**    **E**= Potential

**I**= Current

**Z** =Impedance

There are two formats of evaluating the data obtained with EIS. The first one is by using the Nyquist plot, where the imaginary impedance component ( $Z''$ ) can be plotted against the real impedance component ( $Z'$ ). With the Nyquist plot it is possible to obtain information regarding the solution resistance ( $R_s$ ), Ohmic resistance and estimation of the

circuit components involved in the electrochemical process. Although some of the circuit's elements are easy to read from the Nyquist plot, it doesn't give information regarding the electrode capacitance. The frequency information necessary for the double layer capacitance ( $C_{dl}$ ) can be read with the help of the second format, the Bode plot. With the Bode plot, we are able to plot  $|Z(\omega)|$  and phase shift ( $\phi$ ) versus frequency ( $\log \omega$ ) [97].

With all the combined information obtained from the Nyquist and the Bode plots, it is possible to obtain an equivalent electrical circuit model form which we can determine all the resistance and capacitance components encountered in the circuit of interest.

## **Experimental**

The electrochemical assessments have been carried out using a Reference 600 potentiostat/galvanostat purchased from Gamry Instruments Inc. Both CV and EIS characterizations have been performed in a three- electrode electrochemical cell setting. The electrochemical cell used was a "home-made" Teflon cylindrical cell, with a working volume capacity of maximum 500  $\mu\text{L}$  and a diameter of 0.6 cm. As RE a "home-made" Ag/AgCl [98] quasi reference electrode has been used and a Pt wire was used as a CE.

"Quasi" reference electrodes have been produced by an electrodeposition of Ag/AgCl onto a gold wire according to the protocol described in [98]. After production, the "quasi" RE was calibrated by using a commercial Ag/AgCl RE confined in a saturated potassium chloride solution (KCl), as followed: three separate beakers containing 0.35 M, 0.7 M and 3.5 M KCl solution were prepared. The commercial and the "quasi" REs were connected to a digital multimeter and dipped into each beaker starting from the most concentrated KCl solution and the potential difference was registered. The obtained potential differences were plotted against the logarithm of the concentration and from the slope of the linear fit a potential close to 59 mV was obtained. By using 'pseudo' REs that can be directly

immersed into the electrolyte solution, the effect of the Ohmic resistance is small, the liquid junction potential is inexistent and the test solution will not be contaminated by the solvent molecules that can be in a conventional RE. The obtained “quasi” RE was kept in a saturated KCl solution between experiments and its quality was tested before every usage.

After producing the “quasi” REs, the electrochemical characterization of the ns-ZrO<sub>2</sub> modified electrodes has been performed. The experiments have been performed in 0.1 M PBS (pH=7.5) and afterwards in different concentrations of potassium ferrocyanide/ferricyanide (Fe<sup>3+</sup>/Fe<sup>2+</sup>). For CV measurements, a scan rate of 50 mV/s was set for a range between -0.5 V to +0.5 V. For the square root of the scan rate measurements, rates of 20 mV/s, 50 mV/s and 100 mV/s were chosen.

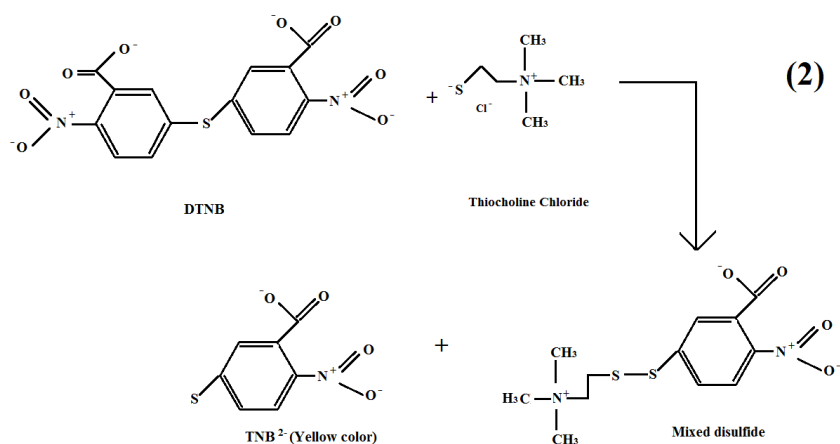
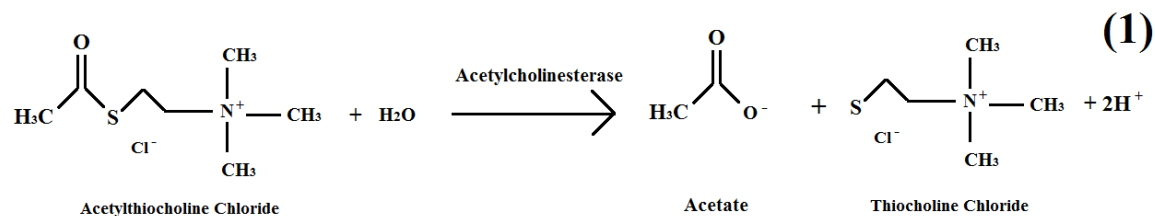
The EIS measurements were also performed in the presence and absence of the electroactive species Fe<sup>3+</sup>/Fe<sup>2+</sup> in 0.1 M PBS (pH=7.5) over a frequency range of 500 KHz to 100 mHz.

Data analysis of the obtained results was obtained using the Gamry Analyst program.

## **2.5. Enzymatic production of thiocholine**

Acetylcholinesterase enzyme helps catalyzing the hydrolysis of acetylcholine into two compounds, choline and acetic acid [54]. Since choline is not an electroactive species and it can't be detected through electrochemical techniques, Acetylthiocholine (ATCh), an artificial analogue of acetylcholine, can be used a substrate to generate TCh which is an electroactive compound (**Scheme 1**) [99]. The synthetically produced TCh and the enzymatic activity can be assessed spectrophotometrically at 412 nm wave length, using the Ellman's method. Basically, the thiol groups in the thiocholine react with the Ellman's

reagent (DTNB) and form TNB (5-thio-2- nitrobenzoate) (**Scheme 2**), a yellow compound that can be read with the spectrophotometer [100].



## Experimental

Since TCh is not commercially available, it was produced daily by enzymatic means. For this, 1 mL of 0.5 M of ATCl was prepared in a phosphate buffer solution 0.1 M with a pH=8. To this solution, 10 U of AchE were added and the mixture was left to incubate for 2 hours. After incubation, the concentration of the obtained TCh was assessed spectrophotometrically with Ellman's method. For this, 2.7 mL of PBS (0.1 M, pH=8) were added in a cuvette along with 300  $\mu\text{L}$  of DTNB solution of 0.1 M and 15  $\mu\text{L}$  of TCh (after it was diluted 1:100 from the stock solution). The obtained enzymatic product was assessed spectrophotometrically at a wave length of 412 nm and the absorbance was measured at different times. From the absorbance values obtained, the real concentration of TCh was evaluated using the Lambert-Beer law with the known molar extinction coefficient of TNB

( $\epsilon=13,600 \text{ M}^{-1} \text{ cm}^{-1}$ ). Therefore, we obtained 1mL of TCh solution of 0.5 M. The TCh stock solution was used only for 24 hours and it was kept at 4°C.

## 2.6. Amperometric detection of Thiocholine

Chronoamperometry (CA) is an amperometric method in which a potential step is applied to the working electrode and the obtained current is measured versus time. CA is suitable for the study of the kinetics of a chemical reaction, adsorption or diffusion processes. In the case of enzymatic products, the information obtained with CA can be used to determine the limit of detection (LOD) of a sensor. The LOD of a biosensor is represented by the lowest quantity of the analyte that can be detected from a blank value within a confidence limit [101]. This value can be determined by using the formula:

$$\text{LOD} = (k * \text{sb}) / m$$

Where: **k** corresponds to the value of confidence level and is chosen to be 2 for a level of confidence above 90% or 3 for a confidence level above 98%

**sb** is the standard deviation of the blank

**m** is the calibration sensitivity

## Experimental

Before the electrochemical detection of TCh, the electrochemical influence of two types of substrate has been tested. For this Acetylthiocholine Chloride (ATChCl) and Acetylthiocholine Iodide (ATChI) substrates have been used in a concentration of 0.5 M in a PBS solution of 0.1 M (pH=7.5). The influence of these substrates has been assessed by CV means and the appropriate substrate was chosen for the enzymatic production of TCh.

For the amperometric detection of TCh 3 electrochemical methods have been used.

The first electrochemical method used was CV and its main purpose was to determine the potential at which the oxidation of TCh takes place. For this, CVs were taken at a 50 mV/s scan rate, with a scanning interval between of 0.2 to 0.9 V. CVs were performed first in a simple PBS solution of 0.1 M (pH=8) and afterwards different concentrations of TCh were added in order to determine the oxidation potential.

Secondly, EIS measurements were performed using a fixed potential obtained from the CV assessment, in PBS solution (0.1 M, pH=8) in the presence of 4 different TCh concentrations in order to determine the double layer capacitance ( $C_{dl}$ ) and charge transfer resistance ( $R_{ct}$ ) values. The information obtained with EIS was processed using Gamry Analyst and the  $C_{dl}$  and  $R_{ct}$  values were obtained after finding an appropriate model fit for the equivalent electric circuit.

The amperometric detection of TCh was performed using chronoamperometry (CA). For this, the potential found for the anodic oxidation of TCh was set during the entire measurement, and after equilibrium was reached with simple 0.1 M PBS solution, different TCh concentration were added to the electrochemical cell, while maintaining a continuous stir of the solution. The current steps were recorded and the peaks for each concentration were plotted together in a graph. From the slope of the obtained curve we were able to calculate the limit of detection (LOD) of our system.

# 3

## Results and Discussion

In the third chapter, the results obtained for this PhD study will be presented. This chapter will be divided into three sections. The first section will be assigned to the morphological and electrochemical characterization of the first generation of ns-ZrO<sub>2</sub> modified electrodes, the second section will be represented by the morphological and electrochemical characterization of the second generation of ns-ZrO<sub>2</sub> modified electrodes and the third section will contain the results obtained from the electrochemical detection of TCh using the second generation of ns-ZrO<sub>2</sub> modified electrodes.

### 3.1. Nanostructured Zirconia

By using SCBD, the gold electrodes were modified with cluster assembled  $\text{ZrO}_2$  nanostructured thin films as described in Section 2.2. For the morphological characterization and the electrochemical behavior assessments two generations of electrodes have been used. For the preliminary morphological and electrochemical studies, modified electrodes with ns- $\text{ZrO}_2$  thicknesses ranging from 50 nm to 200 nm have been used. After completing the preliminary studies, the second generation of modified electrodes with tailored surface morphology characteristics has been produced and the thickness of ns- $\text{ZrO}_2$  thin films ranged between 30 nm and 100 nm.

#### 3.1.1. Morphological characterization of first generation of modified electrodes

Since the thickness of the ns- $\text{ZrO}_2$  thin films plays an important role in the electrochemical behavior of the modified transducers and the surface roughness has been shown to influence the immobilization process of the biological materials, AFM morphological characterization has been performed on all the types of the modified transducers. From the topographical maps presented in **Fig. 12 A-C** as well as the data presented in **Tab 1**, an increase in thickness and roughness can be seen for the samples containing ns- $\text{ZrO}_2$ . Also it is noticeable that when the thickness of the ns- $\text{ZrO}_2$  layer increases, the roughness of the surface increases proportionally.

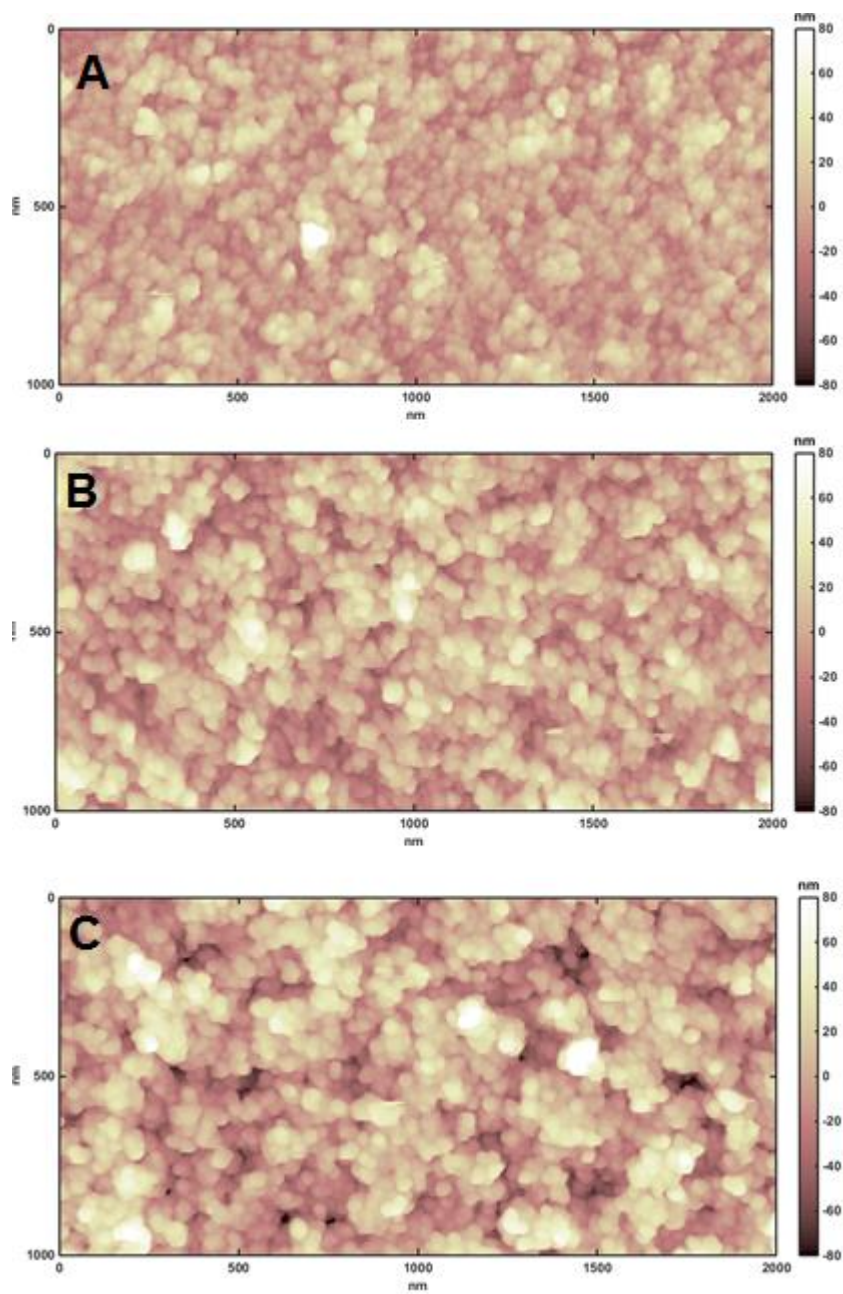


**Fig.12** – AFM analysis of nanostructured ZrO<sub>2</sub> surfaces with increased level of thickness;  
**A-C:** AFM topographic maps of the modified electrodes showing uniform evolution in the surface morphology with increasing film thickness;

Type of sample	Thickness (nm)	Roughness (nm)
NS1	50 ±6	15 ± 0.3
NS2	95 ±7	20 ±06
NS3	210 ± 11	27 ± 1.0

**Table 1.** - Thickness and morphology assessment values performed by tapping-mode AFM on cluster-assembled ZrO<sub>2</sub> nanostructured thin films grown by means of SCBD

### 3.1.2. Electrochemical assessments preparation- “Quasi” Reference electrode production

The calibration curve obtained for the “quasi” reference electrode with the help of a commercial Ag/AgCl RE can be observed in **Fig. 13**. From the linear fit of the obtained calibration curve, the potential of the “quasi” RE can be determined. The quality of the RE can be easily tested before every usage, eyesight by noticing changes in the AgCl layer and also with the help of the multimeter by assessing changes in potential differences.

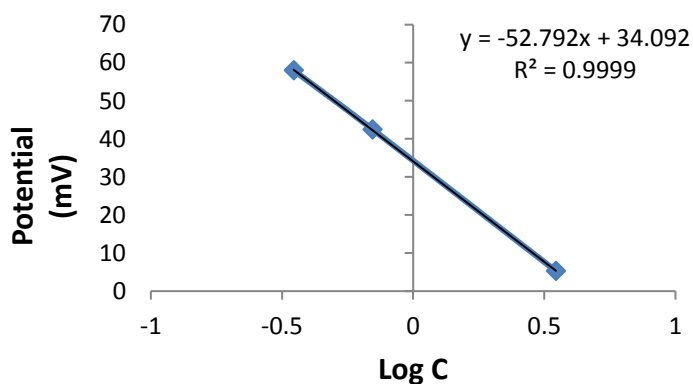


**Fig. 13-** Calibration curve of the “Quasi” RE in KCl solution of difference concentrations

### 3.1.3. Electrochemical behavior of first generation of the modified electrodes – Cyclic Voltammetry study

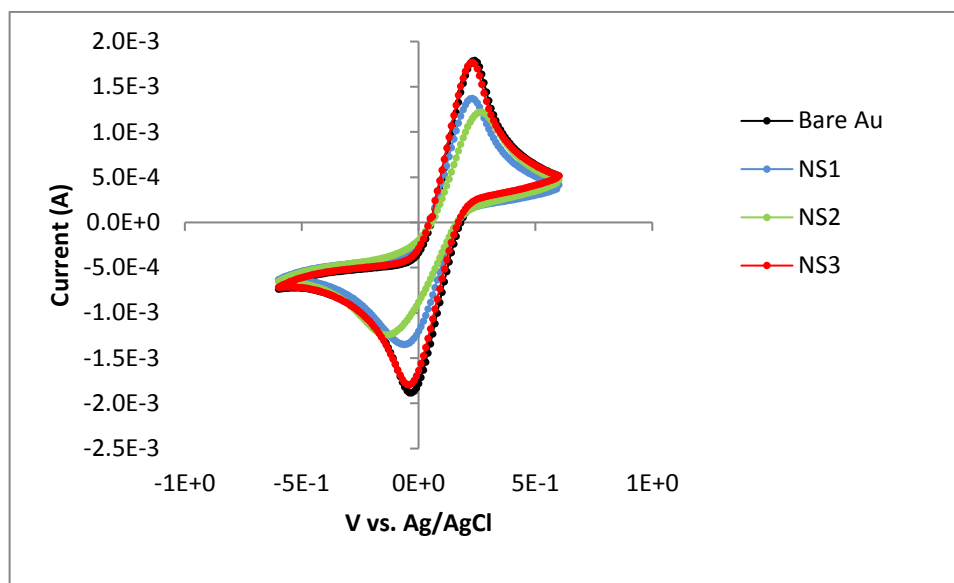


**Fig.14.** - Cyclic voltammograms for all types of ns-ZrO<sub>2</sub> modified working electrodes compared to the bare Au (Control) in the presence of 10 mM Fe<sup>3+</sup>/Fe<sup>2+</sup> and 0.1 M PBS (pH=7.5) at a scan rate of 50 mV/s

Type of sample	I <sub>pa</sub> (mA)	I <sub>pc</sub> (mA)	ΔE <sub>p</sub> (mV)
Bare Au	-1.88	1.8	270
NS 1	-1.34	1.37	290
NS 2	-1.24	1.22	290
NS 3	-1.8	1.76	270

**Table 2-** CV data of anodic and cathodic current peaks as well as the peak-to-peak separation for all types of ns-ZrO<sub>2</sub> modified working electrodes compared to the bare Au

CV study data presented in **Fig. 14.** and **Table 2.** show that by depositing ns-ZrO<sub>2</sub> in various thicknesses onto the thin film of Au, the electrochemical behavior of the electrodes is maintained. This fact is due to the increased surface area offered by the deposited ns-

ZrO<sub>2</sub>, thus we are able to obtain an increased electron transfer process, comparable to bare Au electrodes.

### 3.1.4. Electrochemical behavior of first generation of the modified electrodes – Electrochemical impedance spectroscopy study

EIS assays performed in the presence of a commercial electrolyte have been used for the electrochemical behavior characterization in terms of charge transfer resistance and double layer capacitance of the modified electrodes compared to control samples (**Fig. 15**).

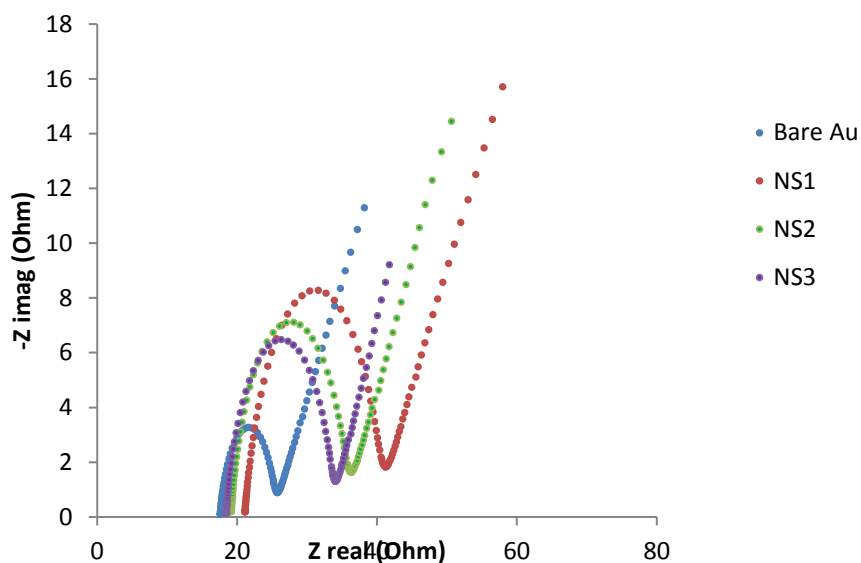


**Fig.15.** - Nyquist plot of the commercial electrolyte (10 mM Fe<sup>3+</sup>/Fe<sup>2+</sup> and 0.1 M PBS pH=7.5) at the surface of the modified electrodes compared to bare Au sample at open potential circuit

The impedance data obtained has been fitted by using a Randles circuit model (**Fig. 16**) and R<sub>ct</sub> and C<sub>dl</sub> values have been determined (**Table 3**). Within the Randles circuit, a constant phase element (CPE) has been used as the equivalent for the double layer capacitance.

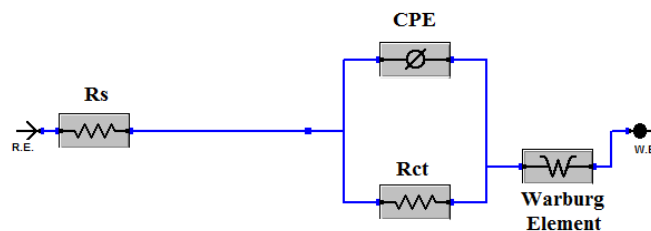


**Fig.16.** - Representation of the Randles circuit model where  $R_s$  is the solution resistance,  $CPE$  is the constant phase element,  $R_{ct}$  is the charge transfer resistance and  $W$  is the Warburg element associated with the diffusion process at low frequencies

Type of sample	$R_s$ (Ohm)	$R_{ct}$ (Ohm)	$C_{dl}$ ( $\mu\text{F}/\text{cm}^2$ )
Bare Au	17.5	7.8	54
NS-1	21.1	19.24	30.5
NS-2	19.1	16.34	33
NS-3	18.42	14.93	43

**Table 3-** Charge transfer resistance, solution resistance and double layer capacitance values for the modified electrodes and bare Au sample in commercial electrolyte solution

Given the obtained results it can be noticed that the  $R_{ct}$  values for the modified electrodes are higher when compared to bare Au, reaction that is expected with the addition of ns-ZrO<sub>2</sub> thin films. When comparing only the modified electrodes it is noticeable that the resistance decreases once the ns-ZrO<sub>2</sub> layer increases. This phenomenon can be explained by the fact that the active surface area is increased and a faster electron transfer is sustained. On the other hand, once the ns-ZrO<sub>2</sub> layer is increased the modified electrodes are showing a behavior that is more capacitive, meaning that the diffusion process takes place longer.

### 3.2.1 Morphological characterization of second generation of the modified electrodes

Given the results obtained from the characterization of the first generation of the modified electrodes, it has been noticed that the thickness of the ns-ZrO<sub>2</sub> thin film layers does not influence in a negative manner the electrochemical behavior of the electrodes. Therefore, for the second generation of modified electrodes the surface morphology characteristics have been tailored in terms of thickness and roughness in order to develop an appropriate platform for the immobilization of AChE for electrochemical detection of TCh.

In **Table 4** as well as the data presented in **Fig. 17 A-D**. The topographical maps of the modified electrodes can be observed.

Type of sample	Thickness (nm)	Roughness (nm)
<b>Bare Au (Control)</b>	160±9	1±0.1
<b>NS 1</b>	35±7	9.1±0.1
<b>NS 2</b>	61±8	10.2±0.1
<b>NS 3</b>	100±10	11.3±0.1

**Table 4.** – Thickness and morphology assessment values performed by tapping-mode AFM on cluster-assembled ZrO<sub>2</sub> nanostructured thin films grown by means of SCBD

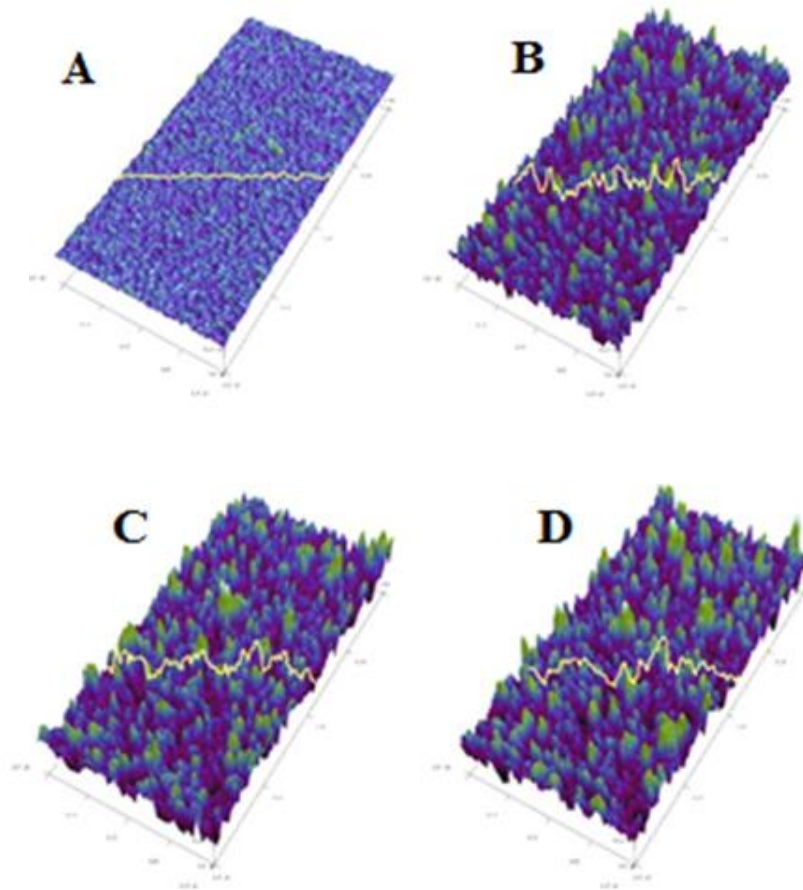


**Fig.17** – AFM analysis of nanostructured ZrO<sub>2</sub> surfaces with increased level of thickness; **B-D** : Three-dimensional visualization of AFM topography along with cross section profiles showing uniform evolution in the surface morphology with increasing film thickness; **A**- Surface topography of E- beam evaporated Au used as control

For the second generation of modified electrodes ns-ZrO<sub>2</sub> thin film thicknesses range from 30 nm to 100 nm and the roughness of the ns-ZrO<sub>2</sub> surface and the roughness of the surface has been tailored in a range comprised between 9 nm and 11 nm.

### 3.2.2. Electrochemical characterization of second generation of the modified electrodes- Cyclic voltammetry study

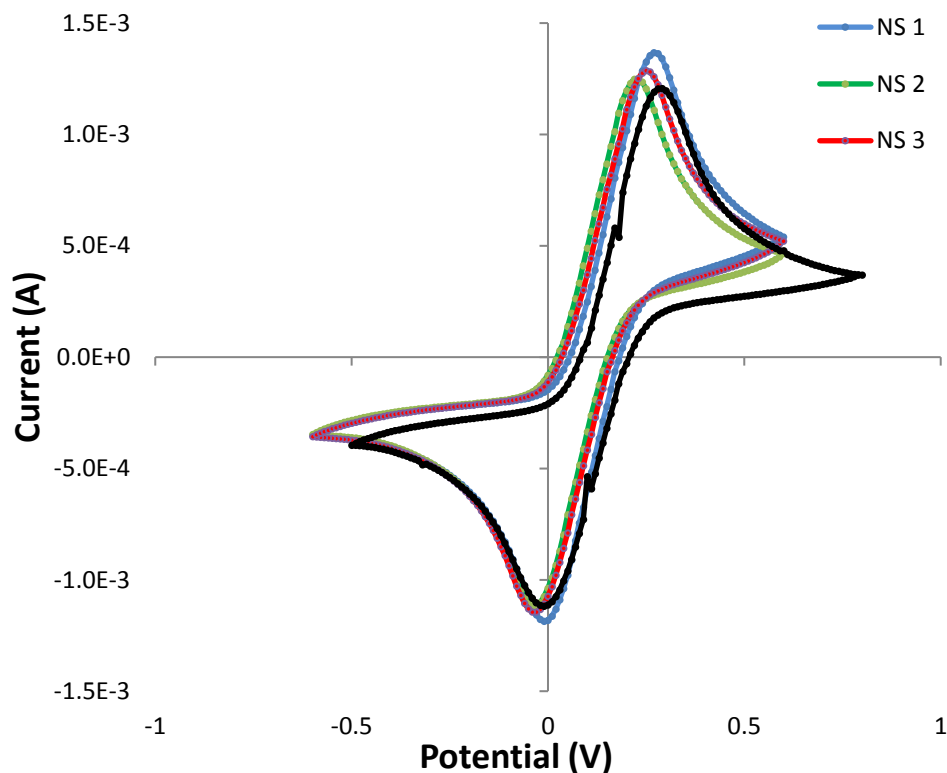


**Fig.18.** - Cyclic voltammograms for all types of ns-ZrO<sub>2</sub> modified working electrodes compared to the bare Au (Control) in the presence of 10 mM Fe<sup>3+</sup>/Fe<sup>2+</sup> and 0.1 M PBS (pH=7.5) at a scan rate of 50 mV/s

Type of sample	I <sub>pa</sub> (mA)	I <sub>pc</sub> (mA)	ΔE <sub>p</sub> (mV)
Bare Au	-1.1	1.2	270
NS 1	-1.2	1.4	280
NS 2	-1.1	1.25	270
NS 3	-1.15	1.3	280

**Table 5** - CV data of anodic and cathodic current peaks as well as the peak-to-peak separation for all types of ns-ZrO<sub>2</sub> modified working electrodes compared to the bare Au

In **Fig. 18** and **Table 5** the results of the CV studies performed for the second generation of modified electrodes are presented. The results obtained are comparable to the ones seen in the case of the first generation of electrodes and moreover it can be noticed that by decreasing the roughness of the ns-ZrO<sub>2</sub> thin film we can still obtain an electrochemical behavior compared to the bare Au electrodes.

The influence of the ns-ZrO<sub>2</sub> thin film layer on the electrochemical behavior of the modified WE has been further tested by calculating the square root of different scan rates in the presence of Fe<sup>3+</sup>/Fe<sup>2+</sup> electrolyte. The obtained results can be observed in **Fig.19-21**.

Analyzing the cyclic voltammograms for all 3 types of modified electrodes as well as the current vs. square root of the scan rate dependency, it can be observed that by increasing the scan rate, the anodic and cathodic current peaks increase linearly as well as the  $\Delta E_p$  values, as expected for a fast electron transfer process with diffusion regime. Also the ratio of the anodic and cathodic peak heights is close to 1 for all electrodes, indicating the reversible character of the redox process.

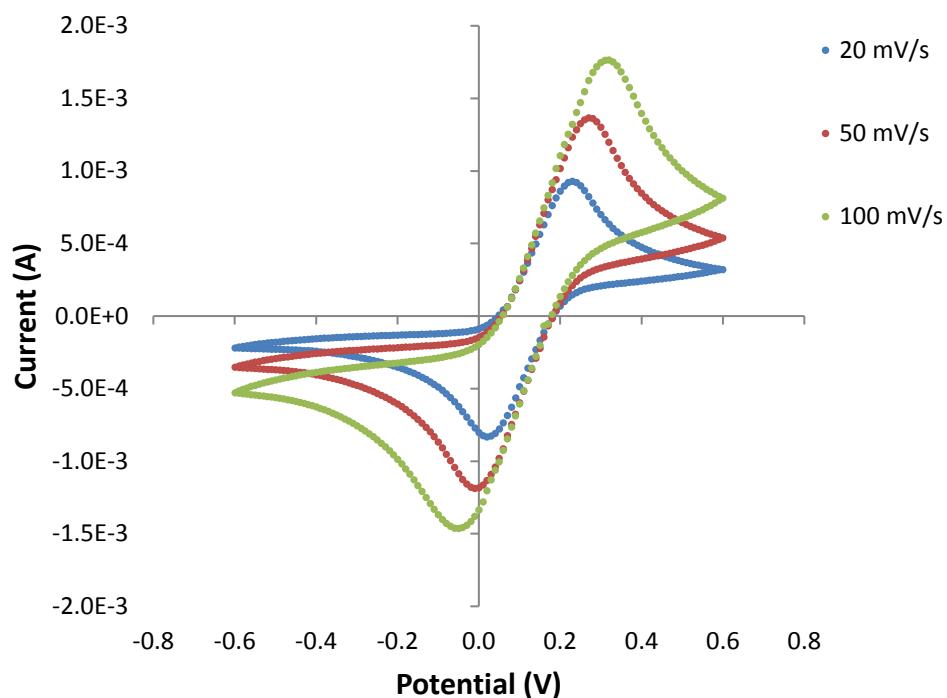


**Fig 19 a-** Cyclic voltammograms for NS-1 working electrodes performed in  $\text{Fe}^{3+}/\text{Fe}^{2+}$  at different scan rates (20 mV/s, 50 mV/s and 100 mV/s)

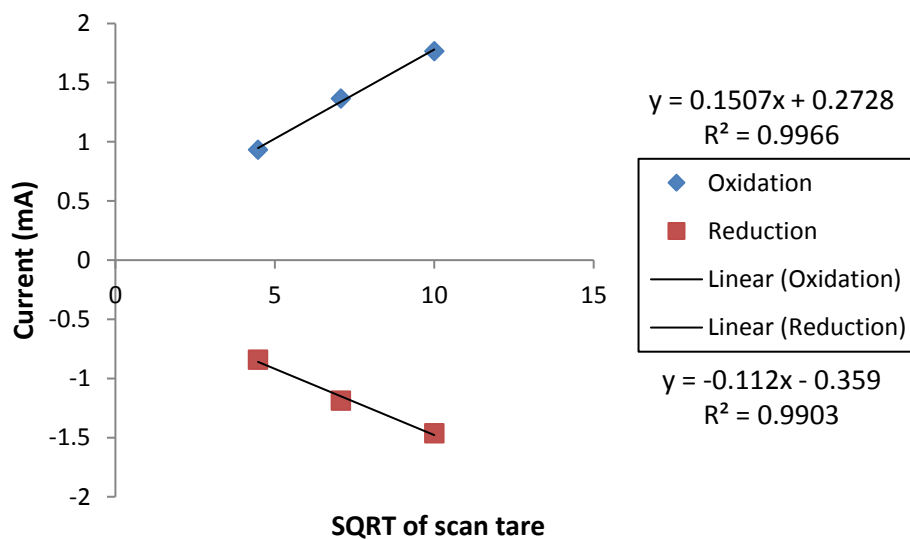


**Fig 19 b-** Variation of anodic and cathodic current peak with the square root of scan rate for the NS-1 working electrodes

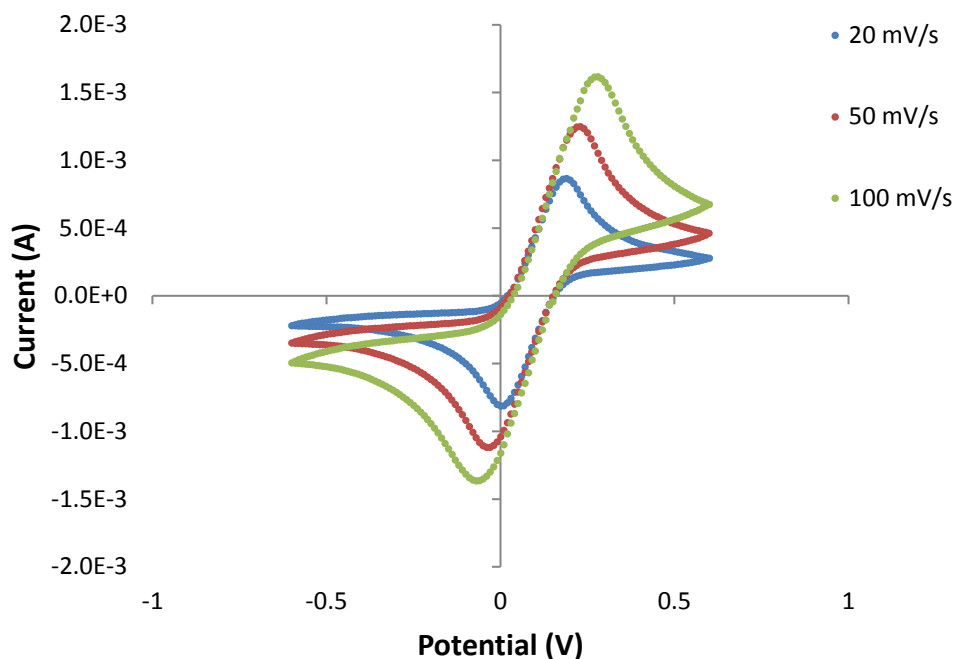


**Fig 20 a-** Cyclic voltammograms for NS-2 working electrodes performed in  $\text{Fe}^{3+}/\text{Fe}^{2+}$  at different scan rates (20 mV/s, 50 mV/s and 100 mV/s)

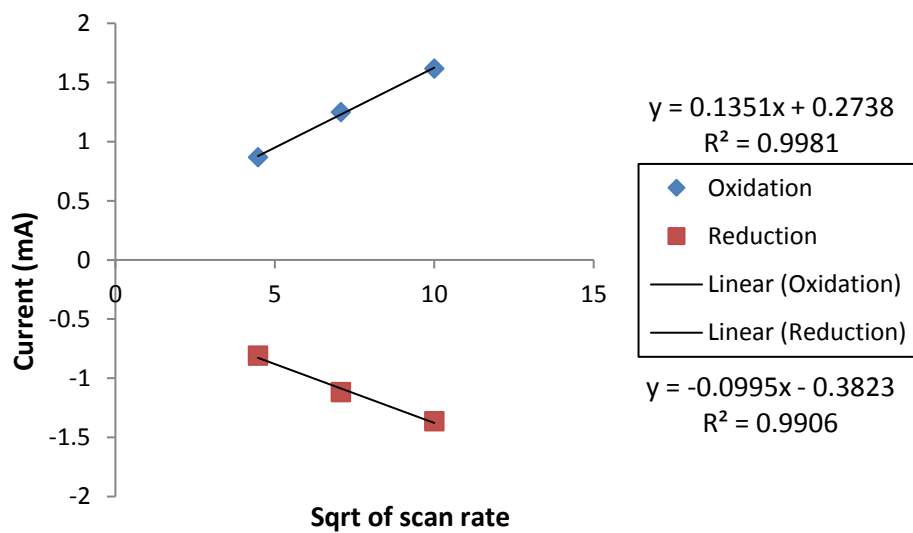


**Fig 20 b-** Variation of anodic and cathodic current peak with the square root of scan rate for the NS-2 working electrodes

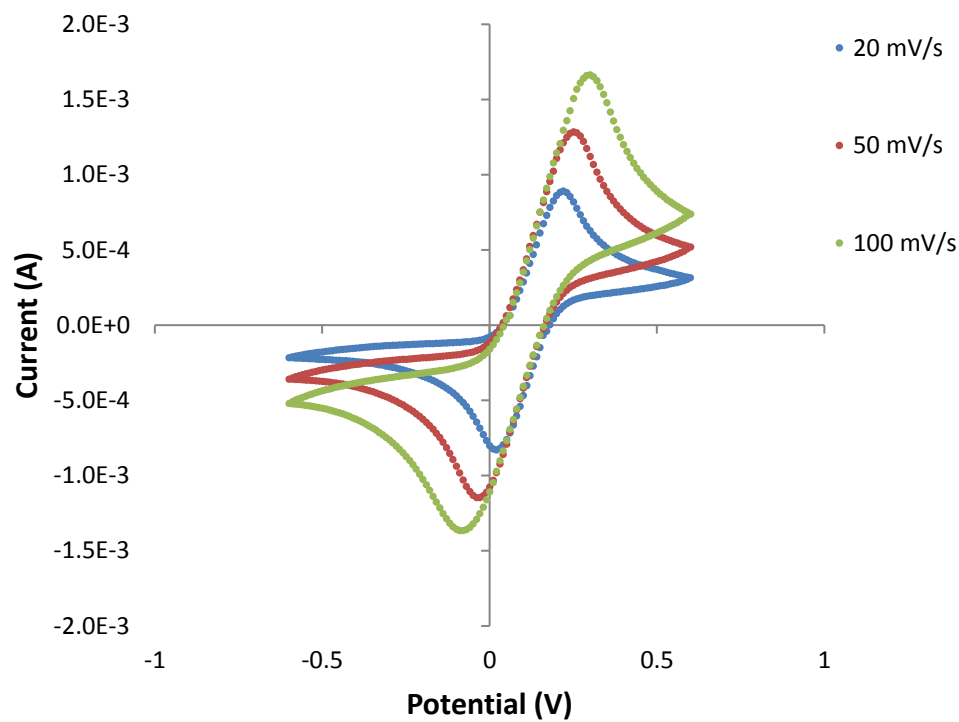


**Fig 21 a-** Cyclic voltammograms for NS-3 working electrodes performed in  $\text{Fe}^{3+}/\text{Fe}^{2+}$  at different scan rates (20 mV/s, 50 mV/s and 100 mV/s)

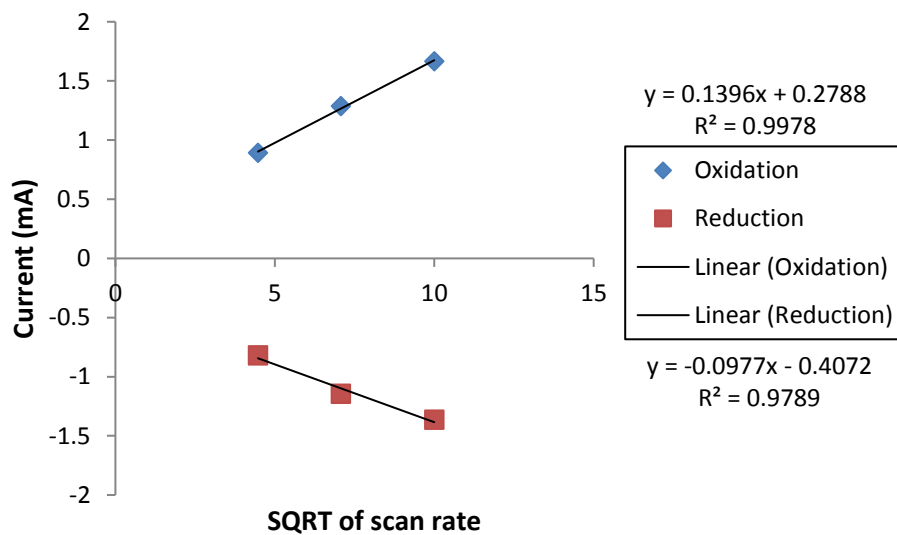


**Fig 21 b-** Variation of anodic and cathodic current peak with the square root of scan rate for the NS-3 working electrodes

### 3.2.3. Electrochemical characterization of second generation of the modified electrodes - Electrochemical impedance spectroscopy study

In **Fig. 22** and **Table 6** the solution resistance ( $R_s$ ) of PBS obtained by EIS assay at the surface of the modified electrodes can be observed. As expected,  $R_s$  values of the modified electrodes are higher compared to the one obtained with the bare Au electrode. This fact is due to the changes in the geometry of the modified electrodes, since it is known to be one of the influencing factors.

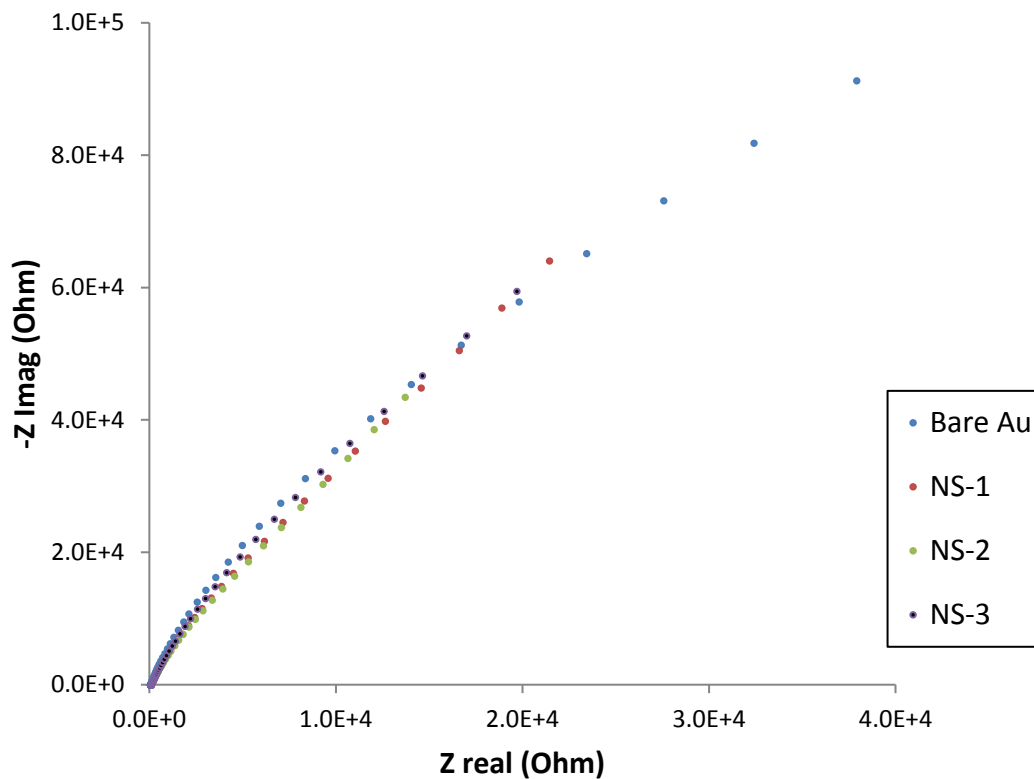


**Fig.22.** – Nyquist plot of PBS (0.1 M, pH= 7.5) at the surface of the modified transducers compared to bare Au electrodes

Type of sample	$R_s$ (Ohm)
Bare Au	60
NS-1	83
NS-2	83
NS-3	75

**Table 6.** - Solution resistance values for the modified electrodes and bare Au (Control) in PBS solution

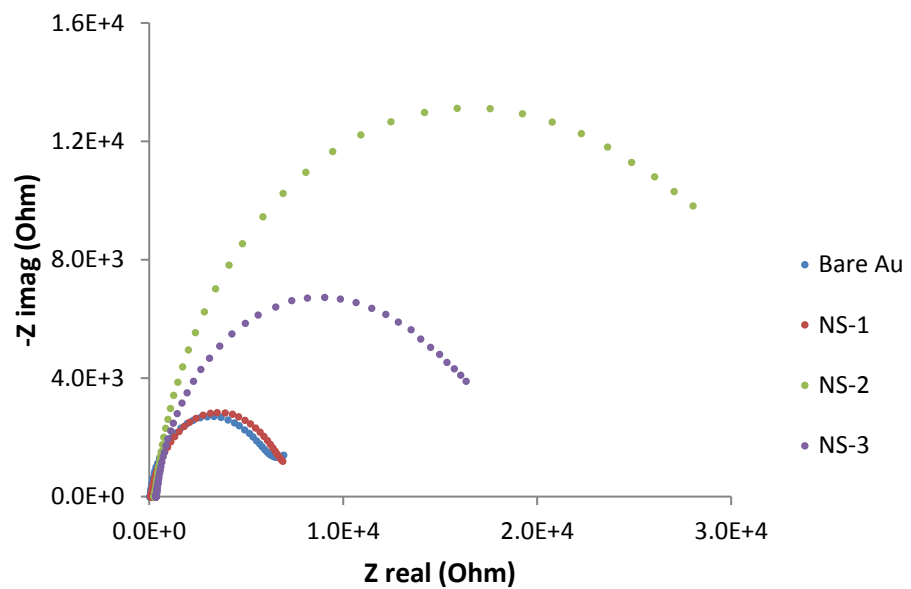


**Fig.23.** - Nyquist plot of the commercial electrolyte at the surface of the modified electrodes compared to bare Au sample at open potential circuit

EIS assays performed in the presence of a commercial electrolyte have been used for the electrochemical behavior characterization in terms of charge transfer resistance and double layer capacitance of the modified electrodes compared to control samples (**Fig. 23**).

The impedance data obtained has been fitted by using a Randles circuit model and  $R_{ct}$  and  $C_{dl}$  values have been determined (**Table 7**).

Type of sample	$R_{ct}$ (KOhm)	$C_{dl}$ ( $\mu\text{F}/\text{cm}^2$ )
Bare Au	5.5	12
NS-1	6.3	24
NS-2	32	15
NS-3	16	21

**Table 7-** Charge transfer resistance and double layer capacitance values for the modified electrodes and bare Au sample in commercial electrolyte solution

Analyzing the results obtained in terms of  $R_{ct}$  and  $C_{dl}$  of the modified electrodes we can observe that for the NS-1 and NS-3 the  $R_{ct}$  is lower, therefore indicating a faster electron transfer. On the other hand, the  $C_{dl}$  values for the same type of samples are doubled when compared to the bare Au samples which indicate a capacitive behavior of these types of modified electrodes. In the case of the modified electrodes NS-2 even though the electron transfer is much slower, the low  $C_{dl}$  values show that there is a diffusion process.

In **Fig. 24-27** and **Table 8-11** the electrochemical behavior of the modified electrodes in terms of charge transfer resistance and double layer capacitance in the presence of different concentrations of a commercial electrolyte at open potential circuit, is presented.

Analyzing the obtained data, it can be observed that by increasing the concentration of the electrolyte both  $R_{ct}$  and  $C_{dl}$  decrease for all the types of produced electrodes.

When a lower concentration of electrolyte is used, the electrochemical behavior of the modified electrodes maintains the same trend in characteristics as seen when higher concentrations are used.

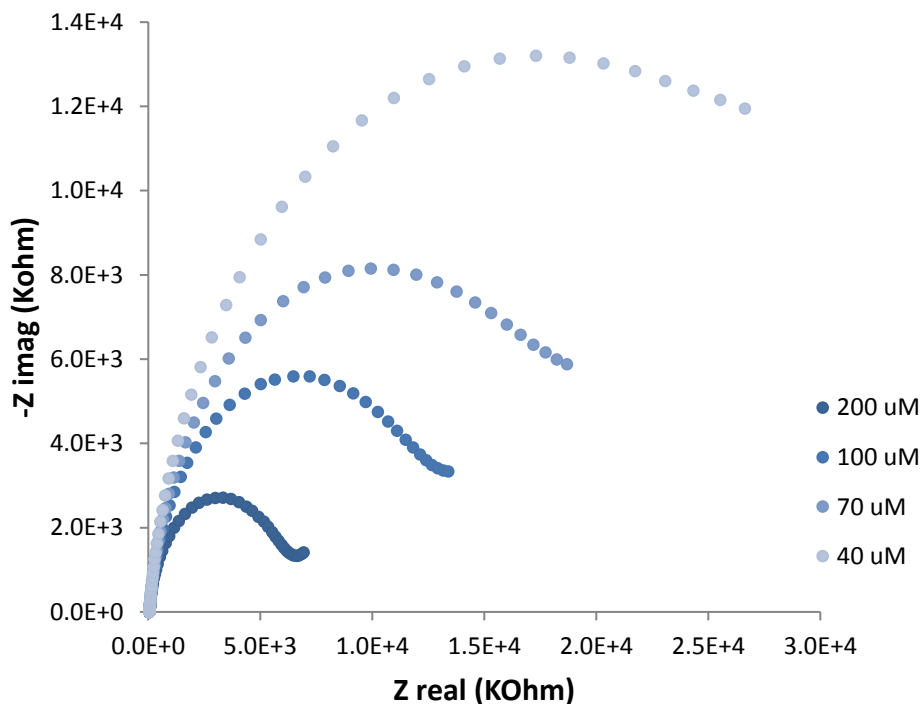


**Fig. 24-** Nyquist plot of different concentration of commercial electrolyte solution at the surface of bare Au electrode

Electrolyte concentration ( $\mu\text{M}$ )	$R_{ct}$ (KOhm)	$C_{dl}$ ( $\mu\text{F}/\text{cm}^2$ )
40	31	16
70	19	15
100	13	13.6
200	6	12

**Table 8. -** Charge transfer resistance and double layer capacitance values for the bare Au sample in commercial electrolyte solution with different concentrations

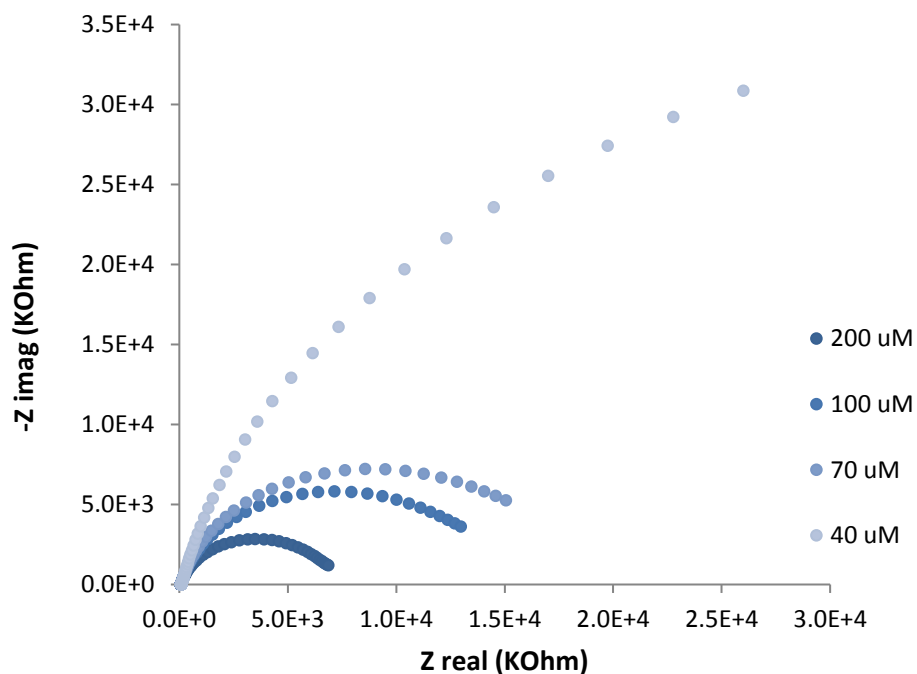


**Fig. 25-** Nyquist plot of different concentration of commercial electrolyte solution at the surface of NS-1 modified electrodes

Electrolyte concentration ( $\mu\text{M}$ )	$R_{ct}$ (KOhm)	$C_{dl}$ ( $\mu\text{F}/\text{cm}^2$ )
40	73	29
70	16	28
100	13	26
200	6	24

**Table 9-**

Charge transfer resistance and double layer capacitance values for the NS-1 modified electrodes in commercial electrolyte solution with different concentrations

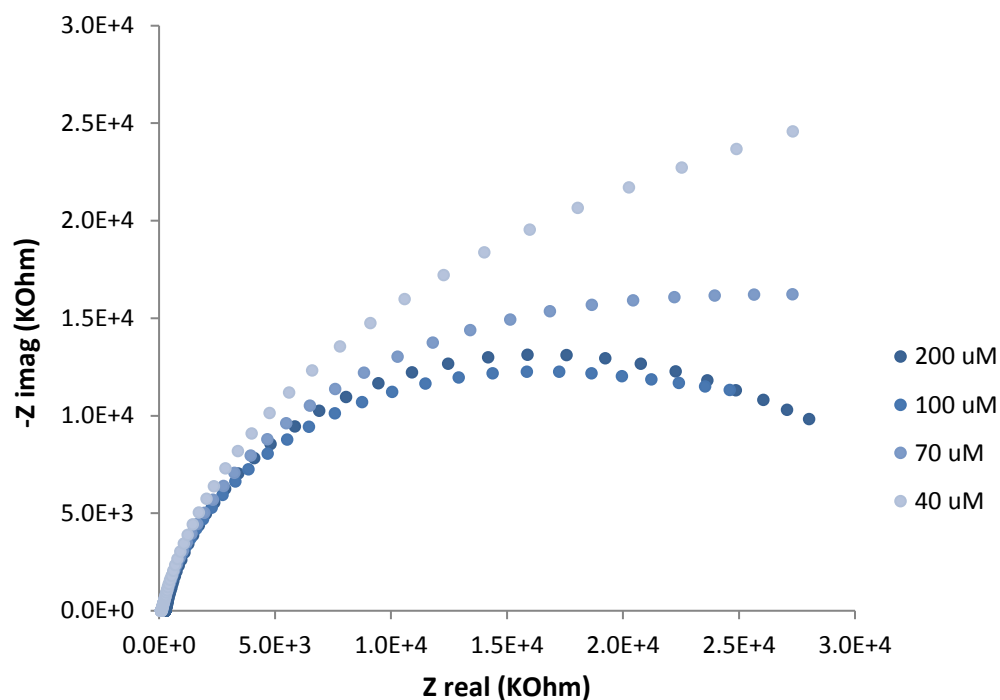


**Fig. 26-** Nyquist plot of different concentration of commercial electrolyte solution at the surface of NS-2 modified electrodes

Electrolyte concentration ( $\mu\text{M}$ )	$R_{ct}$ (KOhm)	$C_{dl}$ ( $\mu\text{F}/\text{cm}^2$ )
40	55	25
70	38	21
100	30	19
200	30	16

**Table 10. -** Charge transfer resistance and double layer capacitance values for the NS-2 modified electrodes in commercial electrolyte solution with different concentrations

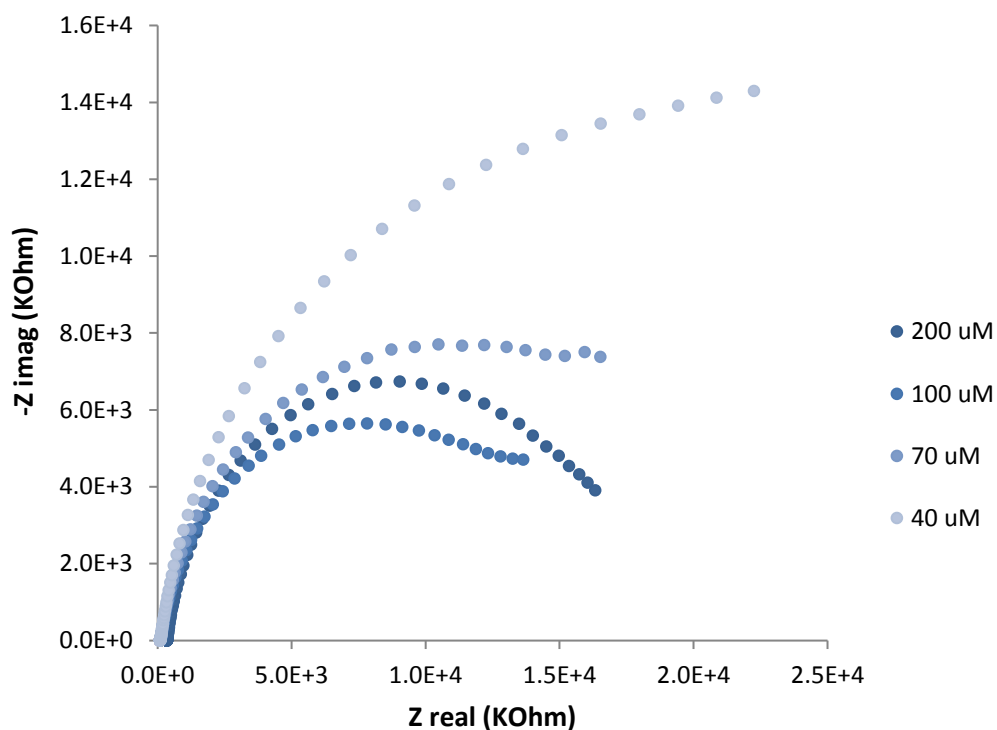


**Fig.27.** - Nyquist plot of different concentration of commercial electrolyte solution at the surface of NS-3 modified electrodes

Electrolyte concentration ( $\mu\text{M}$ )	$R_{ct}$ (KOhm)	$C_{dl}$ ( $\mu\text{F}/\text{cm}^2$ )
40	32	26
70	19	25
100	14	23
200	16	16

**Table 11.** - Charge transfer resistance and double layer capacitance values for the NS-3 modified electrodes in commercial electrolyte solution with different concentrations

### 3.3.1. Enzymatic production of Thiocoline

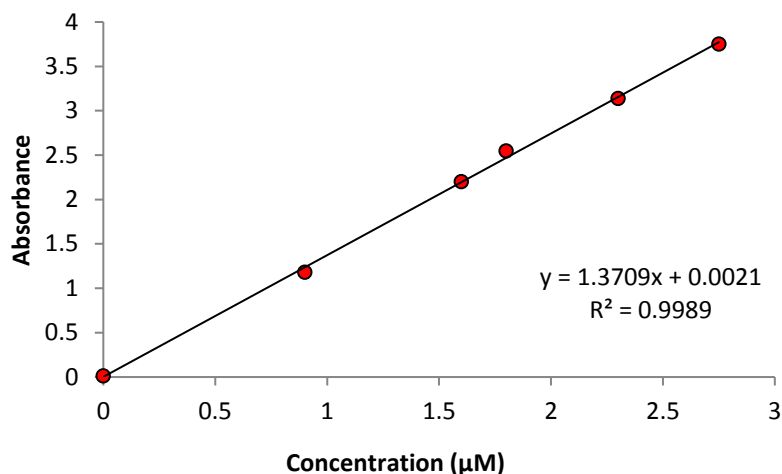


**Fig.28.** – Calibration curve for Thiocoline using the spectrophotometric method

In **Fig.28.** the results obtained after the spectrophotometric assessment of enzymatically produced TCh can be observed. By using the Lambert-Beer law as described in **Section 2.5** the final TCh concentration was determined to be 0.5 M.

### 3.3.2. Electrochemical detection of thiocholine

In **Fig. 29.** the cyclic voltammograms for the ATChCl and ATChI substrates without the presence of the enzyme, can be observed.

The two types of substrates have been tested by CV means. As it can be observed from the obtained results, ATChI substrate gives an electrochemical response which could interfere with the electrochemical signal that we can expect when the electrochemical detection of TCh will be performed. When ATChCl is used, a behavior close to PBS solution response is obtained, therefore this type of substrate was chosen for the enzymatic production of TCH.

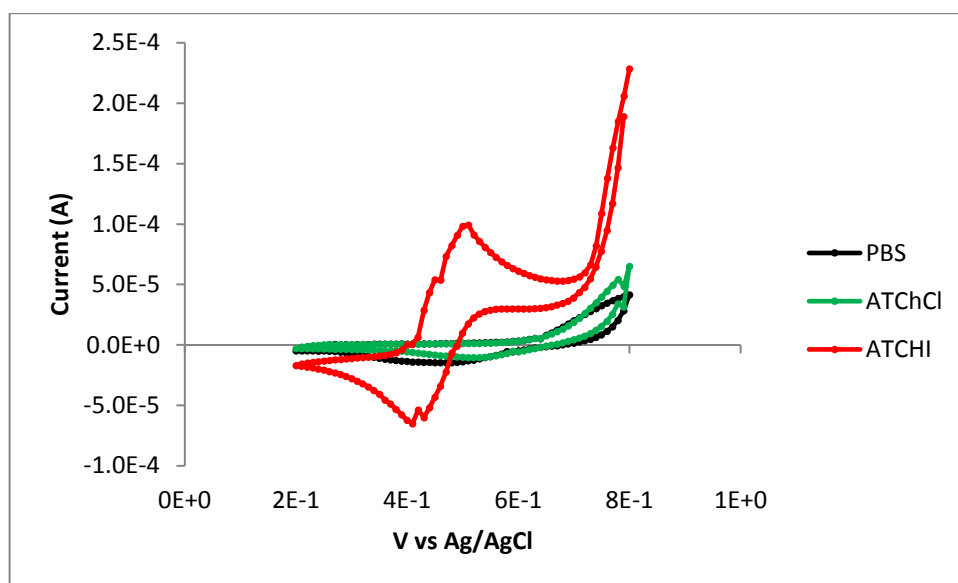


**Fig.29.** - Cyclic voltammograms of ATChCl and ATChI substrates (0.5 M) in PBS solution (0.1 M, pH= 7.5)

In **Fig. 30-33** and **Table 12** the CV data for the determination of the oxidation potential of TCh at the surface of the modified electrodes compared to bare Au sample, can be observed. From the cyclic voltammograms we can see that the electrochemical oxidation of TCh is present for all the types of modified electrodes and the potential of oxidation is kept in the same range. The oxidation current peaks however are different when compared to the bare Au sample and the most suitable type of modified electrode for electrochemical assessment of TCh remains NS-2 with an anodic peak very close to the control sample.

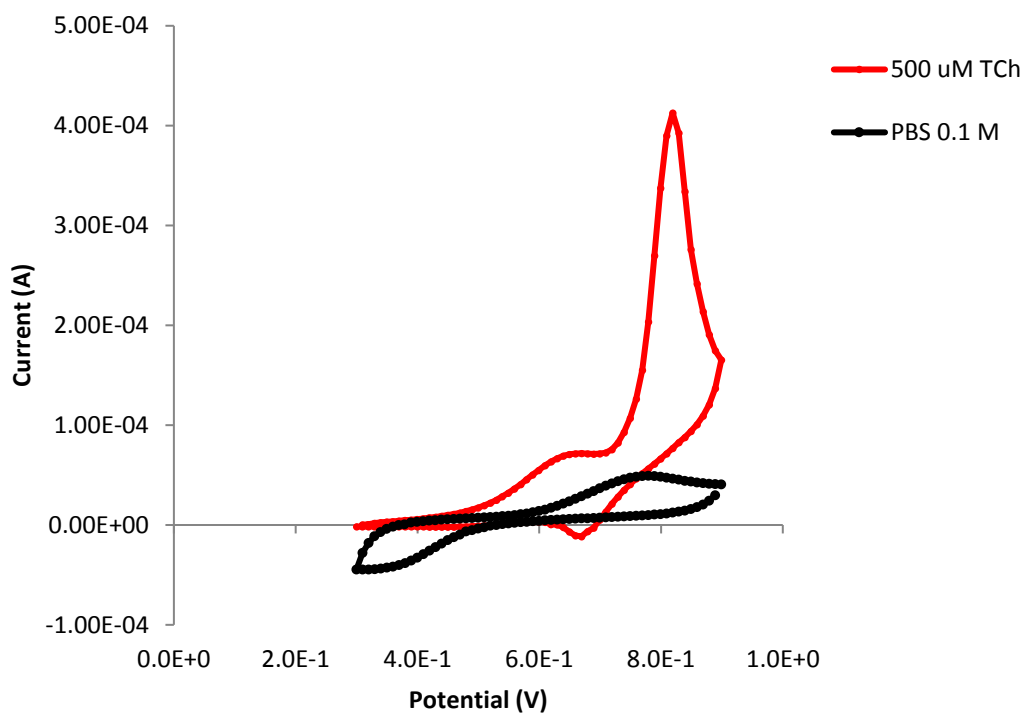


**Fig. 30-** Cyclic voltammogram of TCh oxidation at the surface of Bare Au electrode

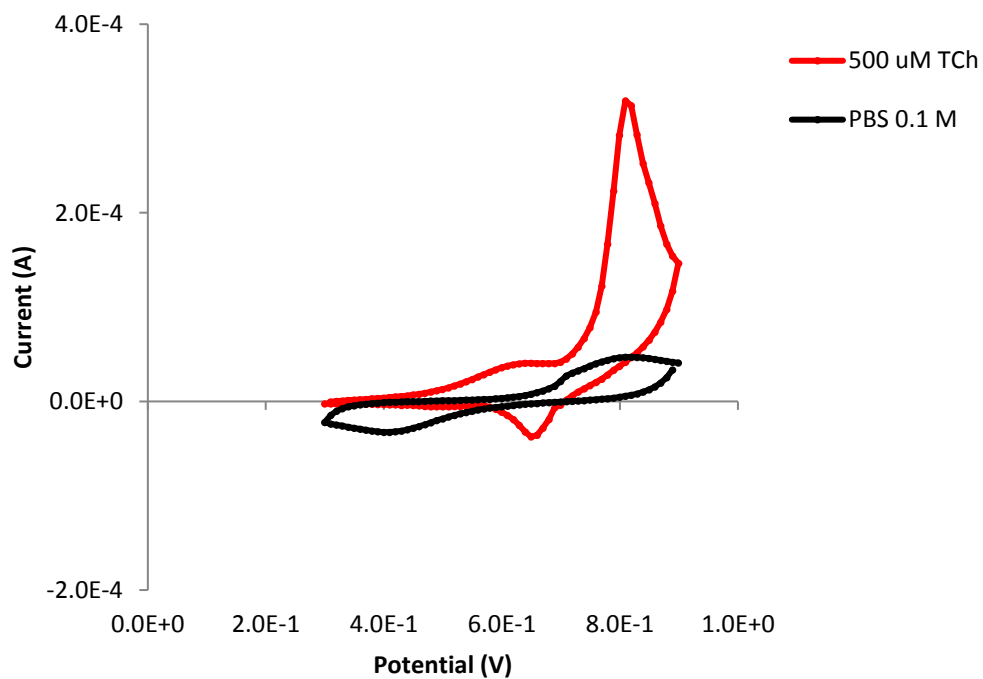


**Fig. 31-** Cyclic voltammogram of TCh oxidation at the surface of NS-1 modified electrode

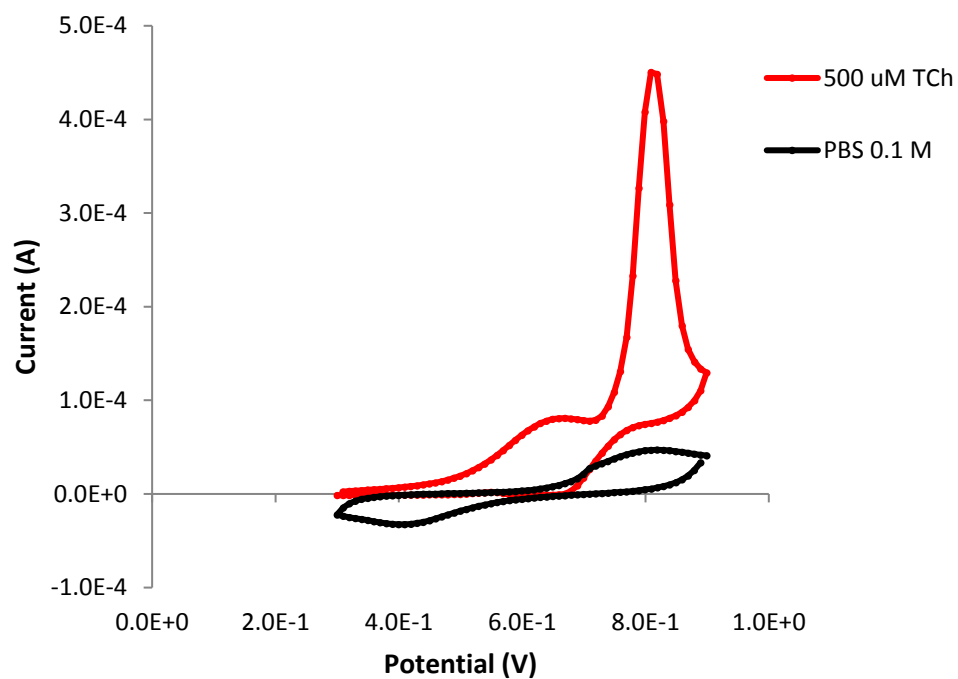


**Fig. 32-** Cyclic voltammogram of TCh oxidation at the surface of NS-2 modified electrode

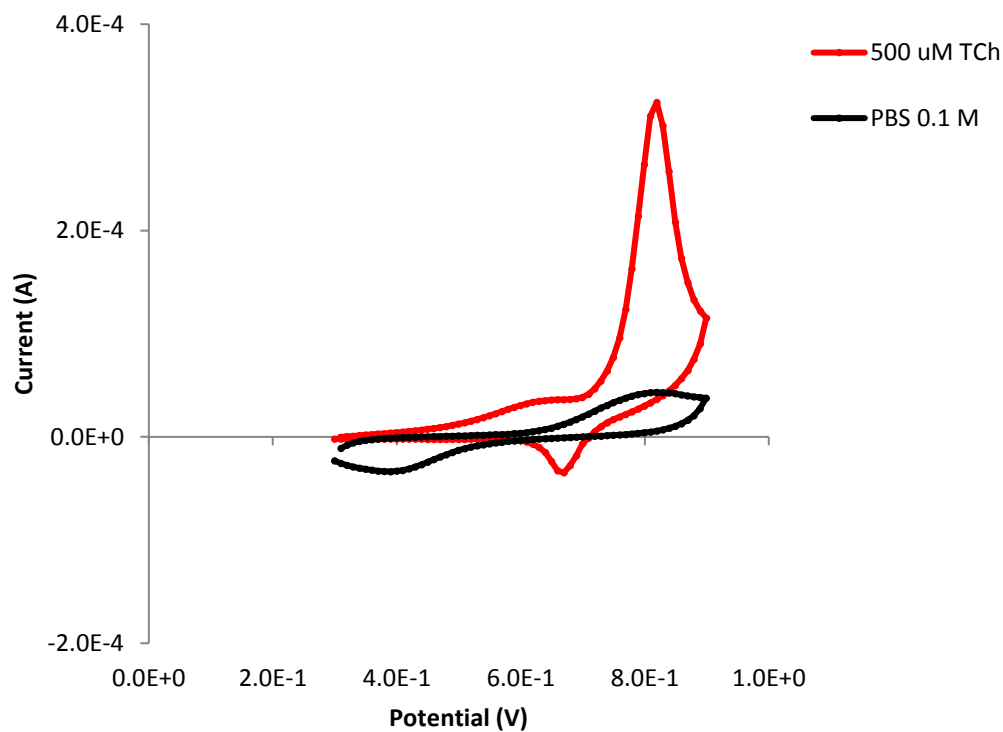


**Fig. 33-** Cyclic voltammogram of TCh oxidation at the surface of NS-3 modified electrode

Type of sample	Oxidation potential (V)	Oxidation current peak ( $\mu\text{A}$ )
Bare Au	0.809	450
NS-1	0.809	318
NS-2	0.819	412
NS-3	0.819	324

**Table 12-** Oxidation potentials and current peaks of TCh at the surface of the modified electrodes and Bare Au sample

### 3.3.3. Electrochemical detection of Thiocholine-Electrochemical Impedance Spectroscopy

In **Fig. 34-37** and **Table 13-16** the EIS study performed for the TCh detection at the surface of the modified electrodes and the bare Au sample is presented.

From the EIS studies performed in the presence of TCh at the chosen potential where the oxidation process takes place it can be seen that in the case of all the batches of modified electrodes the  $R_{ct}$  values decrease by increasing the concentration of TCh and the  $C_{dl}$  increases when the TCh solution is more concentrated, a behavior that is expected when EIS assessments are performed at a chosen potential. Also, if we analyze the obtained results it can be noticed that in the presence of TCh the NS-2 modified electrodes show an improvement in terms of  $C_{dl}$  when compared to bare Au samples and the NS-1 modified electrodes have a similar behavior as the control electrodes, maintaining the diffusion process. In the case of NS-3 modified electrodes the capacitive behavior can still be noticed and at low TCh concentration they express a slow electron transfer.

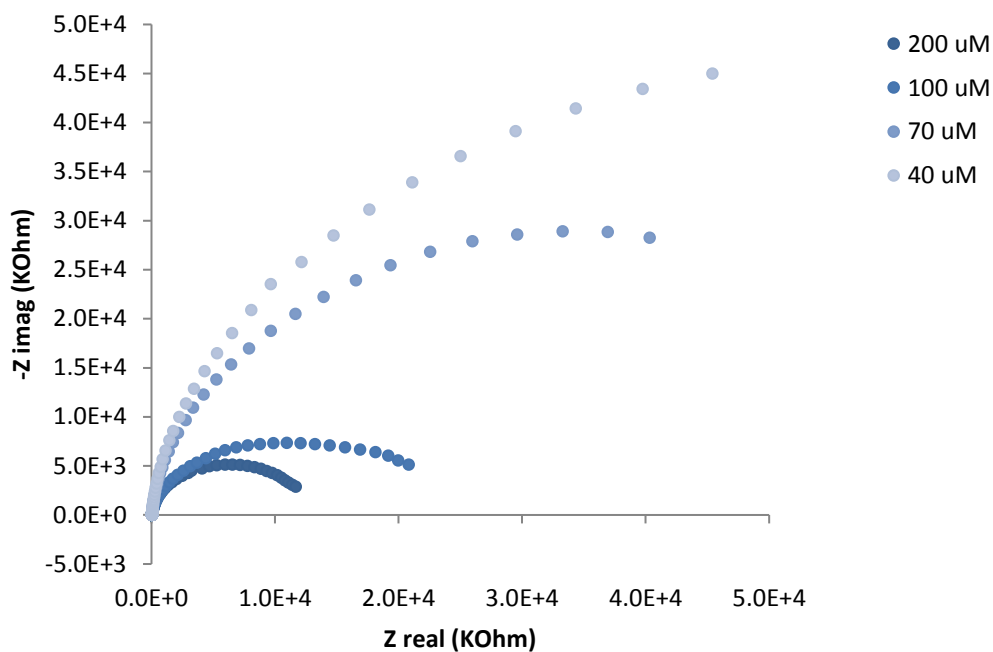


**Fig. 34-** Nyquist plot of different concentrations of TCh solution at the surface of Bare Au electrodes at fixed potential

Electrolyte concentration ( $\mu\text{M}$ )	$R_{ct}$ (KOhm)	$C_{dl}$ ( $\mu\text{F}/\text{cm}^2$ )
40	87	16
70	58	16
100	18	20
200	11	21

**Table 13-** Charge transfer resistance and double layer capacitance values for the Bare Au electrodes in TCh solution with different concentrations

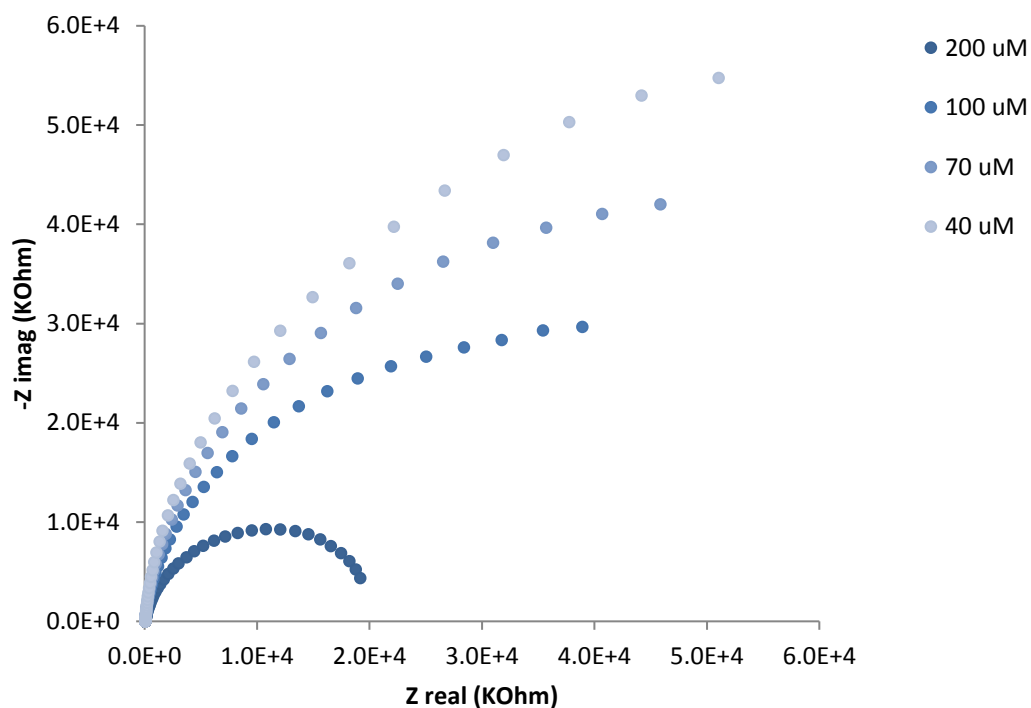


**Fig. 35-** Nyquist plot of different concentrations of TCh solution at the surface of NS-1 modified electrodes at fixed potential

Electrolyte concentration ( $\mu\text{M}$ )	$R_{ct}$ (KOhm)	$C_{dl}$ ( $\mu\text{F}/\text{cm}^2$ )
40	109	15
70	85	16
100	60	17
200	21	21

**Table 14-** Charge transfer resistance and double layer capacitance values for the NS-1 modified electrodes in TCh solution with different concentrations

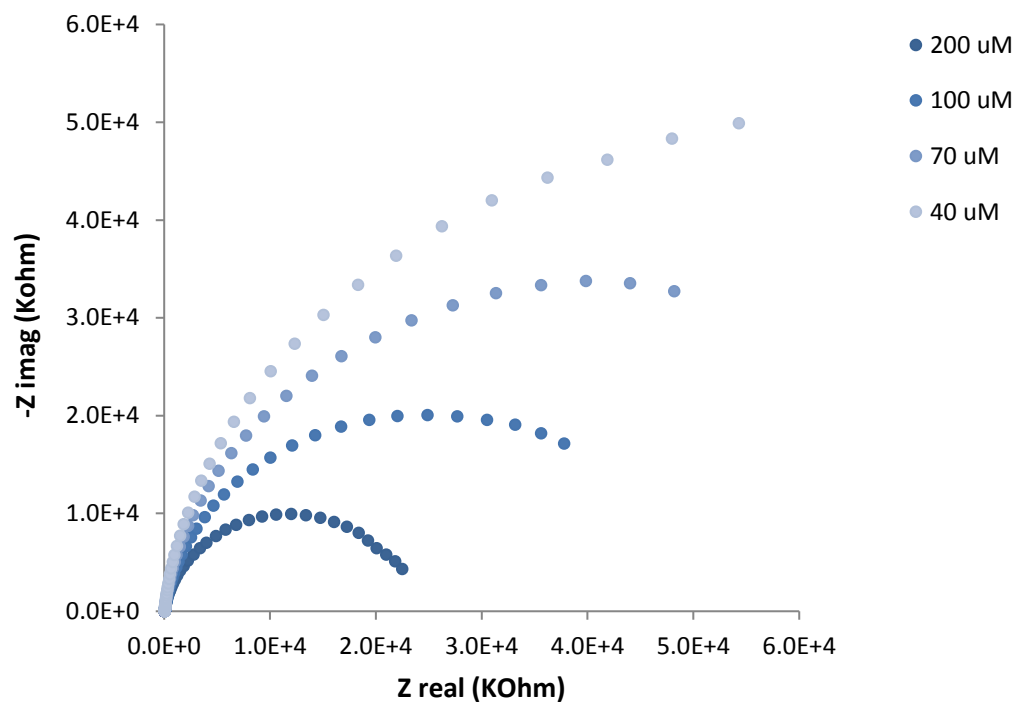


**Fig. 36-** Nyquist plot of different concentrations of TCh solution at the surface of NS-2 modified electrodes at fixed potential

Electrolyte concentration ( $\mu\text{M}$ )	$R_{ct}$ (KOhm)	$C_{dl}$ ( $\mu\text{F}/\text{cm}^2$ )
40	99	14
70	72	14
100	45	16
200	25	16

**Table 15-** Charge transfer resistance and double layer capacitance values for the NS-2 modified electrodes in TCh solution with different concentrations

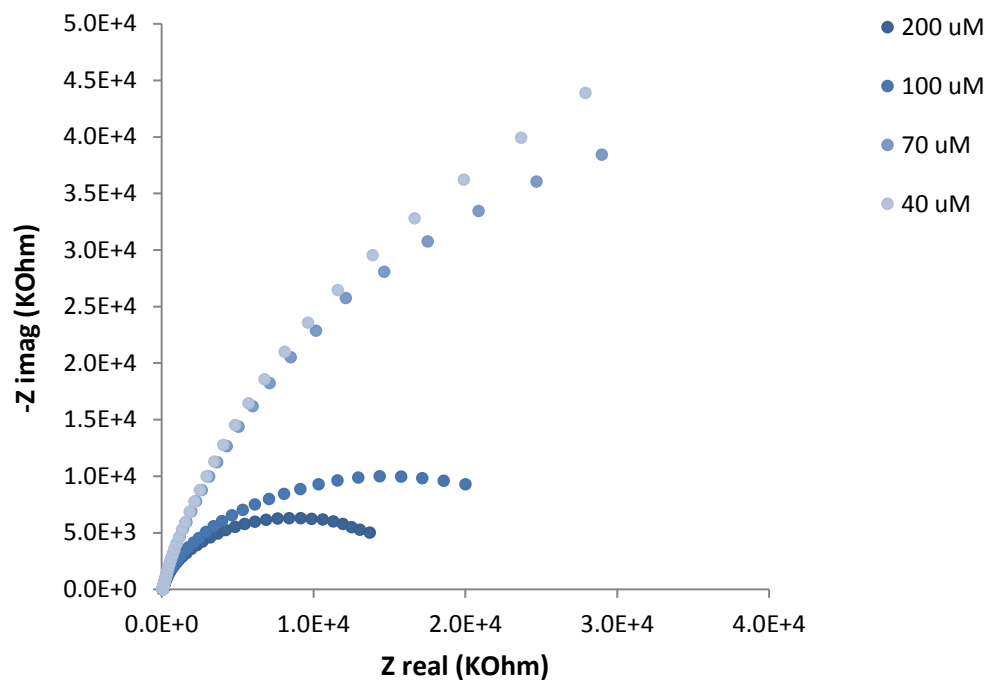


**Fig. 37-** Nyquist plot of different concentrations of TCh solution at the surface of NS-3 modified electrodes at fixed potential

Electrolyte concentration ( $\mu\text{M}$ )	$R_{ct}$ (KOhm)	$C_{dl}$ ( $\mu\text{F}/\text{cm}^2$ )
40	126	26
70	103	26
100	24	31
200	15	30

**Table 16-** Charge transfer resistance and double layer capacitance values for the NS-3 modified electrodes in TCh solution with different concentrations

### 3.3.4. Electrochemical detection of Thiocholine- Chronoamperometry

In Fig.38-41 (a, b) the data corresponding to the amperometric detection of TCh at the surface of all types of modified electrodes as well as the limit of detection of the system is presented.

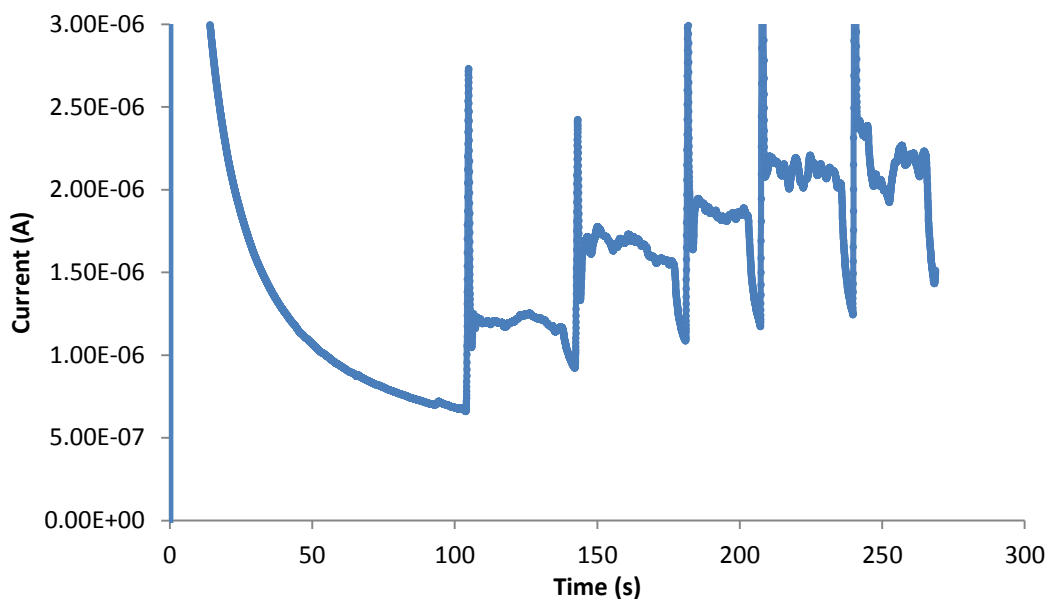


**Fig.-38 a-** Amperometric detection of TCh at the surface of Bare Au electrode (TCh concentrations: 5  $\mu\text{M}$ , 10  $\mu\text{M}$ , 15  $\mu\text{M}$ , 20  $\mu\text{M}$  and 25  $\mu\text{M}$ )

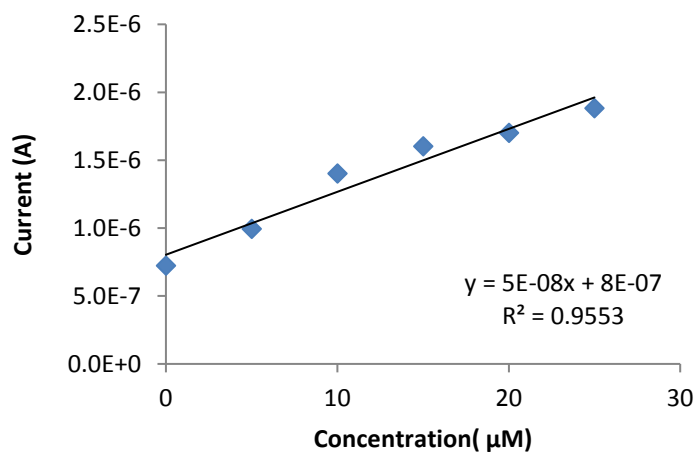


**Fig. 38 b-** Concentration vs. Current of TCh amperometric detection at the surface of Bare Au electrodes

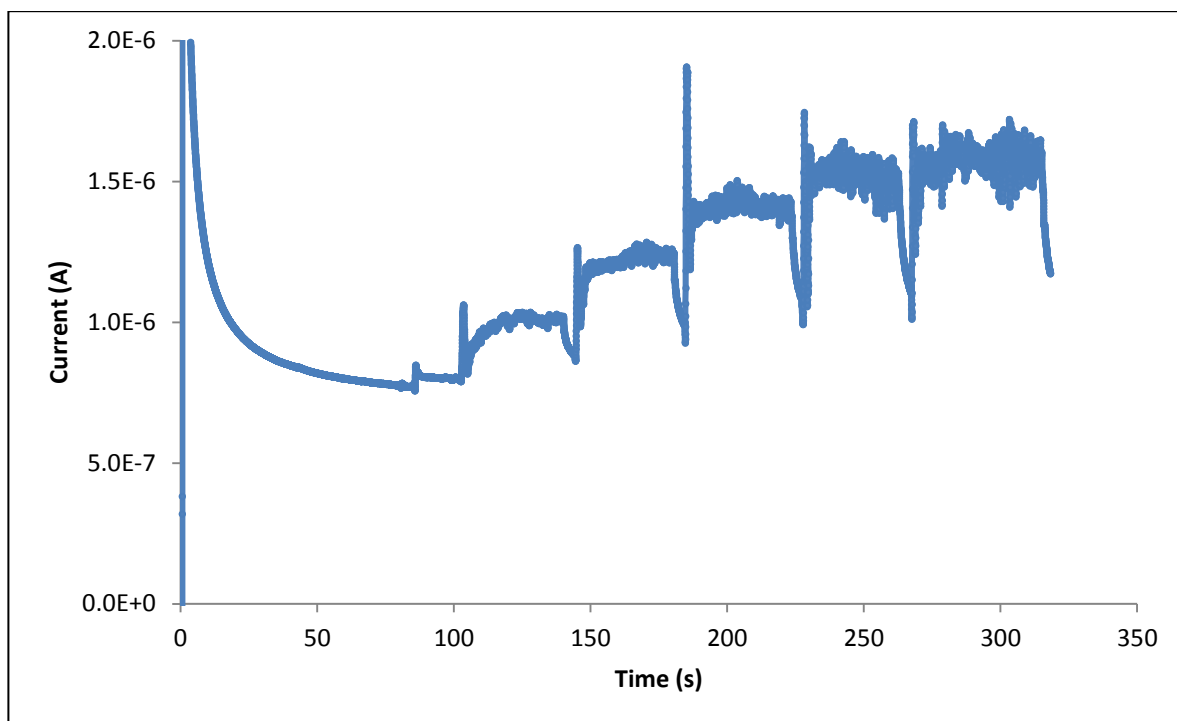


**Fig.-39 a-** Amperometric detection of TCh at the surface of NS-1 modified electrode (TCh concentrations: 5  $\mu\text{M}$ , 10  $\mu\text{M}$ , 15  $\mu\text{M}$ , 20  $\mu\text{M}$  and 25  $\mu\text{M}$ )

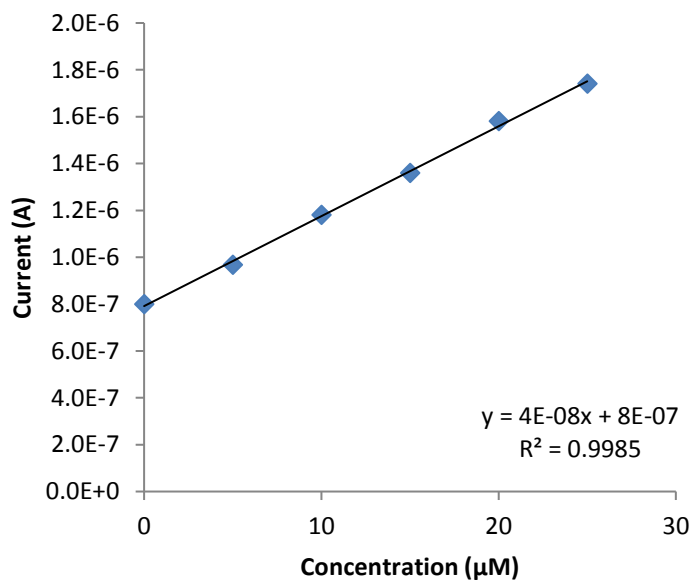


**Fig. 39 b-** Concentration vs. Current of TCh amperometric detection at the surface of NS-1 modified electrodes

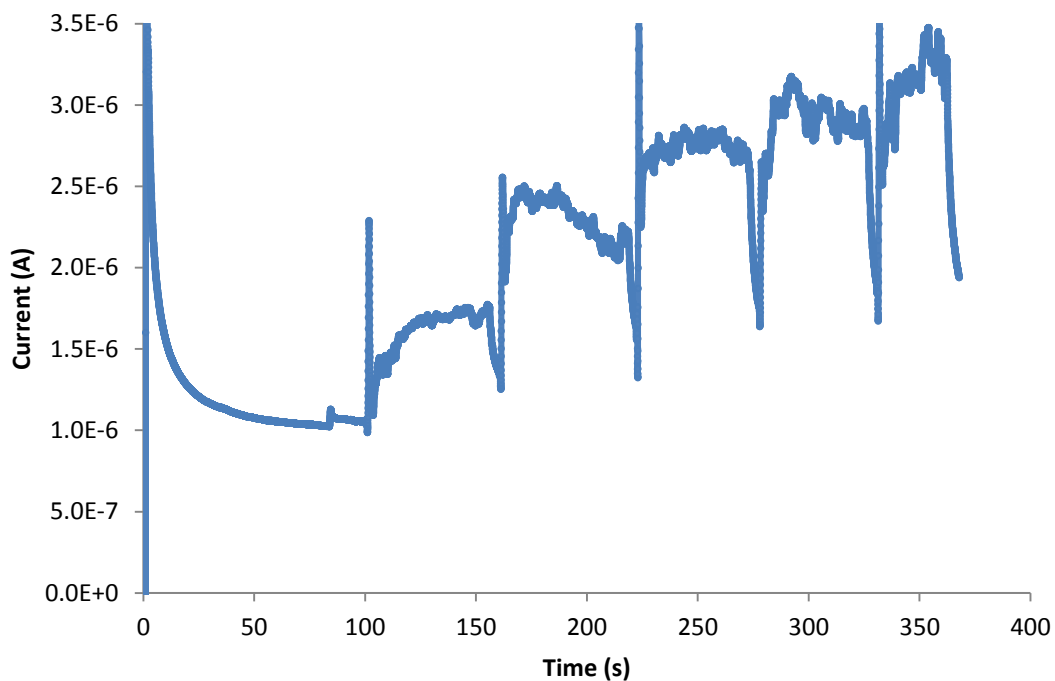


**Fig.-40 a-** Amperometric detection of TCh at the surface of NS-2 modified electrode (TCh concentrations: 5  $\mu\text{M}$ , 10  $\mu\text{M}$ , 15  $\mu\text{M}$ , 20  $\mu\text{M}$  and 25  $\mu\text{M}$ )

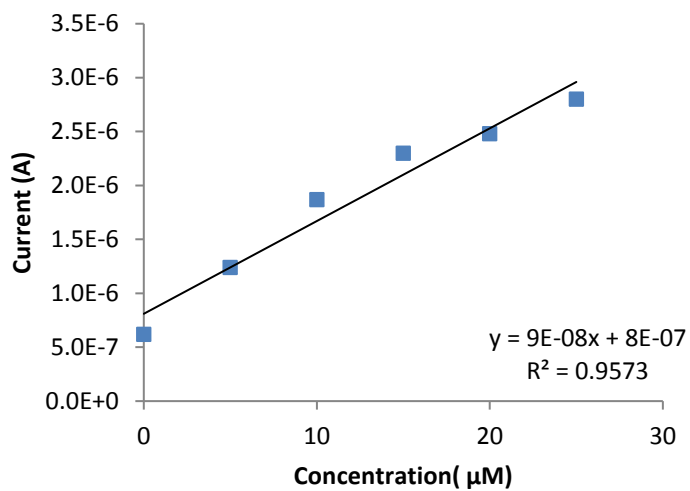


**Fig. 40 b-** Concentration vs. Current of TCh amperometric detection at the surface of NS-2 modified electrodes

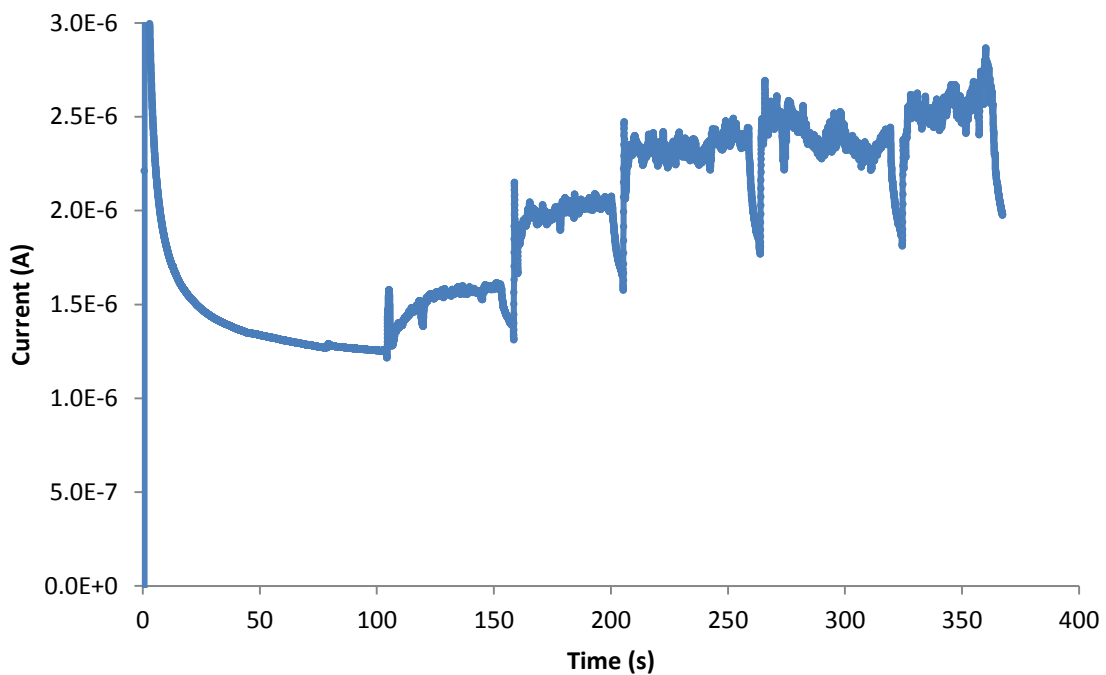


**Fig.-41 a-** Amperometric detection of TCh at the surface of NS-3 modified electrode (TCh concentrations: 5  $\mu\text{M}$ , 10  $\mu\text{M}$ , 15  $\mu\text{M}$ , 20  $\mu\text{M}$  and 25  $\mu\text{M}$ )

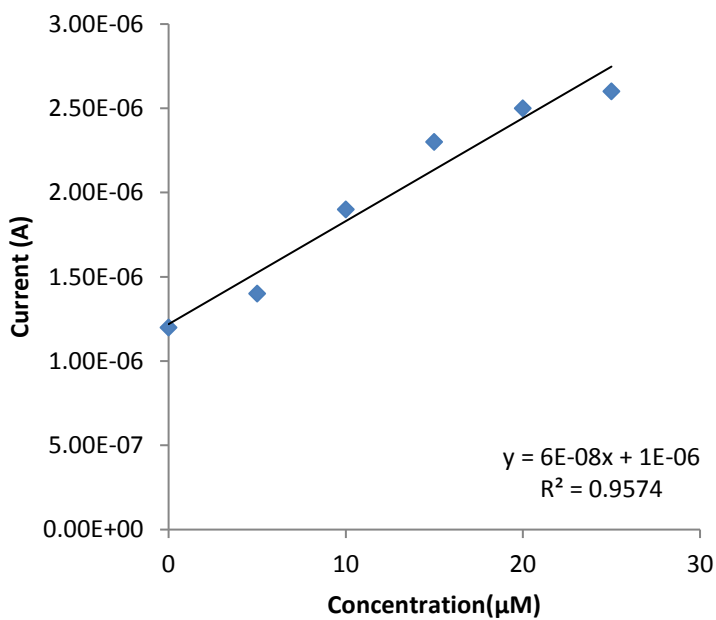


**Fig. 41 b-** Concentration vs. Current of TCh amperometric detection at the surface of NS-3 modified electrodes

Type of sample	Limit of detection ( $\mu\text{M}$ )
Bare Au	0.3
NS-1	0.67
NS-2	0.25
NS-3	1.3

**Table 17-** Limit of detection of TCh at the surface of the modified electrodes and Bare Au control

Chronoamperometry data show that an amperometric detection of TCh is possible using ns-ZrO<sub>2</sub> modified electrodes and the LOD obtained is comparable to the Bare Au electrodes. As shown in the general electrochemical characterization of the modified electrodes, as well as with the EIS assessment in the presence of TCh, the NS-2 modified electrodes show a better response than NS-1 and NS-3 batches, and the obtained LOD of the NS-2 samples is improved when compared to Bare Au electrodes.

# 4

## Discussion

Two generations of cluster-assembled zirconia nanostructured modified electrodes have been developed during this PhD study, to be implemented as platforms for the electrochemical detection of thiocholine.

Cluster-assembled zirconia nanostructured thin films have been deposited using the Supersonic Cluster Beam Deposition technique. With the help of this technique we were able to control the morphological characteristics of the deposited material in order to obtain the most convenient structure for maintaining the electrochemical behavior of the modified electrode.

For the first generation of modified electrodes a combination of high thickness and high roughness of the ns-ZrO<sub>2</sub> has been chosen in order to determine the influence of the morphological characteristics of the deposited material onto the electrochemical performance of the modified electrodes. This type of electrodes has been tested by means of Cyclic Voltammetry and Electrochemical Impedance Spectroscopy in a three-electrode electrochemical setting in batch conditions. The electrochemical cell had a capacity of 10 mL of electrolyte and the area of the assessed modified electrode was kept in the range of 2.25 cm<sup>2</sup>. Electrochemical characterization results for the first generation of modified electrodes have shown that by increasing the thickness of the deposited material the active

surface area is also increased, characteristic that helps lowering the charge transfer resistance and sustains a fast electron transfer of the modified electrodes. In terms of double layer capacitance this type of electrodes have shown that by increasing the thickness the diffusion processes take longer, therefore the second generation of modified electrodes has been developed with different surface morphology characteristics. Taking into consideration also the fact that the electrochemical assessments for this type of electrodes have been performed in batch conditions it was also necessary to develop a new electrochemical setting that would reduce the area of the modified electrode and also the working volume for the electrolyte.

Since it has been seen from the results obtained with the first generation of modified electrodes that the electrochemical behavior is not greatly influenced by a thickness up to 100 nm of deposited material, for the second generation of modified electrodes the thickness of the ns-ZrO<sub>2</sub> has been chosen up to a maximum of 100 nm and the roughness of the electrode's surface was lowered to a maximum of 11 nm. The general electrochemical characterization of this type of modified electrodes has been performed by means of Cyclic Voltammetry and Electrochemical Impedance Spectroscopy in a "homemade" Teflon electrochemical cell which confined a fixed area of the working electrode to 0.6 cm<sup>2</sup> in diameter and a maximum electrolyte volume of 500 μL. With this type of electrochemical setting the errors were greatly reduced and a more precise electrochemical assessment was performed. The CV results obtained in these new working conditions have shown that the electrochemical performance in terms of electron transfer and reversibility of the redox reaction at the surface of all types of modified electrodes are comparable with those obtained in the case of bare Au electrodes. EIS studies have been performed in the presence of a commercial electrolyte for all types of modified electrodes as well as bare Au

electrode. In terms of charge transfer resistance and double layer capacitance NS-2 and NS-3 modified electrodes samples have shown a similar behavior with the one obtained for bare Au electrodes. The increased electron transfer can be allocated to the increase in the active surface area of the modified electrodes. A slightly slower electron transfer could be observed in the case of the NS-1 modified electrodes, fact that can be attributed to a lower active surface area provided by the thinner layer of ns-ZrO<sub>2</sub>.

For the electrochemical detection of the enzymatically produced TCh, the concentration of the product was assessed spectrophotometrically by using the Ellman's method. Before the electrochemical detection of the enzymatic product, two different substrates have been (ATChCl and ATChI) electrochemically assessed in order to establish the substrate's influence upon the electrochemical response of the system. It has been concluded that ATChCl substrate is the appropriate one to be used since the oxidation potential of the ATChI substrate is too high and might interfere with the real electrochemical signal given by the oxidation of TCh.

CV assessment for the determination of the oxidation potential of TCh have shown that for all the types of modified electrodes an electrochemical signal in the range of 0.81 V - 0.82 V has been detected. The obtained oxidation potential values are comparable to the ones obtained by other groups who used Au as conductive material in the design of electrodes for the electrochemical detection of TCH [102]. The obtained potential from the CV studies has been used for EIS assessments as well as chronoamperometric detection of the enzymatic product. The EIS results obtained in the presence of the enzymatic product have shown the same behavior of the modified electrodes as in the case of the commercial electrolyte.

Amperometric detection of TCh has been achieved in the case of all the types of modified electrodes, by maintaining the fixed potential obtained from the CV studies and measuring the current values over a period of time with the change of the enzymatic product concentration. With the information gathered from the CA assessment the limit of detection of the system was calculated. The amperometric detection of TCh was achievable in the case of all the modified electrodes with a limit of detection between 0.25  $\mu\text{M}$  and 1.3  $\mu\text{M}$ , values comparable to the ones obtained with the bare Au electrodes. The detection limit of TCh at the surface of the modified electrodes has been accomplished without any chemical mediators used as enhancers for the electrochemical signal given by the oxidation of the enzymatic product and the obtained values are comparable to the ones described in literature [69],

The general electrochemical characterization of the second generation of modified electrodes in the presence of the commercial electrolyte, as well as their ability to perform electrochemical detection of enzymatic product with three different electrochemical methods give a promising perspective in using ns-ZrO<sub>2</sub> thin films as part of transducers for electrochemical detection of TCh with potential applications in environmental pollution monitoring.

By using the SCBD technique for the cluster-assembled zirconia nanostructured thin films, we are able to produce at a large scale modified electrodes with tailored surface morphology characteristics according to the requirements of the application, making it an attractive technique for industrial production. The good biocompatibility properties of zirconia as well as a precise control over the roughness of the surface of the cluster-assembled nanostructured thin films offered by the SCBD, represents a promising mean of

overcoming the existing drawbacks in terms of transducer/biological compound interactions.

To achieve the final aim represented by the development of a fully functional enzymatic electrochemical detection platform for environmental pollution control, several steps have yet to be accomplished. The design of the modified electrodes has to be reconsidered in order to be able to perform electrochemical assays on very small working areas with total volumes of analyte below 100  $\mu\text{L}$ , therefore eliminating as much as possible the errors during assessments but also making the processes more user-friendly for the general consumers. Physical adsorption of the biological compound onto the surface of the modified electrodes has to be accomplished and the proposed electrochemical detection system has to be assessed in the presence of commercial pesticides based on organophosphorous compounds.

## References

- [1]- D.R. Thevenot, K. Toth, R. A. Durst and G.S. Wilson, *Electrochemical Biosensors: Recommended Definitions and Classification* Pure Appl. Chem., Vol. 71, No. 12, pp. 2333-2348,(1999)
- [2]- D. Grieshaber;, R. MacKenzie;, J. Voros and E. Reimhult, *Electrochemical biosensors- Sensor principles and architectures*, *Sensors*, 8(3), 1400-1458, (2008)
- [3]- N. J. Ronkainen, H. B. Halsall, W. R. Heineman, *Electrochemical biosensors*, *Chem. Soc. Rev.* (39), 265-322, (2010)
- [4]- L. C. Clark,C. Lyons, *.Electrode systems for continuous monitoring in cardiovascular surgery*. *Annals of the New York Academy of Sciences*, Vol.102, No.1, pp. 29-45.(1962)
- [5]- *Commision Recommendation of 18 October 2011 on the definition of nanomaterial*, *Official Journal of the European Union*, (2011)
- [6]- M. Holzinger, A. Le Goff, S. Cosnier – *Nanomaterials for biosensing applications: A review*, *Front Chem*, 2, 63, (2014)
- [7]- B. Malhotra, Md. A. Ali, *Nanomaterials for biosensors*, 1st Edition, *Fundamentals and applications*, (2017)
- [8]- J. Kim, J. W. Grate, P. Wang- *Nanostructures for enzyme immobilization*, *Chemical Engineering Science* 61,1017-1026, (2006)
- [9]- H. Li, S. Liu, Z. Dai, J. Bao, X. Yang- *Applications of nanomaterials in electrochemical enzyme biosensors*, *Sensors*, 9 (11) : 8547-8561, (2009)

- [10]- T. Liu, J. Tang, L. Jiang, *The enhancement effect of gold nanoparticles as a surface modifier on DNA sensor sensitivity*, Biochem. And Biophy. Res. Comm., 313(1), 3-7, (2004)
- [11]- A. L. Ghindilis, P. Atanasov, M. Wilkins, E. Wilkins, *Immunosensors: electrochemical sensing and other engineering approaches*, Biosens Bioelectron, 13(1), 113-131, (1998)
- [12]- A. De la Escosura-Muniz, M. Maltez-da Costa, C. Sanchez-Espinel, B. Diaz-Freitas, J. Fernandez-Suarez, A. Gonzalez-Fernandez, A. Merkoci, *Gold nanoparticle-based electrochemical magnetoimmunosensor for rapid detection of anti-hepatitis B virus antibodies in human serum*, Biosens Bioelectron, 26, 1710-1714, (2010)
- [13]- C.G. Jensen, C.E. Krause, G. A. Sotzing, J. F. Rusling, *Inkjet-printed gold nanoparticle electrochemical arrays on plastic. Application to immunodetection of a cancer biomarker protein*, Phys. Chem. (13), 4888-4894,( 2011)
- [14]- A.Chen, S. Chatterjee, *Nanomaterials based electrochemical sensors for biomedical applications*, Chem. Soc. Rev.,42, 5425-5438, (2013)
- [15]- A. Ahmmad, J. Lee, M. Rahman, *Electrochemical sensors based on carbon nanotubes*, Sensors(9), 2289-2319, (2009)
- [16]- S. Iijima, *Helical microtubules of graphitic carbon*, Nature, (354), 56-58,(1991)
- [17]- P. J. Britto, K. S. V. Sunthanam, P. M. Ayajan, *Carbon nanotube electrode for oxidation of dopamine*, Bioelectrochem. Bioenerg., (41), 121-125, (1996)
- [18]- C. S. S. R., Kumar, *Nanomaterials for biosensors*, Wiley-VCH, Carbon nanotube-based sensor, 27-89, (2007)

- [19]- J. Wang, *Carbon-nanotube based electrochemical biosensors: A review*, *Electroanalysis*, (17) 7-14, (2005)
- [20]- U. S. Mohanty, *Electrodeposition: a versatile and inexpensive tool for the synthesis of nanoparticles, nanorods, nanowires, and nanoclusters of metals*, *Journal of Applied Electrochemistry*, 41,(3), 257-270, (2011)
- [21]- D. Du, J. Liu, X. Zhang, X. Cui, Y. Lin, *One-step electrochemical deposition of a grapheme-ZrO<sub>2</sub> nanocomposite: Preparation, characterization and application for detection of organophosphorus agents*, *J. Mater. Chem.*, 21,8132,( 2011)
- [22]- W. Wu, L. Liu, Z. Dai, J. Liu, S. Yang, L. Zhou, X. Xiao, C. Jiang, V. A. L. Roy, *Low-cost, disposable, flexible and highly reproducible screen printed SERS substrates for the detection of various chemicals*, *Scientific Reports* 5: 10208, (2015)
- [23]- E. Bernalte, C. M. Sanchez, E. P. Gill, C. M. A. Brett, *Characterization of screen-printed gold and gold nanoparticle-modified carbon sensors by electrochemical impedance spectroscopy*, *Journal of Electroanalytical Chemistry*, 709, 70-76,( 2013)
- [24]- S. W. Kim, S. Fujita, *ZnO nanowires with high aspect ratios grown by metal organic chemical vapor deposition using gold nanoparticle*, *Appl Physics Lett.* 86 (15), 1-3,( 2005).
- [25]- P. Xu, X. Han, C. Wang, B. Zhang, X. Wang, H.L. Wang, *Facile synthesis of polyaniline-polypropyrrole nanofibers for application in chemical deposition of metal nanoparticles*, *Macromol Rapid Commun.* 29 (16), 1392-1397, (2008)
- [26]- P. Colson, C. Henrist, R. Cloots, *Nanosphere lithography: A powerful method for the controlled manufacturing of nanomaterials*, *Journal of Nanomaterials*, Art. ID. 948510, (2013)

- [27]- P. Pandey, M. Datta, B.D. Malhotra, *Prospects of nanomaterials in biosensors*, Analytical Letters, 41 (2):159-209, (2008)
- [28]- P. R. Solanki, A. Kaushik, V. V. Agrawal, B. D. Malhotra, *Nanostructured metal oxide-based biosensors*, NPG Asia Mater, 3 (1),17-24, (2011)
- [29]- X. Shi, W. Gu, B. Li, N. Chen, K. Zhao, Y. Xian, *Enzymatic biosensors based on the use of metal oxide nanoparticles*, Microchimica Acta, 181 (1-2), 1-22, (2014)
- [30]- S. Kumar, J. G. Sharma, S. Maji, B. D. Malhotra, *Nanostructured zirconia decorated reduced grapheme oxide based efficient biosensing platform for non-invasive oral cancer detection*, Biosensors and Bioelectronics 78, 497–504, (2016)
- [31]- P. R. Solanki, A. Kaushik, P. M. Chavan, S. N. Maheswari, B. D. Malhotra, *Nanostructured zirconium oxide based genosensor for Escherichia coli detection*, Electrochemistry Communications 11, 2272–2277, (2009)
- [32]- T. Yang, X. Guo, Q. Kong, R. Yang, Q. Li, K. Jiao, *Comparative studies on zirconia and grapheme composites obtained by one-step and stepwise electrodeposition for deoxyribonucleic acid sensing*, Anal Chim Acta., 5;786:29-33, (2013)
- [33]- W. Zhang, T. Yang, C. Jiang, K. Jiao, *DNA hybridization and phosphinothricin acetyltransferase gene sequence detection based on zirconia/nanogold film modified electrode*, Applied Surface Science 254,4750-4756, (2008)
- [34]- B. Liu, J. Hu, J. S. Foord, *Electrochemical detection of DNA hybridization by a zirconia modified diamond electrode*, Electrochemistry Communications, 19, 46-49, (2012)
- [35]- B. Batra, S. Lata, J. S. Rana, C. S. Pundir, *Construction of an amperometric bilirubin biosensor based on covalent immobilization of bilirubin oxidase onto zirconia coated silica nanoparticles/chitosan hybrid film*, Biosensors and Bioelectronics, 44,64-69, (2013)

- [36]- G. Sumana, M. Das, S. Srivastava, B.D. Malhotra, *A novel urea biosensor based on zirconia*, Thin Solid Films, 519 (3), 1187-1191, (2010)
- [37]- J. H. Zhou, C. Y. Deng, S. H. Si, S. E. Wang, *Zirconia electrodeposited on a self-assembled monolayer on a gold electrode for sensitive determination of parathion*, Microchim Acta, 172, 207-215, (2011)
- [38]- M. P. N. Bui, S. S. Seo, *Electrochemical analysis of parathion-ethyl using zirconium oxide-laponite nanocomposites-modified glassy carbon electrode*, J Appl. Electrochem, 45: 365-373, (2015)
- [39]- N. M. Ahmad, J. Abdullah, N. A. Yusof, A. H. A. Rashid, S. A. Rahman, Md. R. Hasan, *Amperometric biosensor based on zirconium oxide/polyethylene glycol/tyrosinase composite film for the detection of phenolic compounds*, Biosensors, 6, 31, (2016)
- [40]- H.Wang, Y. Su, H. Kim, D. Yong, L. Wang, X. Han, *A highly efficient ZrO<sub>2</sub> nanoparticle based electrochemical sensor for the detection of organophosphorus pesticide*, Chin. J. Chem. , 33, 1135-1139, (2015)
- [41]- M. Alvarez-Icaza, U. Bilitewski, *Mass production of biosensors*, Anal. Chem. 65 (11), 525A-533A, (1993)
- [42]- W. Aehle, *Enzymes in industry: Production and application*, 3rd Edition, Wiley-VCH, (2007)
- [43]- S. Datta, C. L. Rene, Y.R.S. Rajaram, *Enzyme immobilization: an overview on techniques and support materials*, Biotech. 3(1), 1-9, (2013)
- [44]- W. Jin, J. D. Brennan, *Properties and applications of protein encapsulated within sol-gel derived material*. Anal. Chim. Acta, 461, 1-36, (2002)

- [45]- Q. Shen, R. Yang, X. Hua, F. Ye, W. Zhang, W. Zhao, *Gelatin-templated biomimetic calcification for  $\beta$ -galactosidase immobilization*. *Process Biochem.* , 46, 1565-1571,(2011)
- [46]- E. Gorecka, M. Jastzerbska, *Immobilization techniques and biopolymer carriers*. *Biotechnol Food Sci.*, (75), 65-86, (2011)
- [47]- R. A. Sheldon, *Cross-linked enzyme aggregates (CLEAs): stable and recyclable biocatalysts*, *Biochem Soc. Trans*, 35 (6), 1583-1587, (2007)
- [48]- U. Hanefeld, L. Gardossi, E. Magner, *Understanding enzyme immobilization*, *Chem. Soc. Rev.* , 38 (2), 453-468, (2009)
- [49]- R. A. Sheldon, *Characteristic features and biotechnological applications of cross-linked enzyme aggregates (CLEAs)*, *Appl. Microbiol. Biotechnol.*, 92(3) 467-477, (2011)
- [50]- K. Ovsejevi, C. Manta, F. Batista-Viera, *Reversible covalent immobilization of enzymes via disulfide bonds*, *Methods Mol Biol.*, 1051,89-116, (2013)
- [51]- L. Huang, Z. M. Cheng, *Immobilization of lipase on chemically modified bimodal ceramic foams for olive oil hydrolysis*, *Chem. Eng. J.*, 144, 103-109, (2008)
- [52]- A. V. Singh, M. Ferri, M. Tamplenizza, F. Borghi, G. Divitini, C. Ducati, C. Lenardi, C. Piazzoni, M. Merlini, A. Podesta, P. Milani, *Bottom-up engineering of the surface roughness of nanostructured cubic zirconia to control cell adhesion*, *Nanotechnology*, 23, 475101,( 2012)
- [53]- C. Schulte, A. Podesta, C. Lenardi, G. Tedeschi, P. Milani, *Quantitative control of protein and cell interaction with nanostructured surfaces by cluster assembling*, *Acc. Chem. Res.* 50(2), 231-239, (2017)
- [54]- D. M. Quinn- *Acetylcholinesterase: Enzyme structure, reaction dynamics, and virtual transition states*, *Chem. Rev.*, 87, 955-979., (1987)

- [55]- J.L. Sussman, M. Harel, F. Frolow, C. Oefner, A. Goldman, L. Toker, I. Silman, *Atomic structure of acetylcholinesterase from Torpedo californica: a prototypic acetylcholine-binding protein*, Science, 253 (5022), 872-9, (1991)
- [56]- V. P. Whittaker, *The contribution of drugs and toxins to understanding of cholinergic function*, Trends Pharmacol Sci, 11 (1), 8-13, (1990)
- [57]- Pediatric Environmental Health Specialty Unit (PEHSU, 2007)
- [58]- United States Environmental Protection Agency- *Recognition and management of pesticide poisonings*, Sixth Edition, Chapter 5, (2013)
- [59]- N. Munro, *Toxicity of the organophosphate chemical warfare agents GA, GB and VX: Implications for public protection*, Environ Health Perspect, 102 (1): 18-37, (1994)
- [60] - [www.aquaportail.com](http://www.aquaportail.com)
- [61]- <https://www.epa.gov/>
- [62]- H. Hrabetz, H. Thiermann, N. Felgenhauer, T. Zilker, B. Haller, J. Nahrig, B. Saugel, F. Eyer, *Organophosphate poisoning in the developed world- A single centre experience from here to the millennium*, Chemico-Biological Interactions 206, 561-568, (2013)
- [63] - [www.netterimages.com/](http://www.netterimages.com/)
- [64]- J.R. Karr, D.R. Dudley *Ecological perspective on water quality goals*. Environ. Manage. Vol.5, pp. 55-68, (1981)
- [65]- A. M. Riederer, K. D. Smith, D. B. Barr, S. W. Hayden, R. E. Hunter, P. B. Ryan, *Current and Historically Used Pesticides in Residential Soil from 11 Homes in Atlanta, Georgia, USA*. Arch. Environ. Con. Tox., Vol.58, pp. 908-917, (2010)

- [66]- S.R. Rissato, M. S. Galhiane, M. V. de Almeida, M. Gerenutti, B.M. Apon, *Multiresidue determination of pesticides in honey samples by gas chromatography–mass spectrometry and application in environmental contamination*. Food Chem., Vol.101, pp. 1719-1726, (2007)
- [67]- Y. Picó, G. Font, M. J. Ruiz, M. Fernández- *Control of pesticide residues by liquid chromatography-mass spectrometry to ensure food safety*. Mass Spectrom. Rev., Vol.25, pp. 917-960, (2006)
- [68]- F. Delattre, F. Cazier, A. Tine -*Use a fluorescent molecular sensor for the detection of pesticides and herbicides in water*. Curr. Anal. Chem., Vol.5, pp. 48-52, (2009)
- [69]- F. Arduini, S. Guidone, A. Amine, G. Palleschi, D. Moscone, *Acetylcholinesterase biosensor based on self-assembled monolayer-modified gold-screen printed electrodes for organophosphorus insecticide detection*, Sensors and Actuators B, 179, 201-208, (2013)
- [70]- P. Raghu, M. R. Mohan Reddy, T. M. Reddy, B. E. Kumara Swamy, K. Reddaiah, *Detection of organophosphorous pesticides using a monoenzyme biosensor : A voltametric study*, Anal. Bioanal. Electrochem. , Vol 4, No 1, 1-16, (2012)
- [71]- A. A. Ciucu, C. Negulescu, R. P. Baldwin- *Detection of pesticides using an amperometric biosensor based on ferrophthalocyanine chemically modified carbon paste electrode and immobilized bienzymatic system*, Biosensors and Bioelectronics, 18 (2-3), 303-310, (2003)
- [72]- S. Andreescu, A. Avramescu, C. Bala, V. Magearu, J. L. Marty- *Detection of organophosphorus insecticides with immobilized acetylcholinesterase- comparative study of two enzyme sensor*, Anal. Bioanal. Chem, 374, 39-45, (2002)

- [73]- N. Kaur, H. Thakur, N. Prabhakar *Conducting polymer and multi-walled carbon nanotubes nanocomposites based amperometric biosensor for detection of organophosphate*. Journal of Electroanalytical Chemistry 775: 121-128, (2016)
- [74]- Q. Long, H. Li, Y. Zhang, S. Yao, *Upconversion nanoparticle- based fluorescence resonance energy transfer assay for organophosphorus pesticides*, Biosens Bioelectron 68, 168-174, (2015)
- [75]- E. Luan, Z. Zheng, X. Li, S. Liu, *Inkjet-assisted layer-by-layer printing of quantum dot/enzyme microarrays for highly sensitive detection of organophosphorous pesticides*, Anal Chim Acta 916, 77-83, (2016)
- [76]- M. Wei, J. Wang *-A novel acetylcholinesterase biosensor based on ionic liquids-AuNPs-porous carbon composite matrix for detection of organophosphate pesticides*. Sensors and Actuators B: Chemical 211: 290-296, (2015)
- [77]- Y. Zheng, Z. Liu, H. Zhan, J. Li, C. Zhang *-Studies on electrochemical organophosphate pesticide (OP) biosensor design based on ionic liquid functionalized graphene and a Co<sub>3</sub>O<sub>4</sub> nanoparticle modified electrode*. Analytical Methods 8(26): 5288-5295, (2016)
- [78]- D. Du, X. Ye, J. Cai, J. Liu, A. Zhang- *Acetylcholinesterase biosensor design based on carbon nanotube-encapsulated polypyrrole and polyaniline for amperometric detection of organophosphates*, Biosens Bioelectron, 25 (11), 2503-2508, (2010)
- [79]- A. Crew, D. Lonsdale, N. Byrd, R. Pittson, J.P. Hart, et al.-*A screen-printed, amperometric biosensor array incorporated into a novel automated system for the simultaneous determination of organophosphate pesticides*. Biosens Bioelectron 26(6): 2847-2851, (2011)

- [80]- Q. Lang, L. Han, C. Hou, F. Wang, A. Liu- *A sensitive acetylcholinesterase biosensor based on gold nanorods modified electrode for detection of organophosphate pesticide.* Talanta 156- 157: 34-41, (2016)
- [81]- R. Sundarmurugasan, M. B. Gumpu, B. L. Ramachandra, N. Nesakumar, S. Sethuraman, et al. -*Simultaneous detection of monocrotophos and dichlorvos in orange samples using acetylcholinesterase-zinc oxide modified platinum electrode with linear regression Calibration.* Sensors and Actuators B: Chemical 230: 306-313, (2016)
- [82]- <http://angstromengineering.com/tech/electron-beam-evaporation/>
- [83]-<http://www.semicore.com>
- [84]- F. Borghi, C. Melis, C. Ghisleri, A. Podestà, L. Ravagnan, L. Colombo, P. Milani,- *Stretchable nanocomposite electrodes with tunable mechanical properties by supersonic cluster beam implantation in elastomers* Appl. Phys. Lett., 106, (2015)
- [85]- Barborini, E., Piseri, P. & Milani, P. *A pulsed microplasma source of high intensity supersonic carbon cluster beams.* J. Phys. Appl. Phys. 32, L105 (1999).
- [86]- E. Barborini, P. Piseri, A. Li Bassi, A.C. Ferrari, C.E. Bottani, P. Milani- *Synthesis of carbon films with controlled nanostructure by separation of neutral clusters in supersonic beams.* Chemical Physical Letters, 300 (56): 633-638, (1999)
- [87]- E. Barborini, P. Piseri, A. Podesta, P. Milani- *Cluster beam microfabrication of patterns of three-dimensional nanostructured objects,* Applied Physics Letters, 77 (7), (2000)
- [88]- Barborini, E., Piseri, P. & Milani, P. *A pulsed microplasma source of high intensity supersonic carbon cluster beams.* J. Phys. Appl. Phys. 32, L105 (1999).

- [89]- G. Binning, C. F. Quate, C. Gerber- *Atomic force microscope*, Phys. Rev. Lett. 56, 930, (1986)
- [90]- D. Rugar, P. Hansma- *Atomic force microscopy*, J. Appl. Phys. , Vol. 61, p 4723, (1987)
- [91] - <http://www.polifab.polimi.it/equipments/afm/>
- [92]- Matlab- version 7. 4. 0. 287 (R2007a) TheMathWorks Inc.
- [93]- A. Bard, L. Faulkner, *Electrochemical Methods – Fundamental and Applications*, 2nd Edition, John Wiley and sons, (2001)
- [94]- <http://compton.chem.ox.ac.uk/>
- [95]- P. T. Kissinger, W. R. Heineman- *Cyclic Voltammetry, Journal of Chemical Education*, Vol 60, No 9, (1983)
- [96]- M. Sluyters-Rehbach, *Impedances of electrochemical systems: terminology, nomenclature and representation. Part 1. Cells with metal electrodes and liquid solutions*. Pure Appl. Chem. 66 (9), 1831–1891 (1994)
- [97]- M. E. Orazem, B. Tribollet, *Electrochemical Impedance Spectroscopy, The Electrochemical Society Series*, Wiley-Interscience, (2008)
- [98]- R. Popovtzer, T. Neufeld, E. Z. Ron, J. Rishpon, and Y. Shacham-Diamand, *Electrochemical detection of biological reactions using a novel nano-bio-chip array*, Sens. Actuator B-Chem., 119, 664-672 (2006).
- [99]- P.C. Pandey, S. Upadhyay, H.C. Pathak, C.M.D. Pandey, I. Tiwari, *Acetylthiocholine/acetylcholine and thiocholine/choline electrochemical biosensors/ sensors based on an organically modified sol–gel glass enzyme reactor and graphite paste electrode*, Sensor. Actuators B-Chem. 62, 109, (2009)

[100]- G. L. Ellman, K. D. Courtney, V. Andres Jr., R. M. Featherstone- *A new and rapid colorimetric determination of acetylcholinesterase activity*, Volume 7, Issue 2, Pages 88-90, IN1, 91-95, **(1961)**

[101]- S. G. Weber, J. T. Long, *Detection limits and selectivity in electrochemical detectors*, Anal. Chem. 60(15), 903A-913A, **(1988)**

[102] - G. Liu, S. L. Riechers, M. C. Mellen, Y. Lin, *Sensitive electrochemical detection of enzymatically generated thiocholine at carbon nanotube modified glassy carbon electrode*, Electrochemistry Communications, 7, 1163-1169, **(2005)**

## **Appendix 1**

# An Amperometric Sensor for Thiocholine based on Cluster-Assembled Zirconia Electrodes

A.Raileanu<sup>1,2</sup>, C. Piazzoni<sup>2</sup>, F. Borghi<sup>2</sup>, L. G. Bettini<sup>2</sup>, Y. Shacham-Diamand<sup>3</sup>, T. Santaniello<sup>2</sup>, P. Milani<sup>2\*</sup>

<sup>1</sup> SEMM, European School of Molecular Medicine, via Adamello, 16, 20139, Milan, Italy

<sup>2</sup> CIMaNa, Interdisciplinary Centre for Nanostructured Materials and Interfaces, via Celoria, 16, 20133, Milan, Italy

<sup>3</sup> School of Electrical Engineering, Tel Aviv University, Chaim Levanon Str, No 30, Tel Aviv, Israel

Corresponding author: CIMaNa, Via Celoria, 16, 20133, Milano, Italy; [pmilani@mi.infn.it](mailto:pmilani@mi.infn.it); Tel: +39 02 5031.17219

## Abstract

Here we report on the fabrication and characterization of cluster-assembled nanostructured zirconia electrodes for the electrochemical detection of enzymatically produced thiocholine. Zirconia nanostructures are produced by Supersonic Cluster Beam Deposition on thin gold films. This technique enables nanoscale control of the deposited film surface morphology, providing high electrochemically active zirconia surface area with low parasitic serial resistance due to high metal wire conductance. The electrochemical behavior of the electrodes has been characterized in the presence of the Potassium ferricyanide/Potassium ferrocyanide redox couple. The electrochemical response for the oxidation of an enzymatic product was assessed by means of cyclic voltammetry, electrochemical impedance spectroscopy and chronoamperometry. The nanostructured zirconia film yields a good electrochemical thiocholine sensing. The limit of detection for thiocholine under working potential of 0.810- 0.820 V vs. reference was found to be comprised between 0.25  $\mu\text{M}$  and 1.3  $\mu\text{M}$ . Nanostructured electrodes, combining gold and zirconia nanoparticles can be implemented as functional transducers in biosensing devices, for example based on Acetylcholinesterase for electrochemical detection of polluting agents.

**Keywords:** Thiocoline, cluster-assembled film, Zirconia, cluster beam deposition, amperometric detection, biosensor

## 1. Introduction

Acetylcholinesterase (AChE) is an enzyme located in the cholinergic and neuromuscular synapses. AChE main role is to catalyze the breakdown of the neurotransmitter acetylcholine (ACh) into two compounds, acetate and choline [1], [2]. Recently, the use of AChE in biosensing technology has gained an increased attention, especially in the field of environmental pollution monitoring where it has been used in pesticide detection systems [3], [4], [5]. The principle of operation of biosensors using AChE as a biological recognition element is based on the irreversible inhibition of the catalytic activity of the enzyme by the compound that has to be detected [6]. In order to facilitate an electrochemical sensing, the product of the enzyme/ substrate reaction can be oxidized or reduced at relatively low bias, typically in the range of 500 mV or less. However, choline that is the product of reaction between AChE and ACh is not an electroactive species and it cannot be detected through electrochemical methods. Therefore, Acetylthiocholine (ATCh), an artificial analogue of ACh, can be used as a substrate to generate Thiocoline (TCh) that is an electroactive compound [3] and can be detected by simple electrochemical methods such as chronoamperometry.

Nowadays, TCh detection methods are traditional laboratory methods such as high purity liquid chromatography (HPLC) [7], gas chromatography [8] or fluorescence spectroscopy [9]. Even though these methods are well established and very precise, they rely on bulky and costly equipment that can be used only in laboratories and that are not suitable for on-site detection outside the labs. Furthermore, laboratory methods require a highly trained personnel, are expensive, and they need a large number of reagents, which add to their

complexity and cost of operation. Therefore, there is a high demand for portable, sensitive, cheap and easy to use detection devices and methods [10].

In recent years, many research groups have been focusing on developing portable biosensors that are robust, precise and easy to use by consumers on-site. Among different approaches for portable detection systems [4], [10], [11], electrochemical real-time detectors have proven to provide a convenient method of enzymatic activity assessments [12], [13]. Electrochemical sensors are easy to use, simple and low cost compared to other methods. Electrochemical sensors require simple low-cost electrodes that can be integrated into compact electronic platforms that can yield rapid responses in user-friendly portable systems [14].

The operating principle of an electrochemical biosensor is based on the reaction of a specific analyte occurring at the electrodes surface generating an electric signal proportional to the analyte concentration. There are several electrochemical methods for detection, such as voltammetry [15], electrochemical impedance spectroscopy [16] and amperometric method, which are the most common in case of enzyme/substrate based sensors [17].

Even though electrochemical methods have their advantages in terms of simplicity and rapid time of detection, the choice of suitable materials constituting the electrodes to tailor the system response to the analyte is a critical point [18]. Actually, the use of thin metal films as the physico-chemical transducer often implies the introduction of chemical mediators through surface functionalization approaches in order to enhance or to hasten the electrical response related to specific chemical reactions. This leads to time-consuming modification procedures and complex post-processing steps of the materials and systems [19]. Moreover, traditional metallization techniques (such as physical vapor deposition or electrodeposition) do not provide fine control on the structure morphology of the electrode and corresponding

specific active area for electrochemical detection, that should be maximized in order to increase the transducer's performance [20].

Recently, nanostructures like nanowires, nanotubes, nanoparticles, and quantum dots have been employed to improve the analytic performance of biosensors. The high surface-to-volume ratio increases the sensitivity and lower the detection limits [17]. More specifically, for TCh based electrochemical detection systems, carbon [20], [21] or gold [4], [22], [23] based nanostructures are the most commonly used. Several research groups have been using different types of materials for electrochemical detection of TCh. Screen printed electrodes modified with Prussian blue have been used for the electrochemical oxidation of TCh at a potential of 0.2 V yielding a limit of detection of 5  $\mu\text{M}$  [24] or carbon nanotube-modified glassy carbon electrodes have yielded a limit of detection of 0.3  $\mu\text{M}$  at an oxidation potential of 0.15 V [20]. Nanostructured metal oxides have been recently used as transducer components, since they show good optical and electrical properties and they also result in a high catalytic efficiency and an improved ability of adsorption of the biomolecules [25].

Zirconium dioxide ( $\text{ZrO}_2$ ) nanostructures have aroused increasing interest to be used as part of the transducer in bio sensing systems, since this material offers high biocompatibility [26], good electron transfer and surface charge properties [27], and a very high affinity to oxygen moieties [28]. The most commonly used methods to produce transducers for TCh electrochemical detection based on  $\text{ZrO}_2$  involve electrochemical deposition [29], [30] and screen printing [31]. Even though these approaches have their advantages in terms of ease of production and standardization, they also present several drawbacks. These are mainly related to the lack of precise control of the film surface morphological characteristics, which would increase the active surface area for detection, and electrical properties, which could enhance the layer's electrochemical characteristics in terms of charge transfer ability. Furthermore, the capability of detecting TCh without the involvement of chemical mediators and the

possibility to pattern the transducer's elements having control on their geometry are difficult to achieve using these techniques.

Here we report the fabrication and characterization of an amperometric sensor for synthetically produced TCh consisting of a transducer based on a cluster-assembled zirconia nanostructured film (ns-ZrO<sub>2</sub>) deposited by Supersonic Cluster Beam Deposition (SCBD) on gold thin film electrodes. This manufacturing approach enables nanoscale control over the electrode morphology, providing large surface area to the transducer which is sufficient for electrochemical detection of TCh, without additional mediators. The electrochemical properties of the cluster-assembled ZrO<sub>2</sub>/gold electrodes were characterized in terms of charge transfer ability, double layer capacitance and their sensing performance yielding the TCh limit of detection (LOD).

## **1. Materials and Methods**

### **2.1 Production of cluster-assembled zirconia modified working electrodes**

The production of cluster-assembled ZrO<sub>2</sub> electrodes was accomplished in two steps. The electrodes were made on 1 mm thick borosilicate glass round coverslip with a diameter of 24 mm (VWR International). A detailed description of the design of the modified working electrode is shown in **Fig.1A**.

The first step was making the metal electrode and a 15 nm thin film Ti adhesion layer was deposited by electron beam evaporation, followed by the deposition of a 160 nm thick gold film.

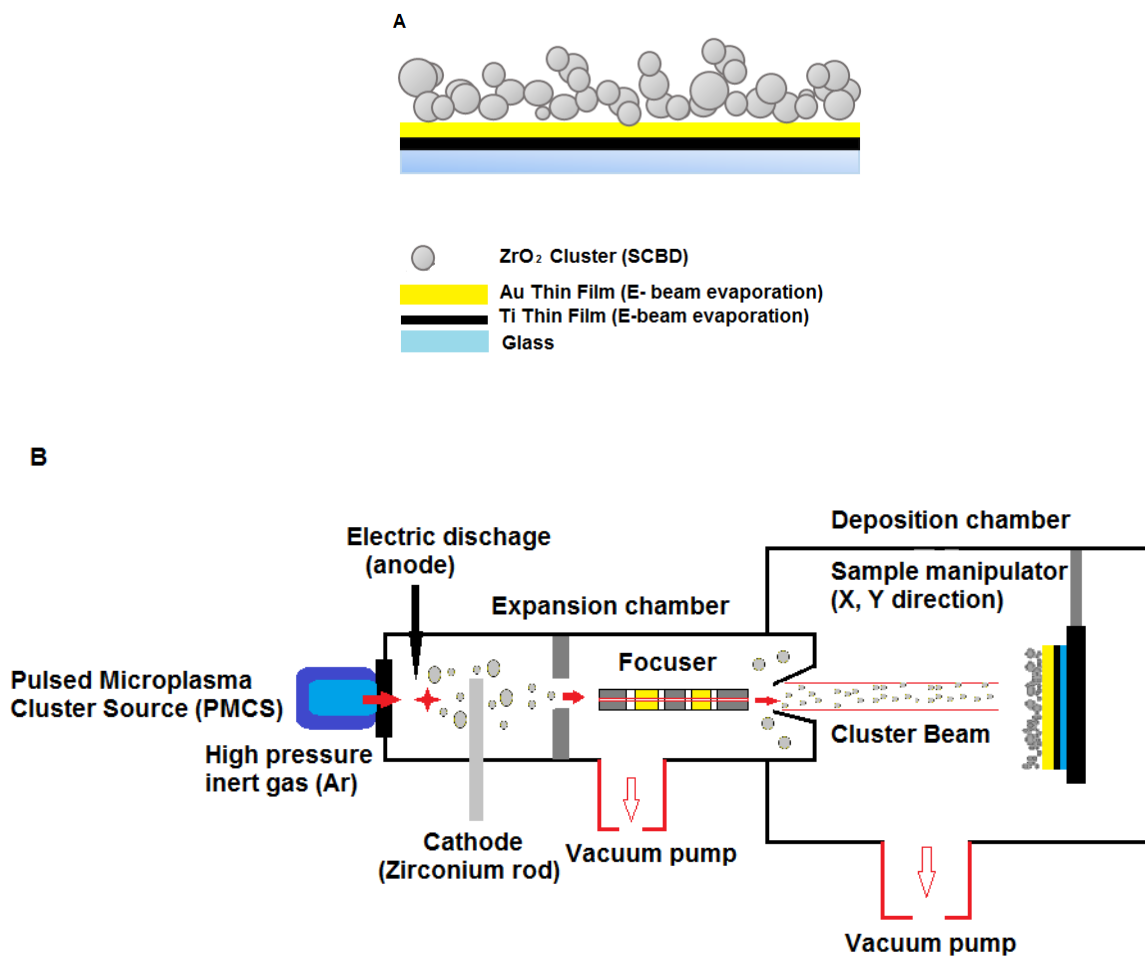


**Figure 1 A-** Schematic representation of the structure of the modified working electrode

**B-** Representation of the SCBD apparatus (adapted with permission [32])

The second step was the deposition of the cluster-assembled zirconia thin film with SCBD. The SCBD apparatus, schematized in **Fig. 1B**, is equipped with a pulsed microplasma cluster source (PMCS) [33]; a detailed description of the PMCS operating principle is presented in [34]. Briefly, the operating principle of PMCS is based on a zirconium rod ablation by argon plasma jet that is ignited by a pulsed electric discharge. The sputtered zirconium atoms and ions thermalize with the gas and the oxygen that is present in the condensation chamber forming ZrO<sub>2</sub> clusters. The mixture of clusters and inert gas is extracted in vacuum through a nozzle and a seeded supersonic beam is formed, which is afterwards collected onto the glass coverslips. Since the supersonic regime implies low

divergence of the cluster beam ( $< 1^\circ$ ) [34], SCBD can be employed to generate patterns of the deposited film using stencil masks, enabling patterning with relatively good lateral resolution with small shadow effects [35]. Furthermore, SCBD is a high-throughput technique suitable for deposition over large surface areas [36].

Due to the low kinetic energy of the nanoparticles, the clusters do not undergo fragmentation or significant deformations upon impact with the target, therefore preserving their original shape and size [37]. This enables the production of an electrochemically active nanostructured surface with tailored morphological features. The surface roughness of the cluster-assembled film can be controlled at the nanoscale by controlling the film thickness [38] since the cluster deposition takes place in a ballistic regime [39]. The quantitative control of the surface roughness at the nanoscale influences the wettability [40] and the absorption of protein and enzymes [41]. Those characteristics are particularly appealing in view of the implementation of enzymatic transducers onto the nanostructures for biosensing applications. For the fabrication of the cluster-assembled  $\text{ZrO}_2$  electrodes reported here we used ns- $\text{ZrO}_2$  layers with variable thickness: 30 nm (NS1), 60 nm (NS2), and 100 nm (NS3). The film thickness was measured off-line by atomic force microscopy [34].

## **2.1. Surface morphology characterization of the cluster-assembled $\text{ZrO}_2$ electrodes**

The surface morphology characterization of the cluster-assembled zirconia thin films has been assessed by means of atomic force microscopy (AFM) in air using a Multimode AFM device equipped with a Nanoscope IV controller (Bruker), operated in Tapping Mode. For this assessment, we have used rigid silicon cantilevers mounting single crystal silicon tips with a nominal radius of 5-10 nm and the resonance frequency was in the range of 250-350 kHz. Several images of  $2\mu\text{m} \times 1\mu\text{m}$  have been acquired for each sample at a scan rate of 1 Hz and 2048 X 512 points. Afterwards, the images have been flattened by line-by-line subtraction of the first and second order polynomials for artifacts removal due to sample tilt

and scanner bow. From the AFM images, root-mean-square surface roughness  $R_q$  and specific area (calculated as the ratio of surface area to the projected area) were calculated. The film thickness used for the modified electrodes was calculated also by AFM by acquiring images across a sharp step produced by applying a mask on the coverslip before the deposition.

### **2.3. Electrochemical characterization of different cluster-assembled $ZrO_2$ electrodes**

The electrochemical characterization of the electrodes has been performed by cyclic voltammetry (CV) and electrochemical impedance spectroscopy (EIS) using a Reference 600 potentiostat/galvanostat (Gamry Instruments Inc.). The measurements were performed in a 3-electrodes electrochemical cell setup with a Pt wire as counter electrode and a Ag/AgCl quasi reference electrode produced by electrodeposition according to a protocol previously described in [42], which was calibrated using a commercial Ag/AgCl electrode (Gamry Instruments Inc.). As electrolyte, a solution containing 10 mM Potassium Ferrocyanide ( $K_4 [Fe (CN)_6]$ , Sigma-Aldrich Chemicals S.A.), 10 mM Potassium Ferricyanide ( $K_3 [Fe (CN)_6]$ , Sigma-Aldrich Chemicals S.A.) and a Phosphate Buffer Solution of 0.1 M (pH=7.5) was used.

Cyclic voltammograms were obtained by scanning the working electrode at a potential range from -0.5 to 0.5 V, with a scan rate of 50 mV/s. For the square root of the scan rate assessments, each type of electrode was scanned at a potential range from -0.5 to 0.5 V, with scan rates of 20 mV/s, 50 mV/s and 100 mV/s respectively.

### **2.4. Enzymatic production of Thiocoline**

Acetylcholinesterase from *Electrophorus electricus* (Type VI-S 500 UN), Acetylthiocholine Chloride (ATCl), 55'-Dithiobis (2-nitrobenzoic acid) (DTNB) were purchased from Sigma-Aldrich Chemicals S.A..

Since TCh is not commercially available, it was produced daily by enzymatic means. For this, 1 mL of 0.5M of ATCl was prepared in a phosphate buffer solution 0.1 M with a pH=8. To this solution, 10 U of AChE were added and the mixture was left to incubate for 2 hours. After incubation, the concentration of the obtained TCh was assessed spectrophotometrically by the Ellman's method [43]. For this, 2.7 mL of PBS (0.1 M, pH=8) was added in a cuvette along with 300  $\mu$ L of DTNB solution of 0.1 M and 15  $\mu$ L of TCh (after it was diluted 1:100 from the stock solution). The obtained enzymatic product was assessed spectrophotometrically at a wavelength of 412 nm and the absorbance was measured at different times. From the absorbance values obtained, the real concentration of TCh was evaluated using the Lambert-Beer law with the known molar extinction coefficient of TNB ( $\epsilon=13,600 \text{ M}^{-1} \text{ cm}^{-1}$  [43]). Therefore, we obtained 1mL of TCh solution of 0.5 M. The TCh stock solution was used for 24 hours and it was stored at 4°C.

## **2.5. Electrochemical detection of Thiocholine**

For the electrochemical detection of the enzymatic product, Cyclic Voltammetry (CV), Electrochemical Impedance Spectroscopy (EIS) and Chronoamperometry (CA) were used.

In order to determine the oxidation potential of the TCh, CV measurements have been performed in the presence and absence of the enzymatic product as followed: the electrodes were first scanned at a potential range from 0.3 to 0.9 V, at a scan rate of 50 mV/s using as electrolyte only the PBS solution adjusted for the use of a biological compound (0.1 M, pH=8). Afterwards, maintaining the same settings, a concentration of 0.5 mM of TCh solution was used in 0.1 M PBS and the oxidation potential was determined.

For the EIS assessments, the equilibrium potential obtained from the cyclic voltammograms was applied, using a frequency range of 500 KHz to 100 mHz with a potential perturbation amplitude of 10 mV. The EIS spectra was determined using 4 different concentrations of TCh, 0.04 mM, 0.07 mM, 0.1mM and 0.2 mM, in PBS solution (0.1 M,

pH=8). All EIS data was processed using Echem Analyst (Gamry Instruments Inc.) and Charge Transfer Resistance was determined after fitting the data with a Randle's circuit [44].

CA was used in order to determine the limit of detection (LOD) of our system. For this, we have used the oxidation potential of TCh determined from the cyclic voltammograms. For each type of electrode, five different concentrations of enzymatic product were used, ranging from 5  $\mu\text{M}$  to 25  $\mu\text{M}$ . The average of the current peaks corresponding to each concentration was plotted against the concentrations used and the LOD of the system was calculated.

### 3. Results and discussion

#### 3.1. AFM characterization of the $\text{ZrO}_2$ films

Typical surface profiles, superimposed to the 3D views of the bare Au electrode compared to cluster-assembled ns- $\text{ZrO}_2$  thin films, are shown in **Fig. 2**.

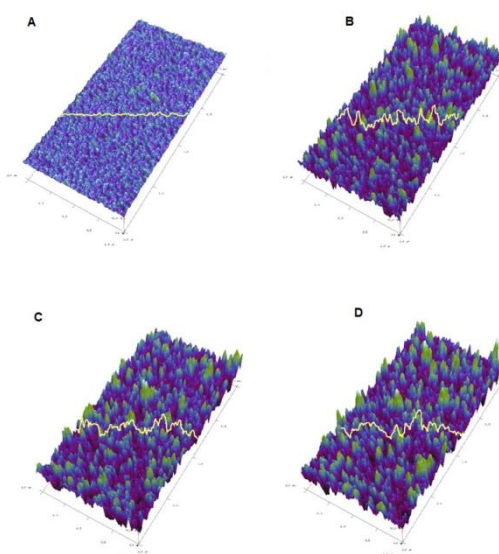


**Figure 2-** Representative surface profiles superimposed to 3D views for: A) Bare Au; B) NS1, C) NS2, D) NS3

As expected, the Au layer is highly flat, with a roughness of 1 nm, compared with the surfaces of the modified ns-ZrO<sub>2</sub> electrodes whose roughness changes from 9 to 11 nm. From the AFM characterization of the interface we can also observe that by increasing the thickness of the ns-ZrO<sub>2</sub> thin film also the specific area increases, therefore leading to a higher surface active area available for the biosensing device. The specific morphological properties of the modified ns-ZrO<sub>2</sub> working electrodes are reported in **Table 1**.

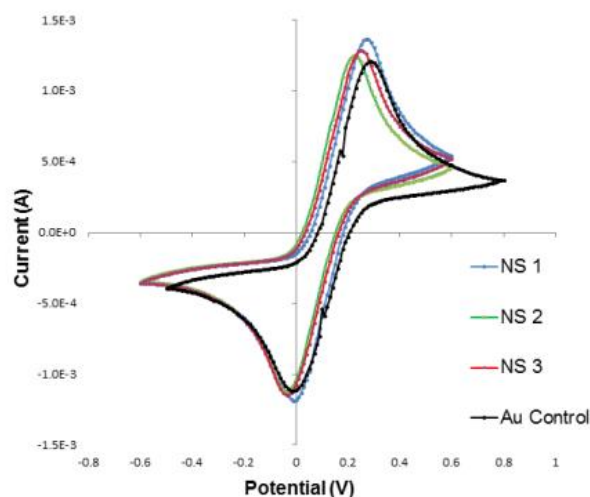
<b>Type of sample</b>	<b>Thickness (nm)</b>	<b>Roughness (nm)</b>	<b>Specific area</b>
<b>Bare Au(Control)</b>	160±9	1±0.1	1.03± 0.01
<b>NS 1</b>	35±7	9.1±0.1	1.38±0.03
<b>NS 2</b>	61±8	10.2±0.1	1.45±0.05
<b>NS 3</b>	100±10	11.3±0.1	1.47±0.03

Table 1 - Morphological characteristics of the cluster-assembled ZrO<sub>2</sub> electrodes

### 3.2. Electrochemical characterization with [Fe(CN)<sub>6</sub>]<sup>3-</sup>/[Fe(CN)<sub>6</sub>]<sup>4-</sup> at different cluster-assembled ZrO<sub>2</sub> electrodes

The cyclic voltammograms obtained for each batch of the produced electrodes and bare Au of the [Fe(CN)<sub>6</sub>]<sup>3-</sup>/[Fe(CN)<sub>6</sub>]<sup>4-</sup> redox couple at a concentration of 10 mM in 0.1 M PBS (pH= 7.5) is shown in **Fig.3**. The peak currents of the redox active species (anodic, I<sub>pa</sub> and cathodic, I<sub>pc</sub>) have slightly increased in the case of the three different modified electrodes in comparison with the bare Au electrode, and a small decrease in the peak-to-peak separation (ΔE<sub>p</sub>) has been observed for the electrodes containing the ns-ZrO<sub>2</sub>, therefore showing a quasi-reversible behavior of the electrodes. The increase of the current peaks at the modified electrodes is attributed to a larger electroactive area and an increased electron transfer rate

due to the addition of the ns-ZrO<sub>2</sub>. The values obtained for the cathodic and anodic processes, as well as the peak separation data, obtained from the cyclic voltammograms of the bare Au and the modified electrodes, are presented in **Table 2**.



**Figure 3** – Cyclic voltammograms obtained for the modified working electrodes in comparison with bare Au electrode in the presence of 10 mM Fe<sup>3+</sup>/Fe<sup>2+</sup> in PBS 0.1 M (pH=7.5) at 50 mV/s

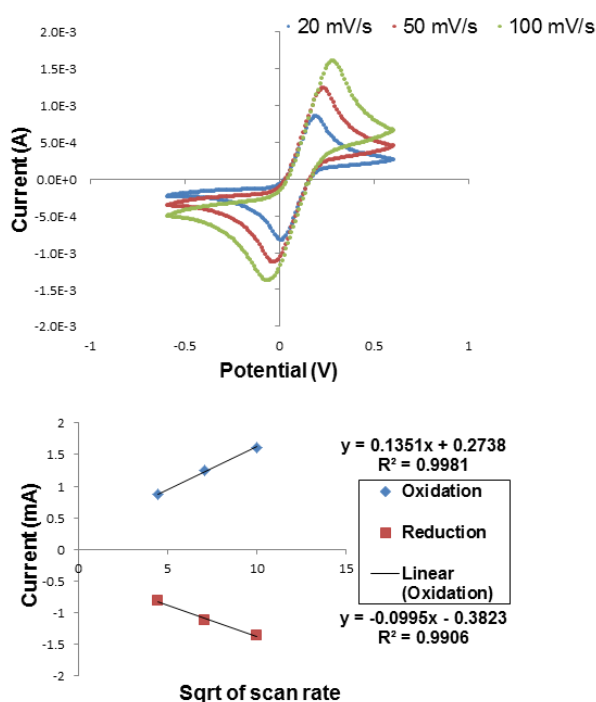
Type of sample	I <sub>pa</sub> (mA)	I <sub>pc</sub> (mA)	ΔE <sub>p</sub> (mV)
Bare Au	-1.1	1.2	270
NS 1	-1.2	1.4	280
NS 2	-1.1	1.25	270
NS 3	-1.15	1.3	280

Table 2 – Description of the redox processes values obtained from the cyclic voltammograms performed on the modified working electrodes compared to the bare Au electrode

The reversibility of the redox reaction has also been tested with CV by using different scan rates and the results obtained are shown in **Fig.4**. As a representative example of this

behavior, the cyclic voltammograms at different scan rates are reported only for the batch of modified working electrodes with a thickness of the ns-ZrO<sub>2</sub> thin film of 60 nm.

By using different scan rates of 20, 50 and 100 mV/s<sup>-1</sup>, we observed that the reduction and the cathodic current peaks for the modified electrodes increase for increasing scan rates, along with a small shift in both cathodic and anodic peak potential, which suggests that there is a good reversibility of the fast charge-discharge response.



**Figure 4-** Cyclic voltammograms of the modified working electrode (ns-ZrO<sub>2</sub> thin film of 60 nm thickness), at different scan rates in the presence of 10 mM Fe<sup>3+</sup>/Fe<sup>2+</sup> in PBS 0.1 M (pH=7.5);

*Inset:* Variation of anodic and cathodic peaks vs. the square root for scan rate

### 3.3. Cyclic voltammetry response of thiocholine at the cluster-assembled ZrO<sub>2</sub> electrodes

The cyclic voltammetry responses of TCh at the modified electrodes as well as at the bare Au electrode have been measured, using a solution of 500  $\mu$ M of TCh in 0.1M PBS (pH=8). In **Table 3** we present the oxidation potential values as well as the cathodic current peak obtained for the oxidation of thiocholine in the case of the modified and bare Au electrodes.

Type of sample	Oxidation potential (V)	Cathodic current peak ( $\mu$ A)
<b>Bare Au</b>	+0.810	450
<b>NS 1</b>	+0.810	320
<b>NS 2</b>	+0.820	413
<b>NS 3</b>	+0.820	325

Table 3- Voltammetric responses of TCh at the modified electrodes and bare Au

Interestingly, the measured cathodic current peaks for all the nanostructured layers were not significantly lower than the one obtained for the control, which suggests that the presence of ns-ZrO<sub>2</sub> do not alter the electrical properties of the gold layer to a great extent, but it rather confers suitable charge transfer properties to the system and preserve the transducer detection activity. More in details, for the electrodes modified with a 60 nm thick layer of ns-ZrO<sub>2</sub> the oxidation current showed to be similar for the one obtained using the bare Au electrodes (413  $\mu$ A against 450  $\mu$ A). For comparison we have performed a CV assay both in the presence as well as in the absence of TCh (**Fig.5**). As expected we see no response when we used only the PBS (0.1 M, pH=8) solution, but a clear peak appears +0.820 V when we add the TCh solution, as previously reported by other groups [20].

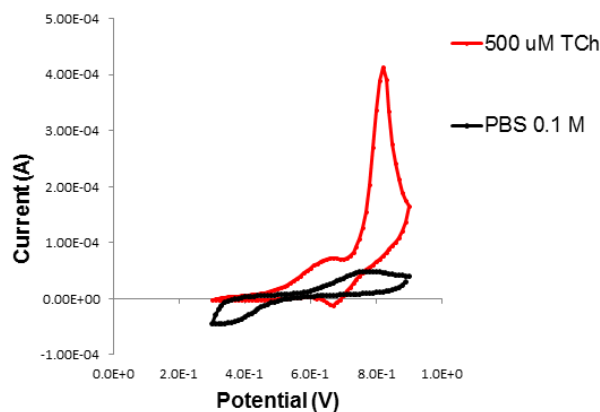


**Figure 5-** Voltammetric response of the modified working electrode in the presence and absence of thiocholine

### 3.2 Electrochemical Impedance Spectroscopy of the thiocholine detection system

For a better understanding of the influence of the ns-ZrO<sub>2</sub> thin layer thicknesses on the electrochemical detection of TCh we have chosen to perform EIS studies at the chosen potential where the oxidation reaction of the enzymatic product takes place, as obtained from the cyclic voltammograms. For this, we have chosen to analyze the response of each type of modified electrode in the presence of the enzymatic product in different concentrations ranging from 40, 70, 100 and 200  $\mu$ M.

After obtaining the EIS spectra, a Randle's circuit model [44] has been used for fitting the data, in order to obtain the charge transfer resistance ( $R_{ct}$ ) values as well as the double layer capacitance ( $C_{dl}$ ).

The EIS spectra of 70  $\mu$ M TCh (**Fig. 6**) shows a diffusion limited process for all the types of modified working electrode, with a Warburg element present at frequencies lower than 1Hz, which enabled us to fit it with the Randle's circuit model.

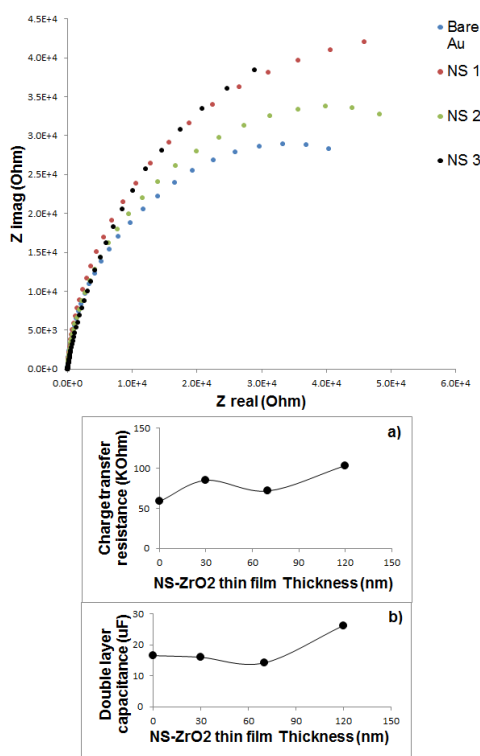


**Figure 6**– Nyquist plot of 70  $\mu\text{M}$  thiocholine at the modified working electrodes compared to bare Au; *Inset a)*  $R_{ct}$  dependence on the ns-ZrO<sub>2</sub> thickness ; *Inset b)*:  $C_{dl}$  dependence on the ns-ZrO<sub>2</sub> thickness

By comparing the  $R_{ct}$  values according to the different thickness of the ns-ZrO<sub>2</sub>, we noticed that for the bare Au electrode we obtain the lowest resistance (58.5 KOhm), as expected, and that the values of  $R_{ct}$  for the sample NS2 are largely similar to that of the bare Au (71.7 KOhm). This observation is compatible with the results obtained from the CV analysis and further confirming that the presence of the nanostructures does not induce significant passivation effects of the metal layer. Taking into account the  $R_{ct}$  value of the NS1 sample (85 KOhm), we notice that is higher than in the case of NS2. This behavior could be explained by the fact that, according to the evolution of the roughness as a function of the layer thickness, the active surface area for NS1 is lower with respect to that of NS2, and therefore the time for the system electron transfer is longer. On the other hand, for the NS3,

we have a large surface area, but the thickness in this case is probably high enough to dampen the electron transfer, giving the highest  $R_{ct}$  value of 103.4 KOhms.

The double layer capacitance values obtained for the NS1 ( $16 \mu\text{F}/\text{cm}^2$ ) and NS2 ( $14.2 \mu\text{F}/\text{cm}^2$ ) are fairly close to the bare Au ( $16.5 \mu\text{F}/\text{cm}^2$ ), but in the case of the NS3 sample ( $27 \mu\text{F}/\text{cm}^2$ ) the behavior is more capacitive and the diffusion process is very low, behavior that can be associated with the larger active surface area and a higher porosity of the thicker sample.

### 3.3 Amperometric response of thiocholine

After determining the oxidation potential of TCh at the modified electrodes, the amperometric response of the enzymatic product was studied by using chronoamperometry. For this, five different concentrations of thiocholine were added and the current response was measured over time. The concentration of the enzymatic product was ranged between  $5 \mu\text{M}$  up to  $25 \mu\text{M}$  and the modified electrode used for this assessment was the Au/NS-ZrO<sub>2</sub> with a thickness of the ZrO<sub>2</sub> thin film of 60 nm (Fig. 7).

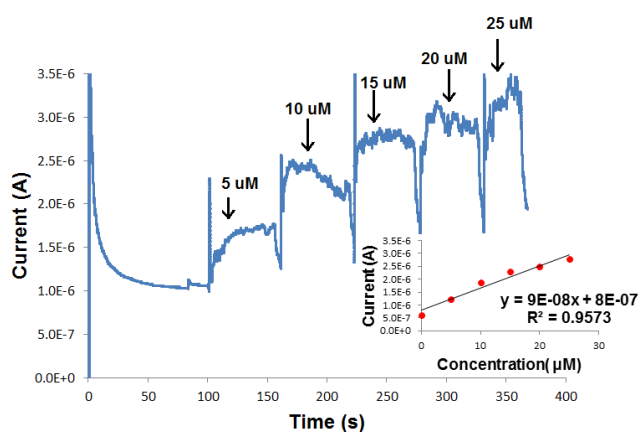


**Figure 7** - Amperometric detection of TCh at the surface of NS2 modified electrode, at a fixed potential of +0.820 V, in PBS 0.1 M (pH=8) and different concentrations of the enzymatic product; *Inset*: Representation of the cathodic current against the different concentrations of TCh

A linear relationship was obtained between the response current and the TCh concentration, but a saturation threshold has been observed for the last concentration, thus giving us a correlation coefficient of 0.924. A detection limit of 0.25  $\mu\text{M}$  was estimated based on a  $S/N=3$ .

Amperometric detection assays for TCh were performed on the other types of the modified electrodes and the LOD obtained are reported in **Table 4**.

Type of sample	Limit of detection ( $\mu\text{M}$ )
Bare Au	0.3
NS 1	0.67
NS 2	0.25
NS 3	1.3

Table 4- Amperometric response of TCh oxidation at different modified working electrode

## Conclusions

We have demonstrated the fabrication of electrochemical transducers for the detection of synthetically produced TCh based on Au electrodes functionalized with cluster-assembled  $\text{ZrO}_2$  nanostructured thin films deposited by SCBD. The electrodes produced were electrochemically characterized using cyclic voltammetry in presence of the  $[\text{Fe}(\text{CN})_6]^{3-}/[\text{Fe}(\text{CN})_6]^{4-}$  redox couple, and the results obtained showed that the presence of the nanostructures do not alter the conductivity of the metal substrate, but that it moderately increased the cathodic and anodic current peaks, preserving the reversibility of the reaction.

By modifying bare Au electrodes with cluster-assembled ns- $\text{ZrO}_2$  thin films with a precise control of the thickness and active surface area, we were able to obtain an efficient

electrochemical detection platform for enzymatically produced TCh, with improved electrochemical characteristics in terms of double layer capacitance and appropriate charge transfer resistance. More specifically, for 60 nm thick ns-ZrO<sub>2</sub> layers, the analyte detection limit was measured as 0.25 μM using amperometric methods, which is a relevant result according to the literature. The modified electrodes presented in this study can represent a promising solution for the development of transducers that can be implemented in electrochemical detection systems based on Acetylcholinesterase for pollution control monitoring.

**Foundings:**

This work was supported by the European Union's Seventh Framework Program FP7/2007-2013 [grant number 607417]

## References:

1. D. M. Quinn, *Chem. Rev.*, 87, 955- 979 (1987)
2. M. R. Picciotto, M. J. Higley, Y. S. Mineur, *Neuron.*, 76 (1), 116- 129 (2012)
3. P. C. Pandey, S. Upadhyay, H. C. Pathak, C. M. D. Pandey, Ida Tiwari, *Sensor. Actuator. B*, 62, 109–116 (2000)
4. F. Arduini, S. Guidone, A. Amine, G. Palleschi, D. Moscone, *Sensors and Actuators B*, 179, 201– 208 (2013)
5. V. Scognamiglio, G. Pezzotti, I. Pezzotti, J. Cano, K. Buonasera, D. Giannini, M. T. Giardi, *Microchimica Acta*, 170, 3–4, 215–225 (2010)
6. H. Schulze, S. Vorlova, F. Villatte, T. T. Bachmann, R. D. Schmid, *Biosens. Bioelectron.*, 18 (2-3), 201-209 (2003)
7. Y. Picó, G. Font, M. J. Ruiz, M. Fernández, *Mass Spectrom. Rev.*, Vol.25, 917-960 (2006)
8. S. R. Rissato, M. S. Galhiane, M. V. de Almeida, M. Gerenutti, B. M. Apon, *Food Chem.*, 101, 1719-1726 (2007)
9. F. Delattre, F. Cazier, A. Tine, *Curr. Anal. Chem.*, 5, 48-52 (2009)
10. B. Srinivasan, S. Tung, *J. Lab. Autom*, 20 (4), 365-389 (2015)
11. P. Ni, Y. Sun, H. Dai, W. Lu, S. Jiang, Y. Wang, Z. Li, *Sensors and Actuators : B*, 240, 1314-1320 (2017)
12. H. Matsuura, Y. Sato, T. Sawaguchi, F. Mizutani, *Sensor. Actuator.B*, 91(1-3), 148-151 (2003)
13. C. S. Fang, K. H. Oh, J. K. Park, H. Yang, *Electroanalysis*, 29, 339-344 (2017)
14. T. Osaka, M. Datta, Y. Shacham-Diamand, *Electrochemical nanotechnologies, Nanostructure Science And Technology*, Springer Science, (2010)
15. Y. Zheng, Z. Liu, H. Zhan, J. Li, C. Zhang, *Analytical Methods*, 8 (26), 5288-5295 (2016)

16. M. Wei, J. Wang, *Sensors and Actuators B: Chemical* 211, 290-296 (2015)
17. Kirsch J, Siltanen C, Zhou Q, Revzin A, Simonian A., *Chem Soc Rev.*, 42 (22), 8733-68 (2013)
18. M. Holzinger, A. Le Goff, S. Cosnier, *Frontiers in Chemistry*, 2-63 (2014)
19. D. Grieshaber, R. MacKenzie, J. Voros, E. Reimhult, *Sensors (Basel)*, 8 (3), 1400-1458 (2008)
20. G. Liu, S. L. Riechers, M. C. Mellen, Y. Lin, *Electrochemistry Communications* 7, 1163–1169 (2005)
21. A. Mulyasuryani, M. Dofir, *Engineering*, 6, 230-235 (2014)
22. Q. Lang, L. Han, C. Hou, F. Wang, A. Liu, *Talanta*, 165-157, 34-41 (2016)
23. N. Dimcheva, E. Horozova, Y. Ivanov, T. Godjevargova, *Cent. Eur. J. Chem.*, 11 (11), 1740-1748 (2013)
24. F. Ricci, F. Arduini, A. Amine, D. Moscone, G. Palleschi, *J. Electroanal. Chem.* 563, 229-237 (2004)
25. P. R. Solanki, A. Kaushik, V. V. Agrawal, B. Malhotra, *NPG, Asia Mater.* 3 (1), 17-24 (2011)
26. S. Kumar, J. G. Sharma, S. Maji, B. D. Malhotra, *Biosensors and Bioelectronics*, 78, 497–504 (2016)
27. P. R. Solanki, A. Kaushik, P. M. Chavan, S. N. Maheswari, B. D. Malhotra, *Electrochemistry Communications* 11, 2272–2277 (2009)
28. T. Yang, X. Guo, Q. Kong, R. Yang, Q. Li, K. Jiao, *Anal Chim Acta.*, 786, 29-33 (2013)
29. H. Zhang, J. Ding, D. Du, *Int. J. Electrochem. Sci.*, 10, 1632 – 1645 (2015)
30. S. Pundir, N. Chauhan, J. Narang, C. S. Pundir, *Analytical Biochemistry*, 427, 26–32 (2012)
31. M. P. Bucur, B. Bucur, G. L. Radu, *Sensors (Basel)*, 13 (2), 1603-1613 (2013)

- 32** F. Borghi, C. Melis, C. Ghisleri, A. Podestà, L. Ravagnan, L. Colombo, P. Milani, *Appl. Phys. Lett.*, 106, 121902 (2015)
- 33.** K. Wegner, P. Piseri, H. V. Tafreshi, P. Milani, *J. Phys. D: Appl. Phys.* 39 (22), 439-459 (2006)
- 34.** P. Piseri, A. Podesta, E. Barborini, P. Milani, *Rev. Sci. Instrum.*, 72, 2261–7 (2001)
- 35.** E. Barborini, P. Piseri, A. Podesta, P. Milani, *Appl. Phys Lett.*, 77, 1059 (2000)
- 36.** P. Milani, P. Piseri, E. Babrborini, L. Diederich, A. Podesta, S. Iannotta, *Journal of Metastable and Nanocrystalline Materials*, 8, 519-524 (2000)
- 37.** P. Milani, S. Iannotta, Springer-Verlag, Berlin, (1999)
- 38.** F. Borghi, C. Lenardi, A. Podesta, P. Milani, E. Sogne, M. Merlini, C. Ducati, *Journal of Applied Physics*, 120 (5), (2016)
- 39.** A. Podesta, F. Borghi, M. Indrieri, S. Bovio, C. Piazzoni, P. Milani, *Journal of Applied Physics*, 118, 234309 (2015)
- 40.** A. Podesta, G. Bongiorno, P.E. Scopelliti, S. Bovio, P. Milani, C. Semprebon, G. Mistura, *J. Phys. Chem. C*, 113 (42), 18264- 11644 (2009)
- 41.** L. Gailite, P. E. Scopelliti, V. K. Sharma, M. Indrieri, A. Podesta, G. Tedeschi, P. Milani, *Langmuir*, 30 (20), 5973- 81 (2014)
- 42.** R. Popovtzer, T. Neufeld, E. Z. Ron, J. Rishpon, Y. Shacham-Diamand, *Sens. Actuator B- Chem.*, 119, 664 (2006)
- 43.** G. L. Ellman, K. D. Courtney, V. Andres Jr., R. M. Featherstone, 7(2), 88-90, IN1, 91-95 (1961)
- 44.** J. E. B. Randles, *Discussions of the Faraday Society*, 1, 11-19 (1947)

## Acknowledgements

I would like to say thank you to my PhD supervisor, Professor Paolo Milani, who taught me in these 4 years, new things regarding physics, biology and how to be a “golf player” in the world of science by working with what is available and having the courage to make my own decisions while trying to get out of a difficult “sand hole”.

I say thank you for the Catsense project which supported my PhD economically and gave me the opportunity to be trained and to interact with amazing researchers all over the world.

In particular, I would like to thank Prof Yosi Shacham-Diamand, Richa Pandey and Giorgia Fiaschi who had the patience and the kindness to help me understand one of the most interesting fields of science, electrochemistry.

Thank you, Claudio Piazzoni for helping me in trying to understand the Supersonic Cluster Beam Deposition device and for providing me with great samples to work with.

Thank you Luca Bettini and Tommaso Santaniello for being the closest things I have for big brothers and supporting me in good times and bad times during these years.

Thank you Francesca Borghi for the great help in AFM assessments and also for the care and support.

Thank you Elisa Sogne, for welcoming me in the beginning in my PhD and for encouraging me when I was panicking at the sight of the SCBD.

Thank you Professor Cristina Lenardi for managing to support me in situations when I couldn't see any light at the end of the tunnel.

Thank you Veronica Viscardi and Francesca Fiore for all the help and the amazing patience you had with me during these years.

And thank you to my parents who unfortunately had to be my psychological support in the darkest times of the research but whom also were taking part at the happy times. I hope I made you proud.